

DTIC FILE COPY

SECURITY CLASSIFICATION OF THIS PAGE

REPORT DOCUMENTATION PAGE				Form Approved OMB No. 0704-0188	
1a. REPORT SECURITY CLASSIFICATION UNCLASSIFIED			1b. RESTRICTIVE MARKINGS NONE		
2a. SECURITY CLASSIFICATION  <b>AD-A218 026</b>			3. DISTRIBUTION/AVAILABILITY OF REPORT APPROVED FOR PUBLIC RELEASE; DISTRIBUTION UNLIMITED.		
6a. NAME OF PERFORMING ORGANIZATION AFIT STUDENT AT Texas A&M Univ			6b. OFFICE SYMBOL (If applicable)		
6c. ADDRESS (City, State, and ZIP Code)			7a. NAME OF MONITORING ORGANIZATION AFIT/CIA		
8a. NAME OF FUNDING / SPONSORING ORGANIZATION			8b. OFFICE SYMBOL (If applicable)		
9. PROCUREMENT INSTRUMENT IDENTIFICATION NUMBER			7b. ADDRESS (City, State, and ZIP Code) Wright-Patterson AFB OH 45433-6583		
10. SOURCE OF FUNDING NUMBERS			11. TITLE (Include Security Classification) (UNCLASSIFIED) Origins of Convective Activity Over Panama		
12. PERSONAL AUTHOR(S) Christopher Stephen Strager			13a. TYPE OF REPORT THESIS/DISSERTATION		
13b. TIME COVERED FROM _____ TO _____			14. DATE OF REPORT (Year, Month, Day) 1989		
15. PAGE COUNT 112			16. SUPPLEMENTARY NOTATION APPROVED FOR PUBLIC RELEASE IAW AFR 190-1 ERNEST A. HAYGOOD, 1st Lt, USAF Executive Officer, Civilian Institution Programs		
17. COSATI CODES			18. SUBJECT TERMS (Continue on reverse if necessary and identify by block number)		
FIELD	GROUP	SUB-GROUP			
19. ABSTRACT (Continue on reverse if necessary and identify by block number)					
<div style="text-align: center;"> <b>DTIC</b>  <b>ELECTE</b>  <b>S FEB 13 1990 D</b>  <i>Co D</i> </div>					
20. DISTRIBUTION / AVAILABILITY OF ABSTRACT <input checked="" type="checkbox"/> UNCLASSIFIED/UNLIMITED <input type="checkbox"/> SAME AS RPT. <input type="checkbox"/> DTIC USERS			21. ABSTRACT SECURITY CLASSIFICATION UNCLASSIFIED		
22a. NAME OF RESPONSIBLE INDIVIDUAL ERNEST A. HAYGOOD, 1st Lt, USAF			22b. TELEPHONE (Include Area Code) (513) 255-2259		22c. OFFICE SYMBOL AFIT/CI

90 02 12 030

# ORIGINS OF CONVECTIVE ACTIVITY OVER PANAMA

A Thesis

by

CHRISTOPHER STEPHEN STRAGER

Submitted to the Office of Graduate Studies of  
Texas A&M University  
in partial fulfillment of the requirements for the degree of

MASTER OF SCIENCE

August 1989

Major Subject: Meteorology

211

11

OTIC COPY INSPECTED

Accession For	
NTIS - GRA&I	<input checked="" type="checkbox"/>
OTIC - TAB	<input type="checkbox"/>
Unannounced	<input type="checkbox"/>
Justification	
By	
Distribution	
Acquisition Source	
Dist	Acquisition or Special
A-1	

90' 02 12 000

## ABSTRACT

Origins of Convective Activity Over Panama. (August 1989)

Christopher Stephen Strager, B.S., The Pennsylvania State University

Chair of Advisory Committee: Dr. Steven W. Lyons

↙ Satellite-derived outgoing longwave radiation (OLR) data were used to examine convective variability over the Panama region. Time series analysis of the area-averaged daily OLR data for 1984 and 1985 revealed a persistent 12-d oscillation in convective activity during each season. Composite analyses of OLR data for the area 120°W-40°W and 35°S-35°N for the 1984 dry (1 January-9 May) and wet (10 May-4 December) seasons showed this oscillation extends beyond Panama and the Central America region into the eastern Pacific.

↘ Composite diagrams of u- and v-wind components and geopotential heights were constructed using daily upper-air soundings from Albrook AFS, Panama in order to infer a vertical structure to the oscillation. These composites showed well-defined trends in all three variables associated with each phase of the 12-d oscillation. The dry season OLR, wind, and geopotential height composites suggest that a west-to-east moving trough in the upper-levels seems to be responsible for the convection anomalies in the Panama region. Wet season OLR, wind, and geopotential height composites suggest that periodic westward migrations of an upper-level anticyclone associated with the subequatorial ridge could be producing the west-northwestward moving periodic convective fluctuations which originate over Panama during that season.

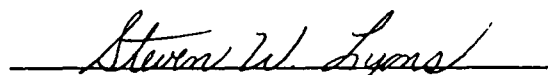
# ORIGINS OF CONVECTIVE ACTIVITY OVER PANAMA

A Thesis

by

CHRISTOPHER STEPHEN STRAGER

Approved as to style and content by:



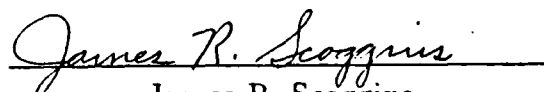
Steven W. Lyons  
(Chair of Committee)



Kenneth C. Brundidge  
(Member)



Rudolf J. Freund  
(Member)



James R. Scoggins  
(Head of Department)

August 1989

A modulation of the 12-d oscillation was found during the 1984 wet season with a period of approximately 70-80 d. It appears to be connected with tropical cyclone activity in the eastern Pacific. For periods when the 12-d oscillation was weak (well-defined) over the Panama region, a significant increase (decrease) in the number of tropical cyclones, as well as an increase (decrease) in the number of systems that developed into hurricanes, was detected.

## ACKNOWLEDGMENTS

I acknowledge the members of my committee for their input and guidance. I would especially like to thank my committee chairman, Dr. Steven W. Lyons, for his ideas, encouragement, and enthusiastic support. The many hours Dr. Lyons spent working with me are very much appreciated.

I thank the U. S. Air Force for giving me the opportunity to continue my education. Within the Air Force, several people have been influential in convincing me to return to school, in particular Lieutenant Colonel Charles French and Major Douglas Pearson. The knowledge I have gained from working with them has been invaluable.

I would like to thank Robert Liles for lending his computer expertise to this project. Space limits me from listing all of the other students in the department who helped me along the way, however, I could not continue without thanking Jeffrey Johnson, Donna Woolley Smith, David Hadley, and Keith Blackwell. Their technical advice and friendship helped smooth out the rough spots in this undertaking.

Finally, I thank my wife Crystal for her love and support during our stay at Texas A&M. Despite attending class full time in pursuit of her degree in accounting, she was always there to console me during the bad times and celebrate with me during the good times.

## DEDICATION

To my wife Crystal, my parents Frank and Mary Lou, and my brother Brian.  
Without your support and encouragement this project would not have been possible.

## TABLE OF CONTENTS

CHAPTER	Page
I INTRODUCTION .....	1
II PREVIOUS WORK .....	3
III RESEARCH OBJECTIVES .....	7
IV DATA .....	9
OLR .....	9
Upper-Air .....	11
Rainfall .....	14
V DETERMINATION OF PERIODIC MODES OF CONVECTIVE ACTIVITY .....	16
Selection of Area of Study .....	16
Methods of Analysis .....	21
VI ANALYSIS OF DOMINANT MODE OF CONVECTIVE ACTIVITY OVER PANAMA .....	36
Examination of 12-Day Oscillation .....	36
OLR Composite Diagrams .....	38
Vertical Structure of 12-Day Oscillation .....	57
Possible Synoptic Scenarios Associated with the 12-Day Oscillation .....	80
Case Study .....	91
Correlation Between OLR Data and Precipitation .....	97
VII MODULATION OF 12-DAY OSCILLATION .....	101
VIII SUMMARY AND AREAS FOR FURTHER STUDY .....	104
REFERENCES .....	109
VITA .....	112



## LIST OF TABLES

Table	Page
1 Resultant winds and height anomalies for Panama corresponding to the four phases of the 12-d oscillation for dry season, 1984. . . . .	82
2 Resultant winds and height anomalies for Panama corresponding to the four phases of the 12-d oscillation for wet season, 1984. . . . .	87

## LIST OF FIGURES

Figure	Page
1 Domain of OLR data used in study. . . . .	12
2 Map of Panama. . . . .	13
3 Location of Panama Canal Commission raingauges across the Panama Canal and Gatun Lake. . . . .	15
4 Average OLR for the period 1 January 1984 through 31 December 1985. . . . .	17
5 OLR variance for the period 1 January 1984 through 31 December 1985. . . . .	19
6 Subset of domain selected as index reference. . . . .	20
7 Time series of daily average OLR for area 5-12°N, 75-85°W for 1984. . . . .	22
8 Time series of daily average OLR for area 5-12°N, 75-85°W for 1985. . . . .	23
9 Trend-removed daily OLR for dry season 1984. . . . .	26
10 Trend-removed daily OLR for wet season 1984. . . . .	27
11 Trend-removed daily OLR for dry season 1985. . . . .	28
12 Trend-removed daily OLR for wet season 1985. . . . .	29
13 Numerical output from IMSL periodogram analysis for dry season and wet season 1984. . . . .	30
14 Numerical output from IMSL periodogram analysis for dry season and wet season 1985. . . . .	31
15 OLR correlograms and 95% confidence bands for 1984. . . . .	33
16 OLR correlograms and 95% confidence bands for 1985. . . . .	34
17 Amplitude response curve of 12-d filter. . . . .	39
18 12-d filtered OLR data for dry season 1984. . . . .	40
19 12-d filtered OLR data for wet season 1984. . . . .	41

Figure	Page
20 12-d filtered OLR data for dry season 1985. . . . .	42
21 12-d filtered OLR data for wet season 1985. . . . .	43
22 OLR composite diagram corresponding to Maximum OLR days over Panama for dry season 1984. . . . .	46
23 OLR composite diagram corresponding to Max-to-Min inflection points over Panama for dry season 1984. . . . .	47
24 OLR composite diagram corresponding to Minimum OLR days over Panama for dry season 1984. . . . .	48
25 OLR composite diagram corresponding to Min-to-Max inflection points over Panama for dry season 1984. . . . .	49
26 OLR composite diagram corresponding to Maximum OLR days over Panama for wet season 1984. . . . .	52
27 OLR composite diagram corresponding to Max-to-Min inflection points over Panama for wet season 1984. . . . .	53
28 OLR composite diagram corresponding to Minimum OLR days over Panama for wet season 1984. . . . .	54
29 OLR composite diagram corresponding to Min-to-Max inflection points over Panama for wet season 1984. . . . .	55
30 Vertical composite for u-wind component corresponding to Maximum OLR days, dry season 1984. . . . .	60
31 Vertical composite for u-wind component corresponding to Max-to-Min OLR inflection points, dry season 1984. . . . .	61
32 Vertical composite for u-wind component corresponding to Minimum OLR days, dry season 1984. . . . .	62
33 Vertical composite for u-wind component corresponding to Min-to-Max OLR inflection points, dry season 1984. . . . .	63
34 Vertical composite for v-wind component corresponding to Maximum OLR days, dry season 1984. . . . .	64

Figure	Page
35 Vertical composite for v-wind component corresponding to Max-to-Min OLR inflection points, dry season 1984. . . . .	65
36 Vertical composite for v-wind component corresponding to Minimum OLR days, dry season 1984. . . . .	66
37 Vertical composite for v-wind component corresponding to Min-to-Max OLR inflection points, dry season 1984. . . . .	67
38 Vertical composite of height anomalies for dry season 1984. . . . .	68
39 Vertical composite for u-wind component corresponding to Maximum OLR days, wet season 1984. . . . .	72
40 Vertical composite for u-wind component corresponding to Max-to-Min OLR inflection points, wet season 1984. . . . .	73
41 Vertical composite for u-wind component corresponding to Minimum OLR days, wet season 1984. . . . .	74
42 Vertical composite for u-wind component corresponding to Min-to-Max OLR inflection points, wet season 1984. . . . .	75
43 Vertical composite for v-wind component corresponding to Maximum OLR days, wet season 1984. . . . .	76
44 Vertical composite for v-wind component corresponding to Max-to-Min OLR inflection points, wet season 1984. . . . .	77
45 Vertical composite for v-wind component corresponding to Minimum OLR days, wet season 1984. . . . .	78
46 Vertical composite for v-wind component corresponding to Min-to-Max OLR inflection points, wet season 1984. . . . .	79
47 Vertical composite for height anomalies for wet season 1984. . . . .	81
48 20 kPa streamline climatology for January. . . . .	84
49 Possible synoptic scenario associated with the four phases of the 12-d oscillation, dry season. . . . .	85
50 20 kPa streamline climatology for August. . . . .	88

Figure	Page
51 Possible synoptic scenarios associated with the four phases of the 12-d oscillation, wet season. . . . .	89
52 GOES enhanced IR satellite photo for 1800 GMT, 3 October 1984. . . .	92
53 GOES enhanced IR satellite photo for 1900 GMT, 6 October 1984. . . .	93
54 GOES enhanced IR satellite photo for 1800 GMT, 8 October 1984. . . .	94
55 GOES enhanced IR satellite photo for 1800 GMT, 11 October 1984. . . .	95
56 12-d filtered OLR time series for wet season 1984 showing active and inactive phases of 12-d oscillation. . . . .	102

## CHAPTER I

### INTRODUCTION

The accurate forecasting of significant precipitation events in the tropics continues to be a problem for the operational forecaster. Recent advances in satellite and radar technology have allowed forecasters to produce reasonable short-range forecasts, but are of little use in developing medium- and long-range forecasts. The scarcity, as well as the questionable accuracy of conventional data throughout the tropical regions, adds to the problem.

These forecasting problems are compounded in Panama where, in the summer wet season (May-November), daily convective activity can be greatly enhanced by the passage of waves in the easterlies. The northward migration of the monsoon trough can also produce significant increases in cloud cover and precipitation amounts. In the dry season, precipitation events along the north coast and central highlands of Panama can be initiated by the southward movement of shear lines into the Caribbean. Early detection of these events is often the key to forecasting precipitation events beyond 24 h. In addition, spectral analyses of tropical wind, pressure, and outgoing longwave radiation (OLR) fields over the past 20 y have revealed periodic fluctuations in these variables ranging from 3 to 60 d. Monitoring the progress of these oscillations could be a key to improving medium- to long-range forecasting in the Panama region and in the tropics in general.

---

The style used is that of the *Monthly Weather Review*

In this study, spectral analysis techniques are applied to time series of OLR over the Panama region to determine if any significant periodic fluctuations in the OLR field are evident. Next, composite OLR diagrams are constructed to determine the spatial extent and strength of the periodicities. Daily rawinsonde analyses are also used to infer the vertical structure and synoptic patterns associated with the oscillation.

Chapter II contains a review of previous work concerning tropical weather systems and their time scales. The objectives and general procedures of this research are outlined in Chapter III. A description of the data sets can be found in Chapter IV. Chapter V describes the methods used in the time series analysis of the OLR and rawinsonde data sets. The results of this research are presented in Chapter VI, along with a case study. Chapter VII shows an interesting relationship between tropical cyclone activity in the eastern Pacific and convective variability over Panama. Finally, a summary and discussion are contained in Chapter VIII.

## CHAPTER II

### PREVIOUS WORK

Over the past 50 y, many studies have attempted to examine convective variability in the tropics. These studies revealed oscillations in atmospheric variables ranging from three days to greater than 60 d. The first synoptic feature detected which produced significant convective variability over Panama were waves in the easterlies. Dunn (1940) was one of the first to recognize these disturbances in the Caribbean region as he tracked isallobaric centers moving westward across the Antilles. Riehl (1945) provided the first comprehensive work on waves in the easterlies, stating that these waves originated over Africa as a result of barotropic instability in the easterly current. He found that these waves have their maximum intensity between 3,000 and 4,500 m, propagate to the west at an average speed of  $5-8 \text{ ms}^{-1}$ , and have a period of roughly 3-4 d. The top of the moist layer to the west of the trough axis can be as low as 1,500 m but rises rapidly near the trough axis, attaining a maximum height of nearly 9,000 m to the east of the trough axis where strong convective activity is found.

Riehl's original work was expanded upon by Merritt (1964) to include several variations of the easterly wave model. Also, during this time, Riehl's original model began to draw criticism. Merritt felt this controversy resulted from a general tendency to label any disturbance in the easterly flow as an easterly wave. Atkinson (1971) agreed with this assessment, claiming that many forecasters used the easterly wave as a "crutch" to attempt to explain all tropical weather occurrences. Further



controversy arose concerning the development of tropical cyclones from waves in the easterlies. While Riehl maintained that tropical storm development resulted from the intensification of waves in the easterlies, Sadler (1967) led the opposing view stating that all tropical vortices form initially in a shear zone between two currents of opposite direction. Despite the controversy concerning an exact definition for waves in the easterlies and their role in tropical cyclone formation, there is little doubt that perturbations in the easterly flow do exist and can produce significant variations in convective activity throughout the Caribbean region.

The use of spectral analysis techniques during the late 1960s led to the discovery of atmospheric oscillations with periods longer than 10 d. Wallace and Chang (1969) used these spectral analysis techniques to further study the characteristics of waves in the easterlies. Their findings confirmed the existence of fluctuations in the zonal and meridional wind components with a periodicity of approximately 4-5 d for several tropical locations, including Balboa, Panama. Similar fluctuations were noted for relative humidity and surface pressure. An additional interesting result was the detection of a longer-period oscillation in these variables having a period greater than 10 d, which was strongest at western Pacific stations. This oscillation was downplayed by the authors and was attributed to the sensitivity of the spectra in the low-frequency end to minor changes in the sampling period. It was felt that if the period of study had been changed by a month or two the spectral peak might have been shifted or completely eliminated.

The first real evidence of a tropical oscillation with a period significantly longer than a wave in the easterlies was presented by Madden and Julian (1971). Their

spectral analysis of daily rawinsonde data for Canton Island ( $3^{\circ}\text{S}$ ,  $172^{\circ}\text{W}$ ) revealed a 41–53 d fluctuation in the 85 and 15 kPa zonal winds, tropospheric temperature, and station pressure in the tropical central Pacific region. Madden and Julian (1972) expanded their original study to include several tropical stations around the globe in order to determine the spatial extent of this oscillation. Their results revealed an eastward-propagating, large-scale (zonal wavenumber one or two) oscillation with a period of roughly 40–50 d. This oscillation was evident in station pressure and zonal winds for all stations within  $10^{\circ}$  latitude of the equator from Singapore eastward to Curacao. Balboa, Panama was included in this study and showed spectral peaks in pressure and upper tropospheric zonal winds at or near 40–50 d.

As the use of satellite data increased during the 1970s, cloud cover and outgoing longwave radiation (OLR) data began to be used to detect low-frequency oscillations in the tropics. Using satellite cloud data and geopotential height, Yasunari (1980) found that intraseasonal variation of the Indian monsoon during northern summer is dominated by the 40–50 d oscillation. Murakami (1980) found significant 15–30 d peaks in OLR data over regions of southeast Asia during winter, while Lyons (1981) found similar spectral peaks over Indonesia and the equatorial Pacific regions. These studies demonstrated the ability of OLR data to represent convective activity in the tropics, with small OLR values indicating areas of high cloudiness (associated with convective activity) and larger OLR values showing relatively cloud-free areas. The success of those studies led to a series of papers which used OLR data to detect low-frequency tropical oscillations, including studies by Weickmann (1983); Weickmann, Lussky, and Kutzbach (1985); Lau and Chan (1983); and Knutson, Weickmann, and

Kutzbach (1986). The results of these studies confirmed the original description of the oscillation as stated by Madden and Julian and showed that the OLR anomalies have a characteristic propagation speed of  $3\text{--}6\text{ ms}^{-1}$  and are strongest over the tropical Indian and the western Pacific oceans.

While most of the studies mentioned above have concentrated on low-frequency oscillations over the Indian Ocean and western Pacific region, Knutson and Weickmann (1987) state that some potentially-significant OLR fluctuations seem to be occurring over parts of Central and South America. To date, very little research has dealt with the detection and significance of low-frequency oscillations in this tropical region. They also go on to state that the practical importance of the oscillation, in terms of relating the low-frequency oscillations to a local forecast, is a topic that needs to be investigated. This research will address both subjects.

The majority of work done in analyzing tropical oscillations to date has focused on atmospheric variables such as OLR, geopotential height, temperature, and zonal and meridional wind measurements. Hartmann and Gross (1988) were the first to detect low-frequency oscillations using daily precipitation records. Their results showed significant spectral peaks in the 40–50 d range for several Indonesian and western Pacific locations. This study was also significant in that it began to focus attention on the effect these atmospheric oscillations can have on day-to-day weather conditions such as daily rainfall amounts at specific locations. Once it's been determined that these oscillations can significantly affect rainfall and cloud cover at a location, the next important step is to develop techniques to forecast the day-to-day changes associated with these oscillations.

## CHAPTER III

### RESEARCH OBJECTIVES

The main research objective was to examine convective variability over Panama through spectral analysis of OLR time series data. Any significant periodicities in the OLR time series would reflect periodic variations of cloud cover and convection over the Panama region. The spatial extent of this oscillation would then be determined through the construction of composite OLR anomaly diagrams over a larger domain ( $120^{\circ}\text{W}$ - $40^{\circ}\text{W}$ ,  $35^{\circ}\text{S}$ - $35^{\circ}\text{N}$ ) corresponding to four phases (maximum, minimum, and two inflection points) of the oscillation cycle. By following the four phases of the oscillation, a direction of movement of the OLR anomalies could be inferred. Similar composites of rawinsonde data corresponding to the four parts of the oscillation would be constructed which, along with satellite imagery, would allow for a rough analysis of the associated synoptic pattern.

Another objective was to identify, quantitatively (through use of rawinsonde wind and geopotential height composites) and qualitatively (through use of satellite imagery), the atmospheric conditions that would forecast any change in cloud cover and convective activity over Panama. By maintaining daily continuity on these conditions, operational weather forecasters in Panama would be able to distinguish between each phase of the oscillation, allowing them to significantly improve their medium- to long-range forecasts.

An additional goal was to examine the correlation between daily-averaged OLR values over Panama and daily rainfall totals from the dense network of raingauges in

the Panama Canal region. A comparison of the rainfall totals and OLR values would help determine the usefulness of OLR values in estimating rainfall over a region.

## CHAPTER IV

### DATA

#### OLR

A 2-y subset (1 January 1984 through 31 December 1985) of the National Oceanic and Atmospheric Administration (NOAA) Outgoing Longwave Radiation (OLR) data set provided the primary tool used in this research. This data set was established in June 1974 and since that time numerous studies have used these OLR values to study convective activity in the tropics. These OLR data were derived from window radiance measurements obtained from a scanning radiometer flown aboard the NOAA 7 polar-orbiting satellite. The NOAA 7 is one in a series of sun-synchronous satellites and has equator crossing times of 0230 and 1430 LST. The spatial resolution, as originally measured, was 8 km but the observations have been spatially-averaged, digitized, and stored in a  $2.5^\circ$  latitude-longitude array. A more detailed description of the process is provided by Gruber and Winston (1978).

A brief summary of the procedures used to obtain the OLR values follows:

The Temperature Humidity Infrared Radiometer (THIR) on the NOAA 7 satellite senses window radiance ( $E_\lambda$ ) in the infrared window region of 11.5 to 12.5  $\mu\text{m}$ . Radiance equivalent brightness temperatures ( $T_{rb}$ ) are obtained by solving Planck's law

$$E_\lambda = \frac{c_1 \lambda^{-5}}{c_2 / e^{T_{rb} / \lambda} - 1} \quad (1)$$

for  $T_{rb}$ . The result is

$$T_{rb} = \frac{c_2 \lambda^{-1}}{\ln(c_1 \lambda^{-5} E_{\lambda}^{-1} + 1)} \quad (2)$$

where  $\lambda$  is the wavelength in  $\mu\text{m}$ ,  $c_1 = 3.74 \times 10^{-16} \text{Wm}^2$ , and  $c_2 = 1.44 \times 10^{-2} \text{mK}$ .

At this point, an empirical regression formula developed by Ohring, Gruber, and Ellingson (1984) and refined by Gruber and Krueger (1984) is used to convert  $T_{rb}$  to flux equivalent brightness temperatures ( $T_{fb}$ ):

$$T_{fb} = aT_x + bT_x^2 \quad (3)$$

where  $T_x = -3.66\text{K} + 1.015(T_{rb})$ ,  $a = 1.249$ , and  $b = 0.001055\text{K}^{-1}$ .

Finally, through use of the Stefan-Boltzman law

$$F_{olr} = \sigma T_{fb}^4 \quad (4)$$

where  $\sigma = 5.67 \times 10^{-8} \text{Wm}^{-2}\text{K}^{-4}$ , the actual OLR flux emittance values ( $F_{olr}$ ) used in this study were obtained.

A relationship between OLR values and equivalent cloudtop temperatures ( $T_e$ ) provided by Cahalan, Short, and North (1982) states

$$\frac{\Delta \text{OLR}}{\Delta T_e} \approx 2 \text{Wm}^{-2}\text{K}^{-1}$$

with a reference point of  $\text{OLR} \approx 250 \text{Wm}^{-2}$  at  $T_e = 273 \text{K}$ .

The assumption made in using these data is that small values of OLR represent areas of deep convection and cloud cover, while large OLR values represent relatively clear conditions. This leads to the major disadvantage of using OLR data, which is that it is only one-dimensional and does not allow for an analysis of the vertical

structure of the system. For example, a small OLR value of  $130 \text{ Wm}^{-2}$  would suggest that convective activity and precipitation were occurring at a location. However, that low OLR value could be reflecting only the cold cloud tops of a cirrus anvil associated with convective activity occurring far from that location.

Although the objective of this study was to examine convective variability over Panama, it became apparent during the research that the factors affecting convection in that area were originating well outside of the Panama region. The original area of study continued to expand, with the eventual domain of the OLR field shown in Fig. 1.

### Upper-Air

The upper-air data used in this study are from Albrook Air Force Station, Panama (see Fig. 2) for the time period 1 January through 31 December 1984. Vertical soundings were taken twice daily at the site, at 0000 and 1200 GMT. Only the 1200 GMT soundings are used in this study since thunderstorms are often still in the local area during the 0000 GMT run and can affect the ability of the sounding to represent conditions on a larger spatial scale.

Three variables were used from the soundings: u- and v-wind components and height of the significant pressure surfaces. The wind data were obtained from pilot-balloon (PIBAL) observations while the height data were obtained from radiosonde observations (RAOBS). Missing data for any of the variables were resolved through linear interpolation over time.



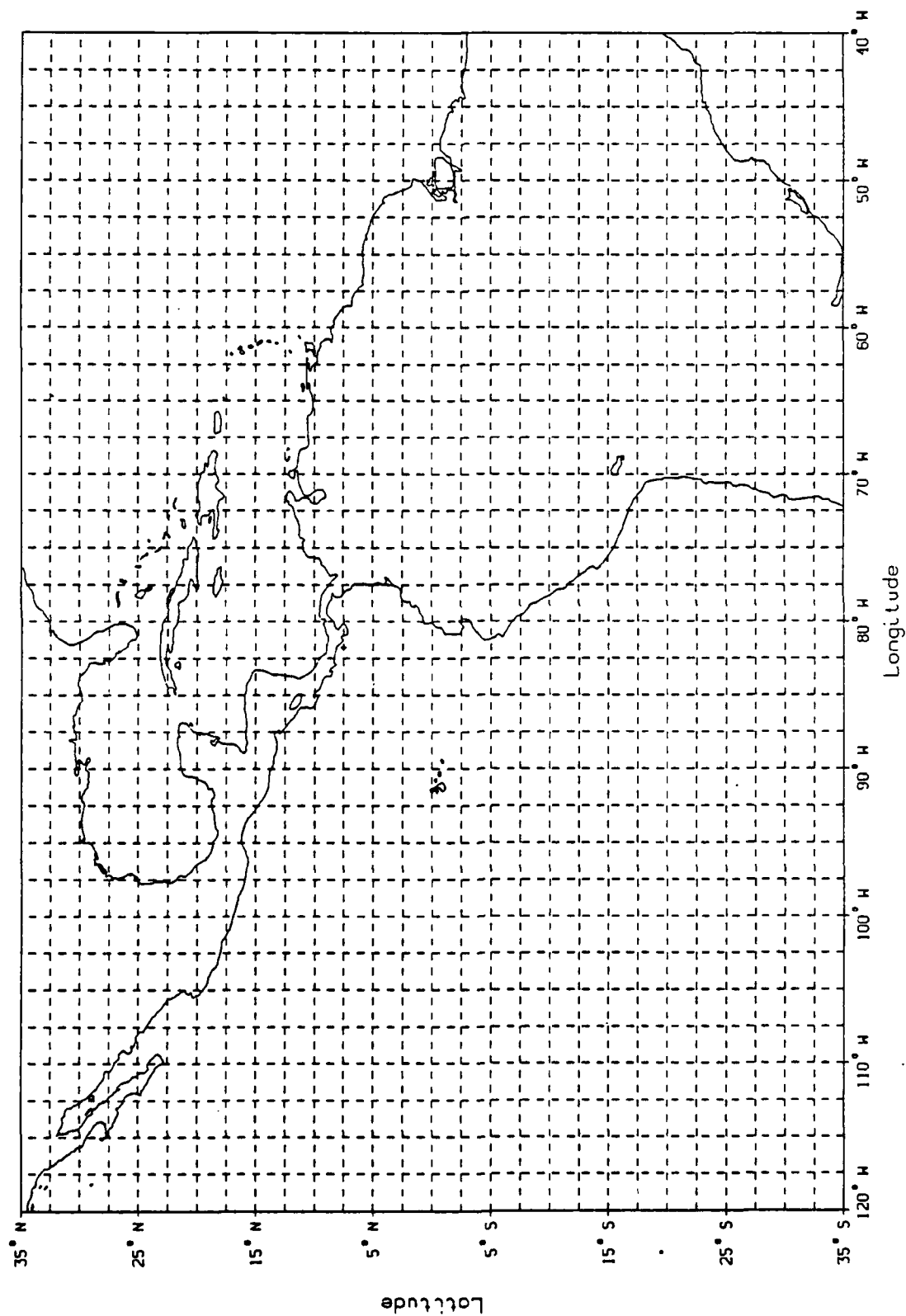


Figure 1. Domain of OLR data used in study. Dashed grid represents 2.5° latitude-longitude OLR data spacing.



## Rainfall

Rainfall data for 1984 and 1985 were provided by the Meteorology and Hydrology Branch of the Panama Canal Commission. Their network of 26 automated raingauges provides a complete coverage of rainfall within the Panama Canal region. The exact locations of these raingauges are shown in Fig. 3. For this study, daily rainfall totals from each raingauge site were summed to provide one daily rainfall total for the entire Canal region. Analysis of this time series of daily rainfall totals is discussed in Chapter VI.

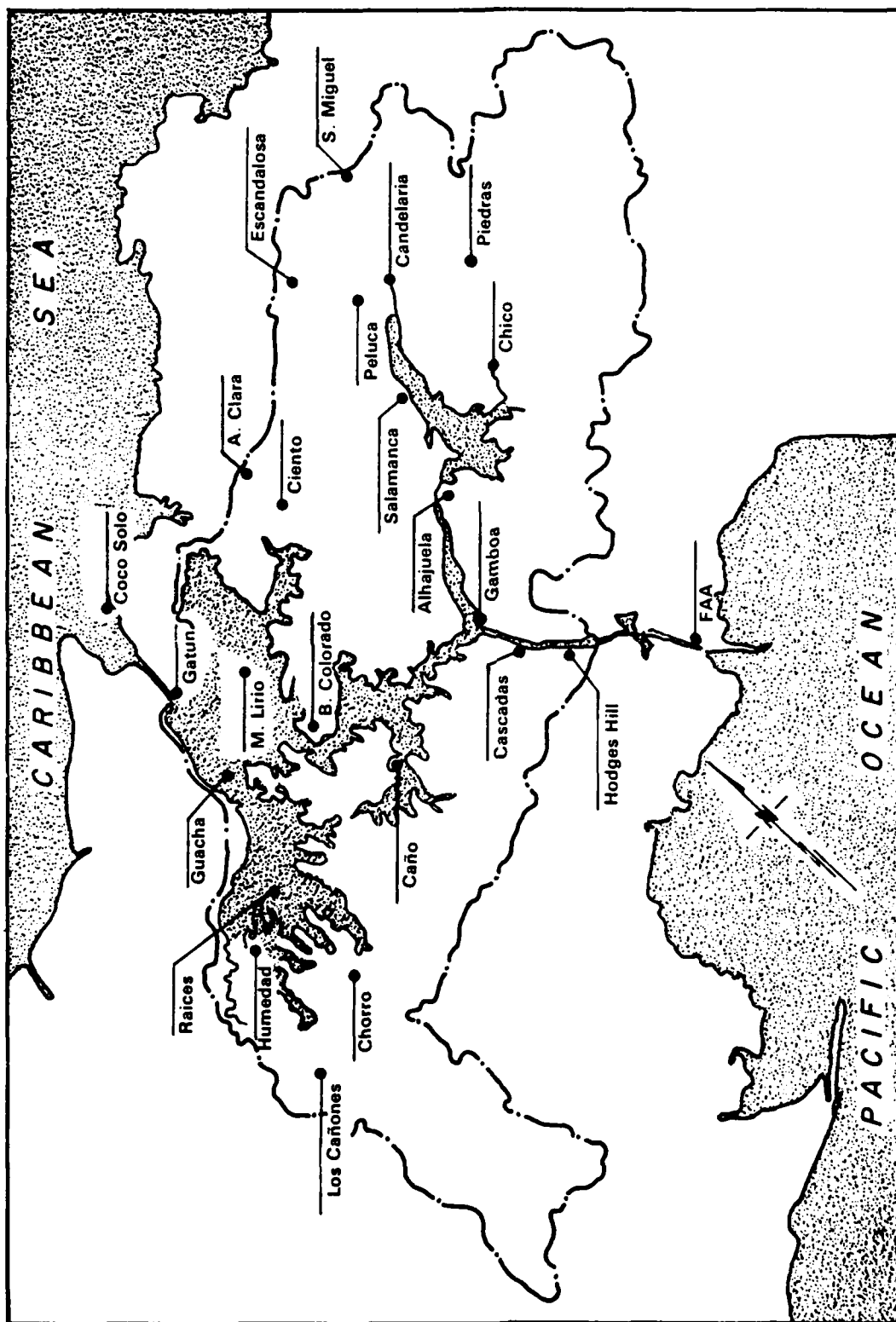


Figure 3. Location of Panama Canal Commission rain gauges across the Panama Canal and Gatun Lake (adapted from Daily Rainfall Map, Panama Canal Commission).

## CHAPTER V

### DETERMINATION OF PERIODIC MODES OF CONVECTIVE ACTIVITY

#### Selection of Area of Study

Periodic fluctuations in an area's OLR time series are easier to detect if an area has relatively small average annual OLR values, indicating that large amounts of cloud cover are present throughout the year. Average OLR values of the domain for the period 1 January 1984 through 31 December 1985 are shown in Fig. 4. These average OLR values were calculated for each  $2.5^\circ$  latitude-longitude grid point using both the 0230 and 1430 LST observations. Note the relative OLR minima extending from central Mexico southeastward through Central America. The lowest OLR values in all of Central America, as well as some of the lowest OLR values in the entire domain, are found in the Panama area, especially in the eastern portions of the country. Also note the relatively low OLR values associated with the trade wind/monsoon trough beginning at  $10^\circ\text{N}$ ,  $120^\circ\text{W}$  and extending eastward into extreme eastern portions of Colombia.

In addition to having low average OLR values, an important criterion in selecting an area of study is the total variance of OLR. If a region is cloudy all year but has little or no fluctuations in the cloud cover, an analysis of that OLR time

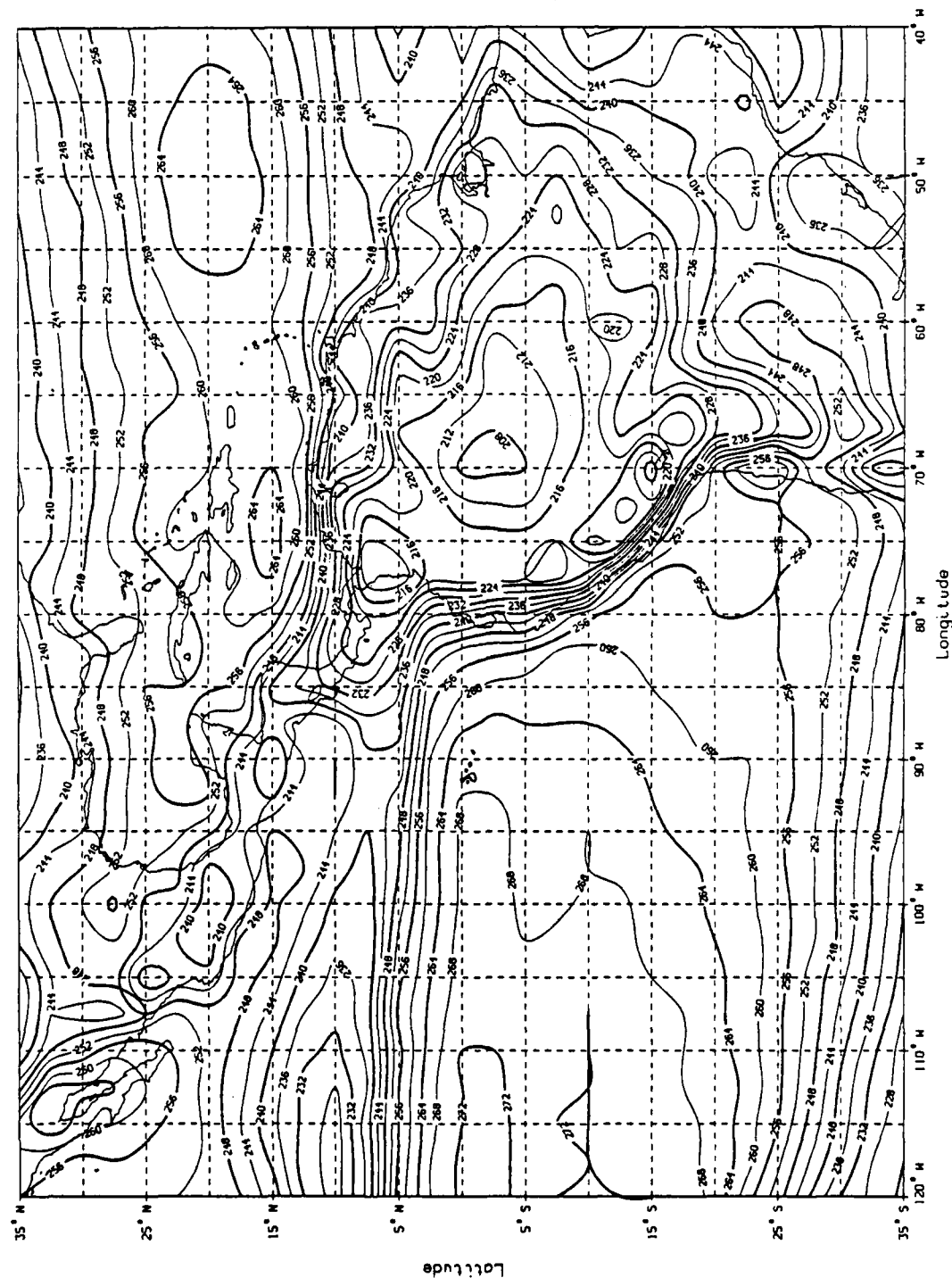


Figure 4. Average OLR for the period 1 January 1984 through 31 December 1985. Contoured values are in units  $Wm^{-2}$ .

series would not detect any significant periodicities. The variance was calculated for each grid point in the domain for the same 2-y period using the formula

$$s^2 = \sum_{i=1}^n (Y_i - \bar{Y})^2 / (n - 1) \quad (5)$$

where  $Y_i$  represents the daily averages of the 0230 and 1430 LST observations,  $\bar{Y}$  is the 2-y average OLR for that point, and  $n$  equals the total number of daily average OLR values over the 2-y period, which was 731. In these calculations the average of the two daily OLR observations was used to eliminate any variance resulting from the diurnal cycle. The total variance for the domain is shown in Fig. 5. It can be seen that the highest total variance in the entire domain is a 2000 ( $\text{Wm}^{-2}$ )<sup>2</sup> contour located just to the southwest of Panama City. In addition, the entire country of Panama, as well as the surrounding area, has some of the highest OLR variance values in the domain. This combination of low average OLR values and maximum OLR variance should make the Panama area daily OLR values favorable for time series analysis.

The exact boundaries of the area of study must now be specified. They must be broad enough to be representative of the region as a whole, but small enough so that the changes in the OLR field that could be associated with synoptic-scale features are not averaged out. Figure 6 shows the portion of the domain selected for analysis, with the boundaries extending from 5°-12.5°N and 85°-75°W. These boundaries were selected on the basis of the average OLR values and total OLR variance as shown in Figs. 4 and 5, as well as the fact that this area is subject to the influence of large-scale effects such as northward migrations of the monsoon trough, the passage of

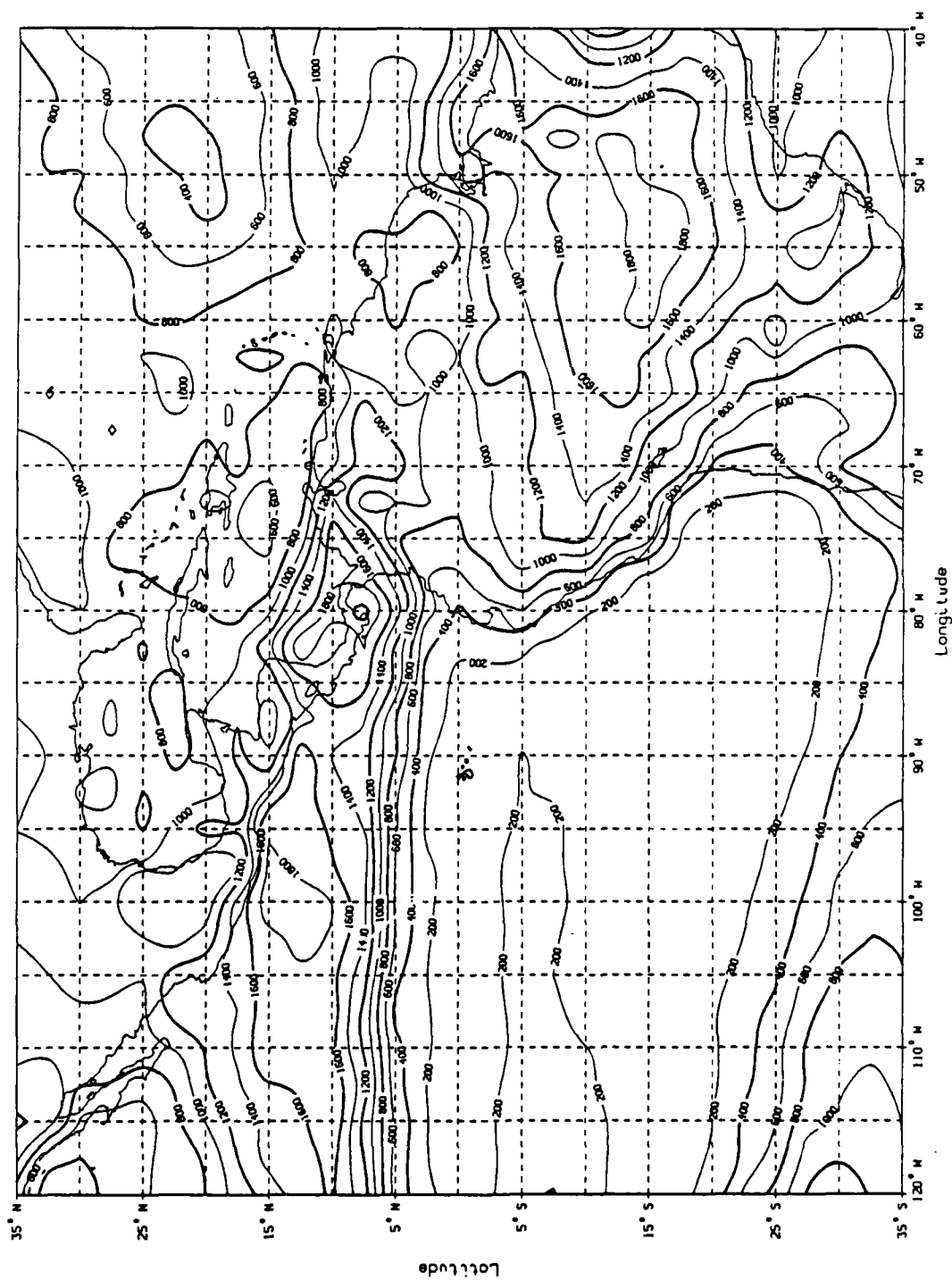


Figure 5. OLR variance for the period 1 January 1984 through 31 December 1985. Contoured values are in units of  $(Wm^{-2})^2$ .



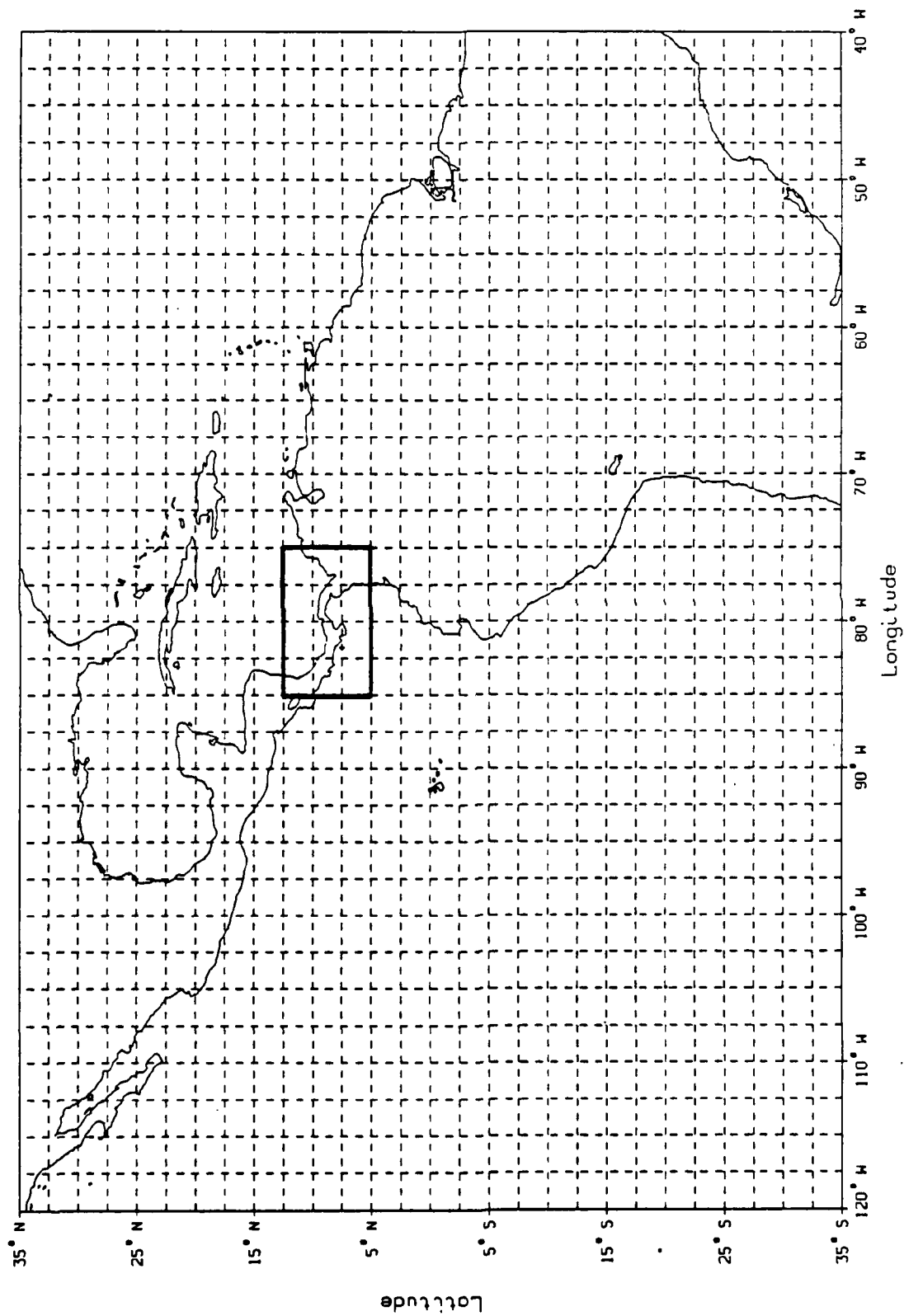


Figure 6. Subset of domain selected as index reference.

waves in the easterlies, and the occasional southward advance of shear lines towards the Panama area.

### Methods of Analysis

There are 20 OLR grid points contained in the area of study shown in Fig. 6. A single daily OLR value was calculated for the area of study by taking the average of the 20 0230 LST and the 20 1430 LST OLR point values. A study of the area-averaged OLR as opposed to a single grid point greatly reduces the noise in the OLR time series, allowing a differentiation between local and large-scale effects. These area-averaged daily OLR values comprise the OLR time series for the Panama area and will be used in the time series analysis. Plots of these time series of daily OLR averages for 1984 and 1985 are shown in Figs. 7 and 8.

### Division of Data into Dry and Wet Seasons

The next step in preparing the data for analysis is to recognize that the conditions in the Panama area are not constant throughout the year but are divided into dry and wet seasons. Several studies over the past 20 y have concerned themselves with detecting periodicities in tropical variables and have chosen not to deal with these two seasons separately. This would not be an appropriate method of study for the Panama area since the two seasons are so distinctly different in terms of cloud cover and precipitation as well as the upper-level wind patterns associated with these features. A periodicity that is detected in both the dry and wet seasons could be the reflection of two completely different synoptic or local conditions depending

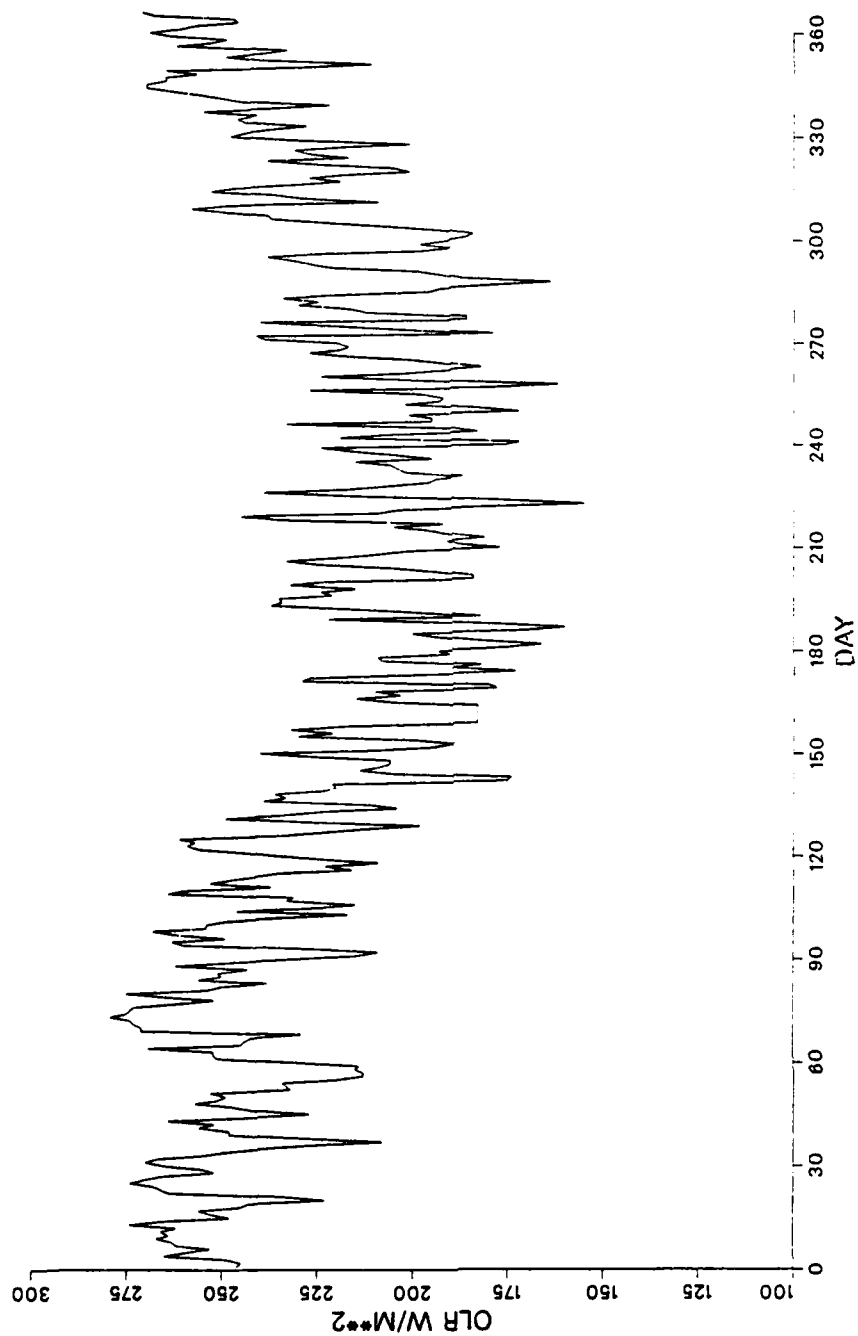


Figure 7. Time series of daily average OLR for area 5-12°N, 75-85°W for 1984.

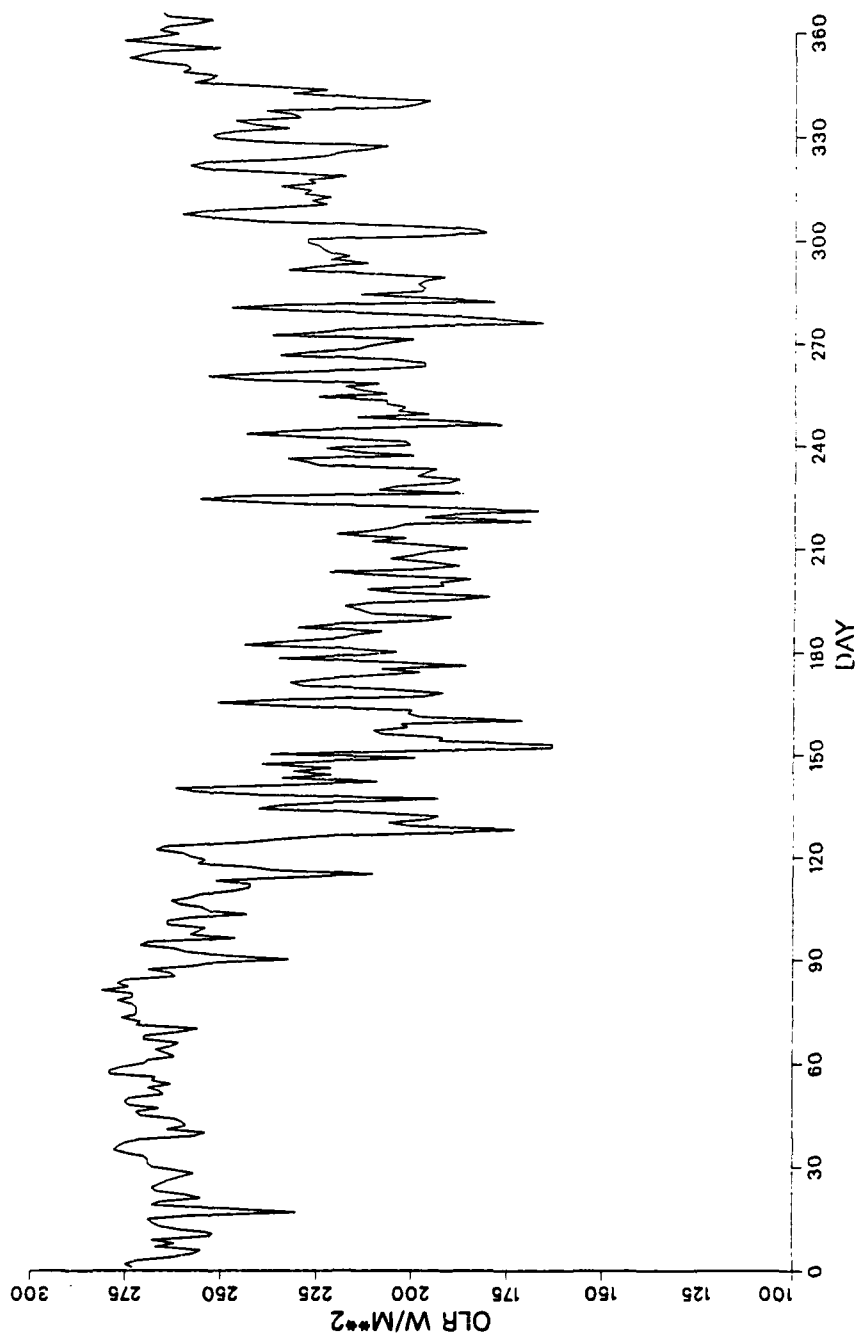


Figure 8. Time series of daily average OLR for area 5-12°N, 75-85°W for 1985.

on the time of the year. For this reason, the 2-y period has been divided into dry and wet seasons through the subjective analysis of raw OLR values as well as daily precipitation totals. Both time series show distinct delineations between the two seasons, which are as follows:

- Dry season 1984: 1 January–9 May (130 days)
- Wet season 1984: 10 May–4 December (209 days)
- Dry season 1985: 5 December 1984–2 May 1985 (149 days)
- Wet season 1985: 3 May–8 December (220 days).

#### Removal of Seasonal Trends

Although a distinct discontinuity in the raw OLR and precipitation data marks each change of season, a long-period seasonal trend is clearly visible in each season. This can be seen in the OLR time series shown in Figs. 7 and 8. In preparing each season's OLR time series for spectral analysis, Chatfield (1980) recommends removing any obvious long-period seasonal trends from the time series so that this trend does not detract from the power of any higher-frequency oscillations. To eliminate these seasonal trends, a 2nd degree polynomial trend remover method was used, as described by Neiswanger (1948). This method fits the data to a polynomial curve, with the fitted function providing a measure of the trend. The residuals about this fitted curve provide an estimate of local fluctuations which are independent from the long-period trend. These fluctuations about the fitted curve (which has been

set to zero) for each season's OLR time series are shown in Figs. 9, 10, 11, and 12. Note that the broad curves associated with seasonal trends in the OLR time series of Figs. 7 and 8 have been removed and the daily OLR values are now represented as deviations about the fitted curves. These four OLR time series are now ready for time series analysis.

### Time Series Analysis

The method used to determine whether any significant periodicities were present in the OLR time series was harmonic analysis, which is the process of decomposing a time record into the sum of sinusoids of various frequencies and amplitudes. The idea behind harmonic analysis is that a complicated time series can be understood by breaking it up into these simple frequency components and studying them separately. A detailed discussion of harmonic analysis is provided by Panofsky and Brier (1968). One type of harmonic analysis which is used to decompose this OLR time series into its sine and cosine components is the fast Fourier transform (FFT) method. The International Mathematical and Statistical Library (IMSL) User's Manual describes the FFT method and provides a computer routine that uses the FFT method to perform a periodogram analysis. This periodogram analysis calculates the sum of the squared amplitudes of the sinusoids, or spectral density, for each frequency. The IMSL periodogram analysis was done for the box-averaged OLR time series of each season, with the results shown in Figs. 13 and 14.

As seen in Fig. 13, dry season 1984 shows a spectral peak at around 65 d, but the largest spectral peak for this season is concentrated in the 11-12 d range.

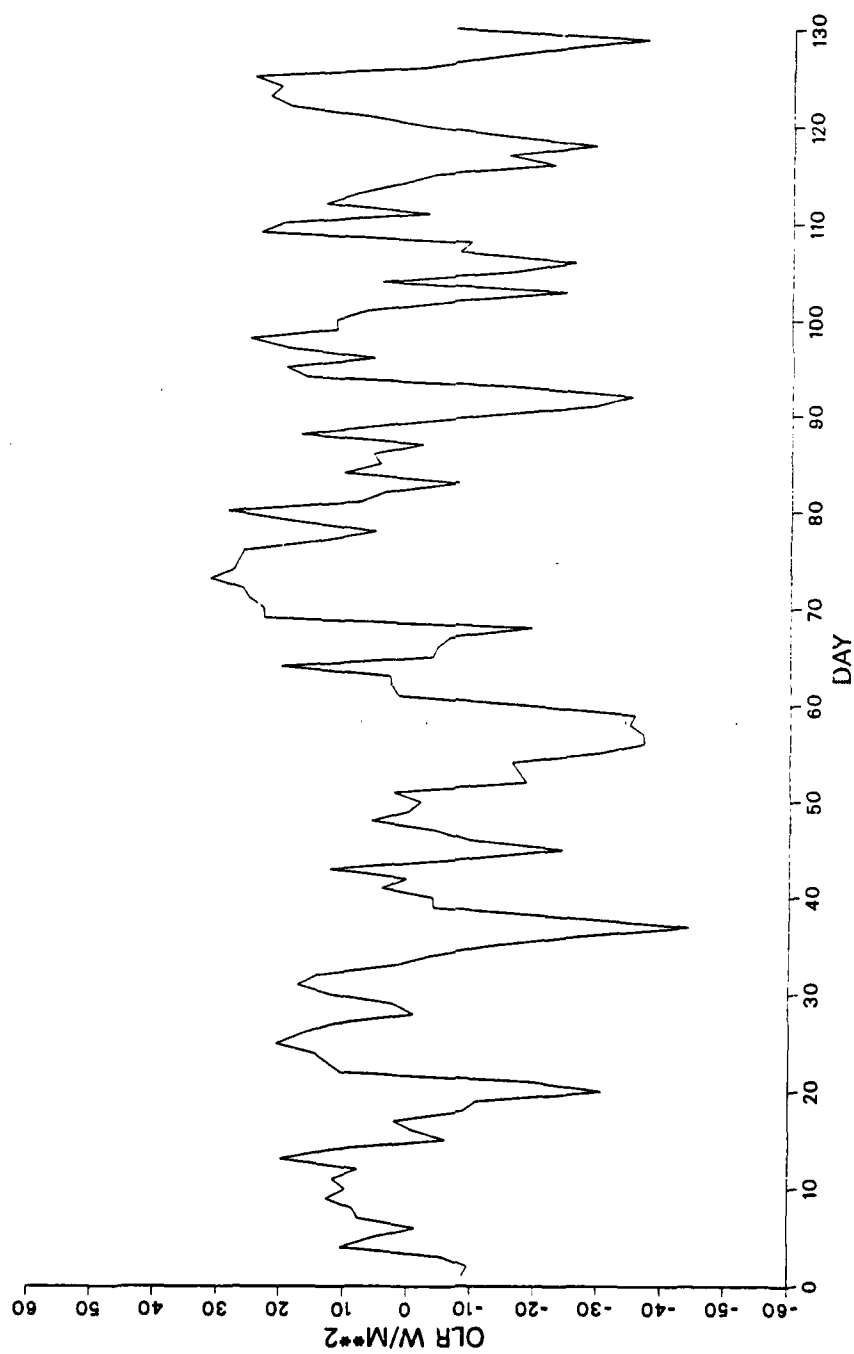


Figure 9. Trend-removed daily OLR for dry season 1984.

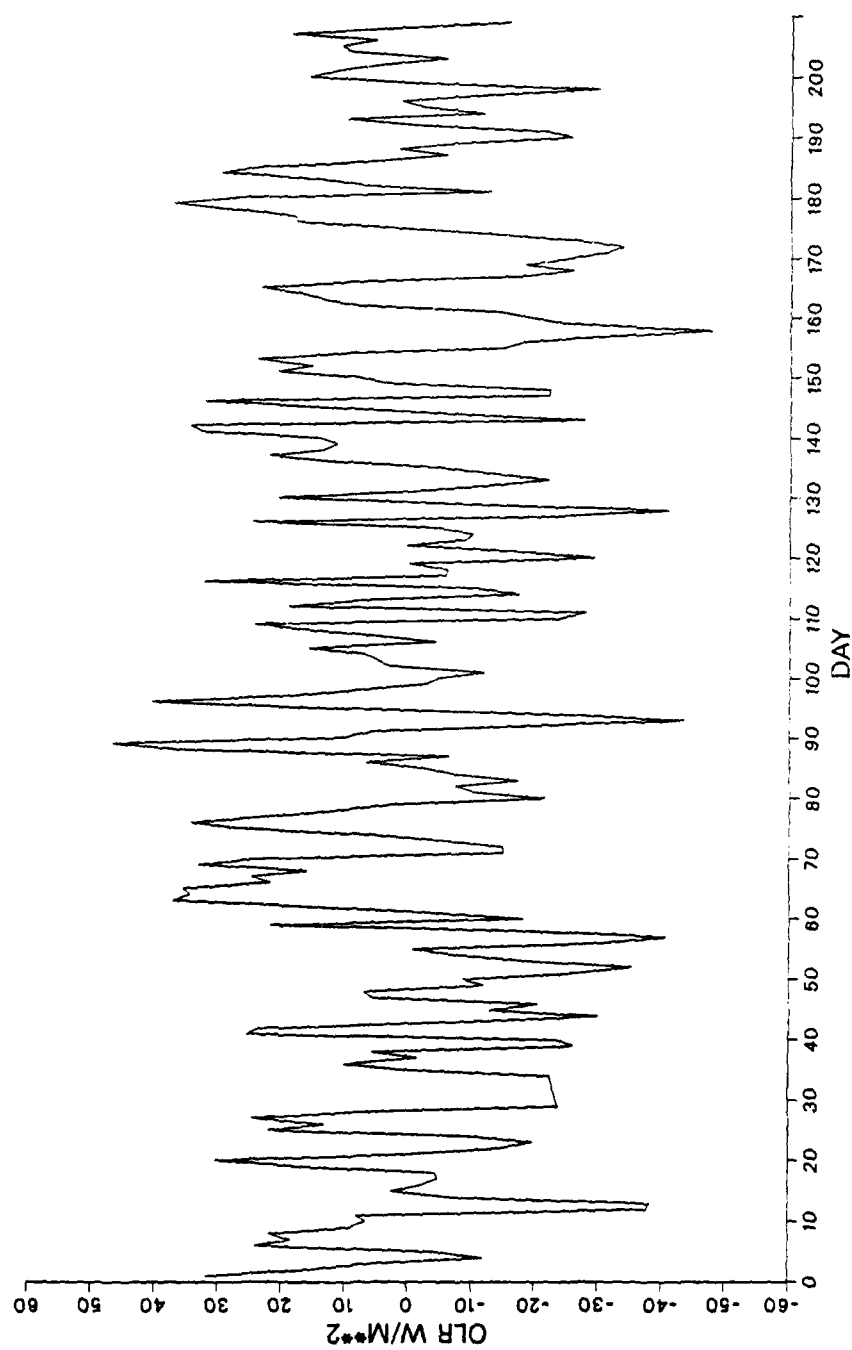


Figure 10. Trend-removed daily OLR for wet season 1984.



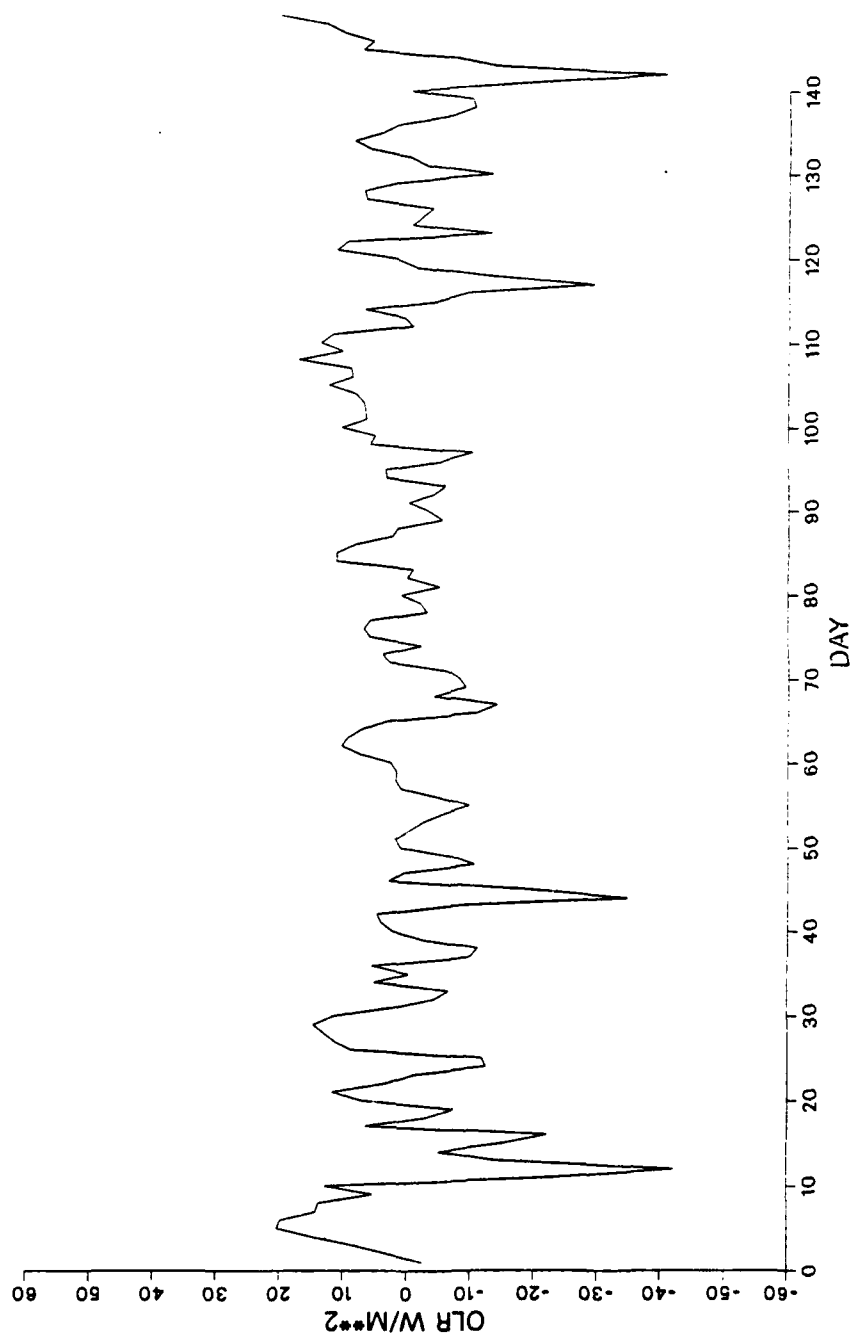


Figure 11. Trend-removed daily OLR for dry season 1985.

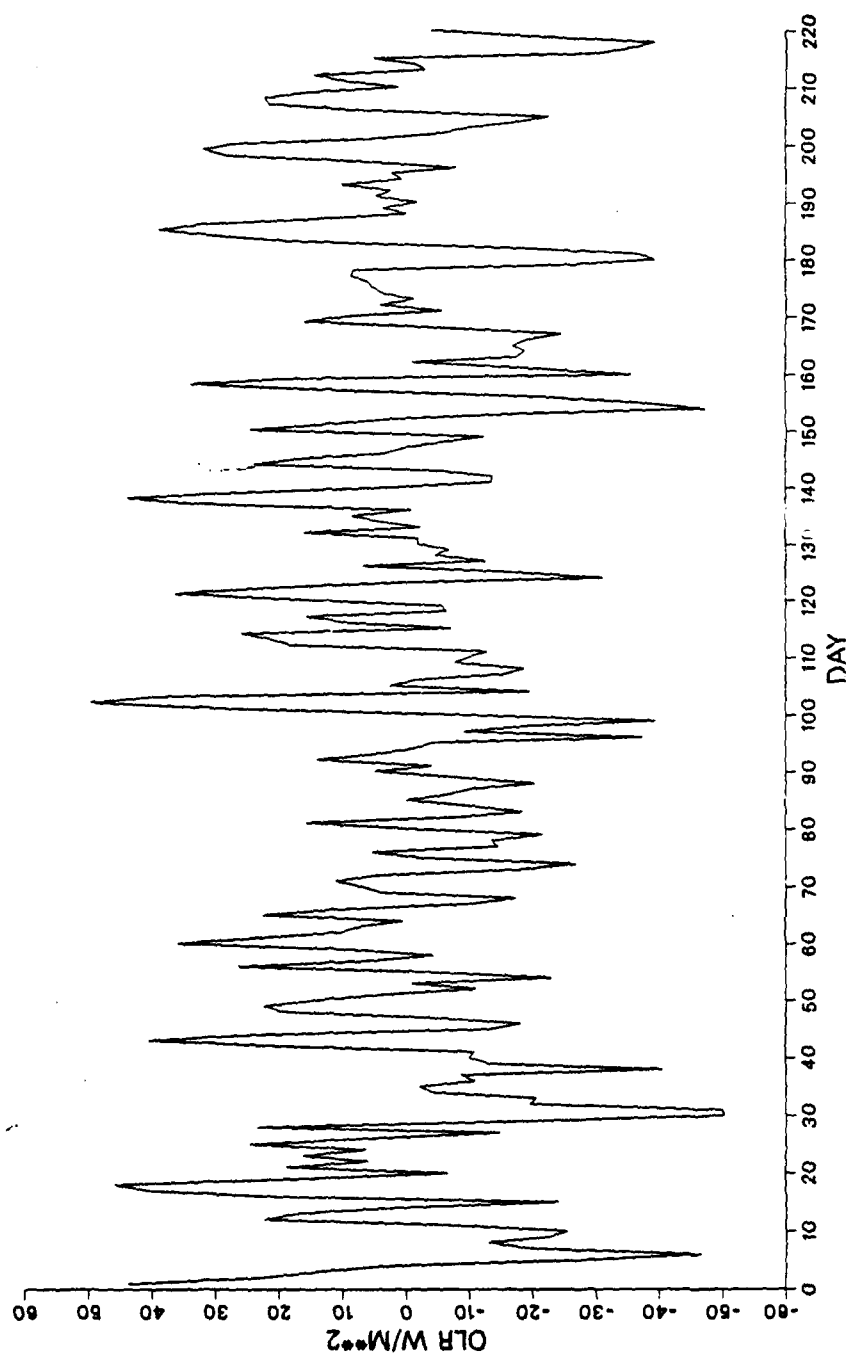


Figure 12. Trend-removed daily OLR for wet season 1985.

## PERIODOGRAM ANALYSIS - DRY SEASON 1984

Freq. w(k)	Period	I(w(k))
0.0000	.....	0.
0.0039	259.00	28.
0.0077	129.50	940.
0.0116	86.33	3607.
0.0154	64.75	4440.
0.0193	51.80	3136.
0.0232	43.17	2172.
0.0270	37.00	1884.
0.0309	32.38	1708.
0.0347	28.78	1326.
0.0386	25.90	1516.
0.0425	23.55	2780.
0.0463	21.58	1918.
0.0502	19.92	1078.
0.0541	18.50	2307.
0.0579	17.27	1855.
0.0618	16.19	2065.
0.0656	15.24	264.
0.0695	14.39	1341.
0.0734	13.63	1606.
0.0772	12.95	2313.
0.0811	12.33	5508.
0.0849	11.77	4753.
0.0888	11.26	1778.
0.0927	10.79	30.
0.0965	10.36	918.
0.1004	9.96	1796.
0.1042	9.59	419.
0.1081	9.25	1976.
0.1120	8.93	2286.
0.1158	8.63	67.
0.1197	8.35	862.
0.1236	8.09	872.
0.1274	7.85	1205.
0.1313	7.62	1536.
0.1351	7.40	391.
0.1390	7.19	114.
0.1429	7.00	467.
0.1467	6.82	101.
0.1506	6.64	55.
0.1544	6.47	254.
0.1583	6.32	327.
0.1622	6.17	13.

## PERIODOGRAM ANALYSIS - WET SEASON 1984

Freq. w(k)	Period	I(w(k))
0.0000	.....	0.
0.0024	417.00	1.
0.0048	208.50	139.
0.0072	139.00	1121.
0.0096	104.25	1963.
0.0120	83.40	1527.
0.0144	69.50	2399.
0.0168	59.57	2196.
0.0192	52.13	301.
0.0216	46.33	367.
0.0240	41.70	2019.
0.0264	37.91	4806.
0.0288	34.75	4337.
0.0312	32.08	326.
0.0336	29.79	995.
0.0360	27.80	1454.
0.0384	26.06	271.
0.0408	24.53	620.
0.0432	23.17	4243.
0.0456	21.95	2401.
0.0480	20.85	685.
0.0504	19.86	4794.
0.0528	18.95	1275.
0.0552	18.13	572.
0.0576	17.38	1207.
0.0600	16.68	118.
0.0624	16.04	936.
0.0647	15.44	382.
0.0671	14.89	1309.
0.0695	14.38	3082.
0.0719	13.90	1118.
0.0743	13.45	786.
0.0767	13.03	4061.
0.0791	12.64	5668.
0.0815	12.26	3602.
0.0839	11.91	425.
0.0863	11.58	641.
0.0887	11.27	2848.
0.0911	10.97	2575.
0.0935	10.69	1328.
0.0959	10.42	997.
0.0983	10.17	536.
0.1007	9.93	3981.
0.1031	9.70	4485.
0.1055	9.48	790.
0.1079	9.27	5.
0.1103	9.07	661.
0.1127	8.87	2529.
0.1151	8.69	1303.
0.1175	8.51	485.
0.1199	8.34	348.
0.1223	8.18	411.
0.1247	8.02	2553.
0.1271	7.87	1113.
0.1295	7.72	166.
0.1319	7.58	715.
0.1343	7.45	236.
0.1367	7.32	311.
0.1391	7.19	240.
0.1415	7.07	545.
0.1439	6.95	3918.
0.1463	6.84	5829.
0.1487	6.73	1978.
0.1511	6.62	533.
0.1535	6.52	111.
0.1559	6.42	121.
0.1583	6.32	322.
0.1607	6.22	669.
0.1631	6.13	197.
0.1655	6.04	23.

Figure 13. Numerical output from IMSL periodogram analysis for dry season and wet season 1984. Periods are in days,  $I(w(k))$  represents spectral density.

## PERIODOGRAM ANALYSIS - DRY SEASON 1985

Freq. $w(k)$	Period	$I(w(k))$
0.0000	.....	0.
0.0034	297.00	7.
0.0067	148.50	238.
0.0101	99.00	703.
0.0135	74.25	338.
0.0168	59.40	175.
0.0202	49.50	172.
0.0236	42.43	255.
0.0269	37.13	455.
0.0303	33.00	507.
0.0337	29.70	433.
0.0370	27.00	1076.
0.0404	24.75	2872.
0.0438	22.85	431.
0.0471	21.21	1282.
0.0505	19.80	718.
0.0539	18.56	361.
0.0572	17.47	617.
0.0606	16.50	199.
0.0640	15.63	255.
0.0673	14.85	485.
0.0707	14.14	1236.
0.0741	13.50	46.
0.0774	12.91	1246.
0.0808	12.38	341.
0.0842	11.88	1925.
0.0875	11.42	1174.
0.0909	11.00	749.
0.0943	10.61	1002.
0.0976	10.24	75.
0.1010	9.90	175.
0.1044	9.58	9.
0.1077	9.28	257.
0.1111	9.00	230.
0.1145	8.74	259.
0.1178	8.49	76.
0.1212	8.25	53.
0.1246	8.03	1.
0.1279	7.82	23.
0.1313	7.62	1.
0.1347	7.42	32.
0.1380	7.24	290.
0.1414	7.07	684.
0.1448	6.91	201.
0.1481	6.75	186.
0.1515	6.60	837.
0.1549	6.46	195.
0.1582	6.32	266.
0.1616	6.19	846.
0.1650	6.06	171.

## PERIODOGRAM ANALYSIS - WET SEASON 1985

Freq. $w(k)$	Period	$I(w(k))$
0.0000	.....	0.
0.0023	439.00	3.
0.0046	219.50	59.
0.0068	146.33	37.
0.0091	109.75	88.
0.0114	87.80	773.
0.0137	73.17	3250.
0.0159	62.71	4573.
0.0182	54.88	778.
0.0205	48.78	1243.
0.0228	43.90	3651.
0.0251	39.91	1288.
0.0273	36.58	1107.
0.0296	33.77	190.
0.0319	31.36	2336.
0.0342	29.27	2124.
0.0364	27.44	208.
0.0387	25.82	1248.
0.0410	24.39	3027.
0.0433	23.11	3614.
0.0456	21.95	634.
0.0478	20.90	3360.
0.0501	19.95	1080.
0.0524	19.09	2420.
0.0547	18.29	1246.
0.0569	17.56	1368.
0.0592	16.88	967.
0.0615	16.26	38.
0.0638	15.68	129.
0.0661	15.14	1390.
0.0683	14.63	650.
0.0706	14.16	2030.
0.0729	13.72	1584.
0.0752	13.30	3695.
0.0774	12.91	1844.
0.0797	12.54	2610.
0.0820	12.19	4622.
0.0843	11.86	1403.
0.0866	11.55	3609.
0.0888	11.26	1578.
0.0911	10.97	2377.
0.0934	10.71	1149.
0.0957	10.45	570.
0.0979	10.21	380.
0.1002	9.98	1006.
0.1025	9.76	1681.
0.1048	9.54	1629.
0.1071	9.34	2080.
0.1093	9.15	1878.
0.1116	8.96	836.
0.1139	8.78	1404.
0.1162	8.61	1004.
0.1185	8.44	1787.
0.1207	8.28	3326.
0.1230	8.13	366.
0.1253	7.98	2837.
0.1276	7.84	5245.
0.1298	7.70	98.
0.1321	7.57	2748.
0.1344	7.44	1629.
0.1367	7.32	320.
0.1390	7.20	2304.
0.1412	7.08	2765.
0.1435	6.97	1200.
0.1458	6.86	2104.
0.1481	6.75	2011.
0.1503	6.65	192.
0.1526	6.55	235.
0.1549	6.46	1516.
0.1572	6.36	2449.
0.1595	6.27	2043.
0.1617	6.18	1563.
0.1640	6.10	1790.
0.1663	6.01	1618.

Figure 14. Numerical output from IMSL periodogram analysis for dry season and wet season 1985. Periods are in days,  $I(w(k))$  represents spectral density.

On all of the analyses the spectral density begins to decrease rapidly below 6 d, so those portions of the analyses have been omitted. The periodogram analysis for wet season 1984 shows a spectral peak of approximately 35–40 d, which was not evident in the dry season. A spectral peak is also found at 6–7 d, however, another high concentration of spectral density in this season can again be found at around 12 d. The largest spectral peak in dry season 1985 is found at approximately 25 d, but another large peak is evident at 11–12 d. Finally, wet season 1985 shows a spectral peak in the 60–70 d range, but the strongest peak again appears to be located at roughly 11–12 d.

The periodogram analyses of Figs. 13 and 14 show there are several frequencies that display spectral peaks through the 2-y period, but by far the strongest and most consistent is found in the 12-d range. The next step is to apply a different analysis technique to the data to see if the results are consistent. Several additional techniques, as well as a comprehensive discussion on time series analysis, are presented by Newton (1988). One of the methods outlined in his book *TIMESLAB* is the correlogram. The correlogram is a plot of the autocorrelation coefficient ( $\rho(\nu)$ ) vs the lag period ( $\nu$ ). In other words, it is measuring the correlation of the data with themselves except “lagged” by a certain number of time units. This technique was applied to the OLR time series for each season and the results are shown in Figs. 15 and 16. Although the  $\rho(\nu)$  trace never exceeds the 95% confidence band, the correlogram for dry seasons 1984 and 1985 exhibit sinusoidal patterns with a periodicity in the time frame of around 12 d. The correlograms for both wet seasons indicate a weak 12-d periodicity, but not nearly as strong as the dry seasons.

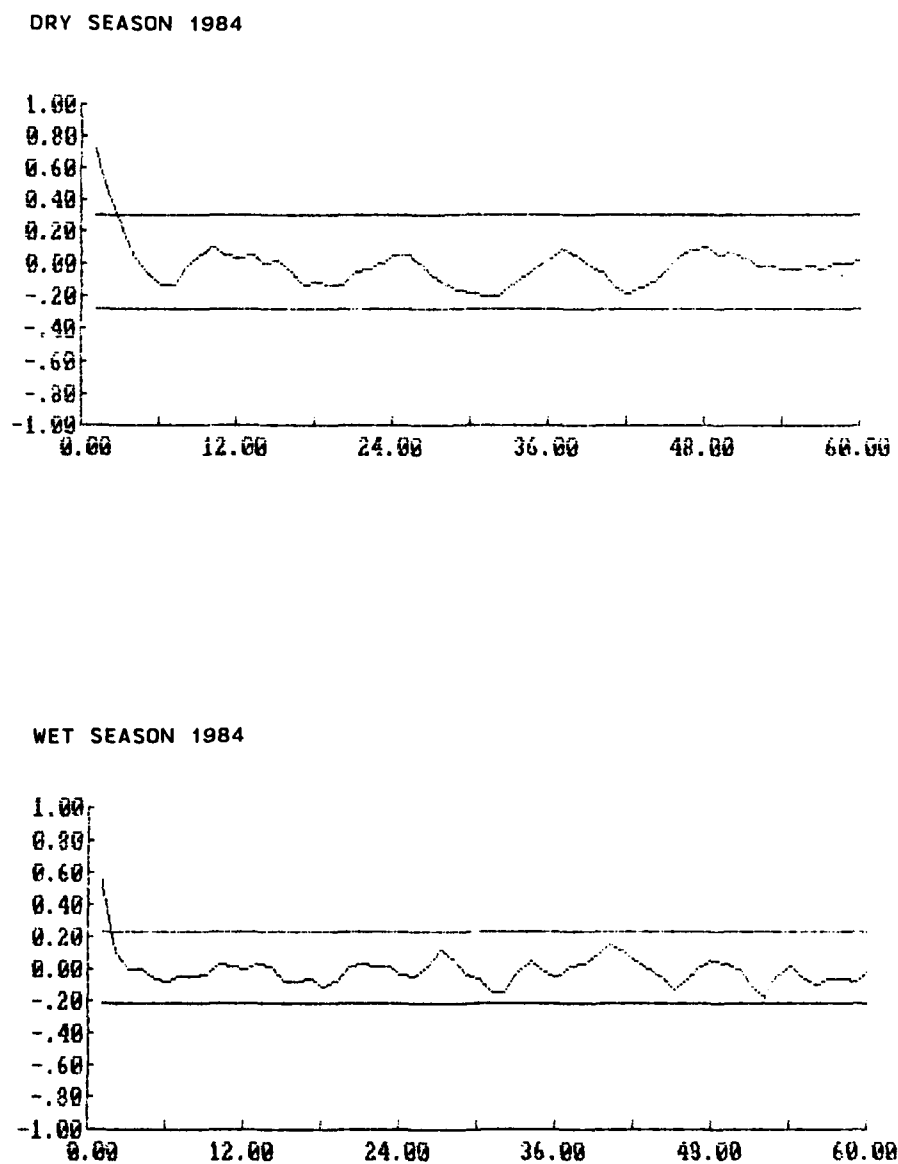


Figure 15. OLR correlograms and 95% confidence bands for 1984. Y axes represent autocorrelation coefficient ( $\rho(\nu)$ ), X axes represent lag period in days ( $\nu$ ).

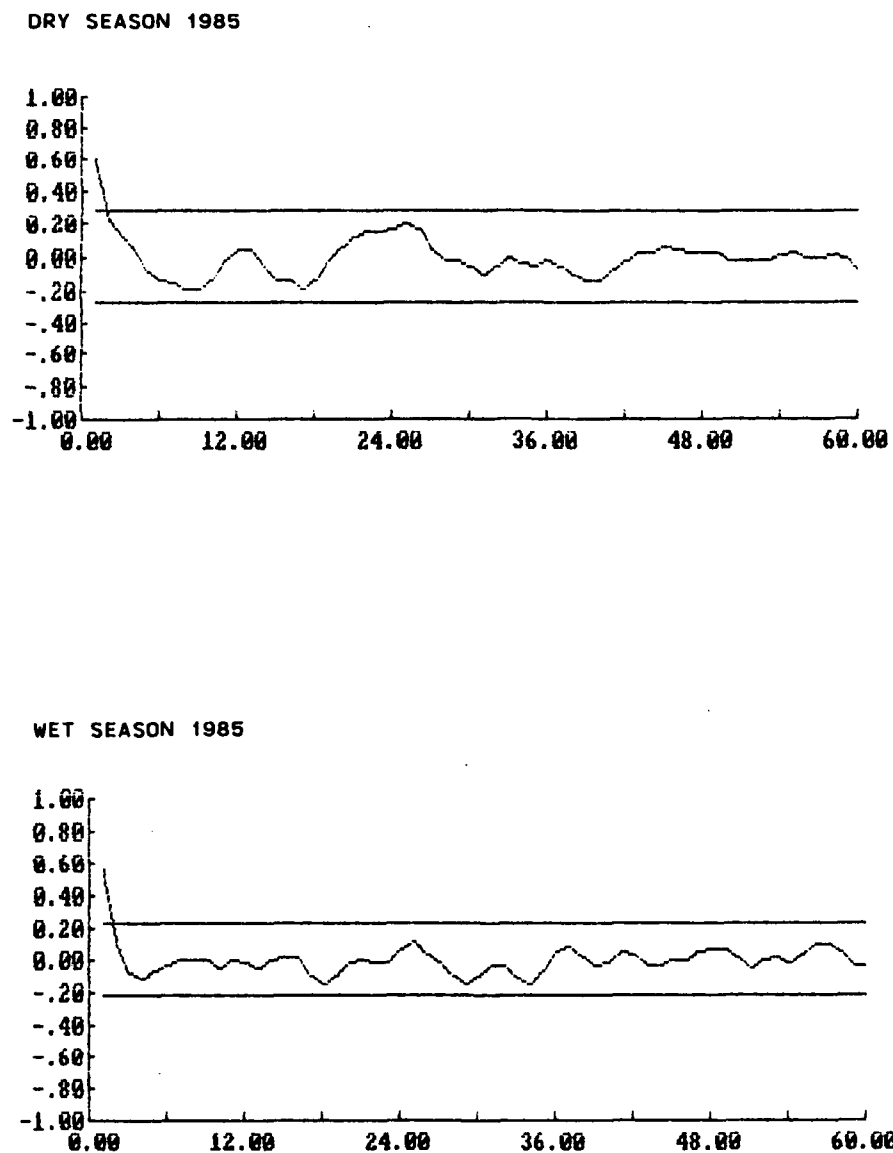


Figure 16. OLR correlograms and 95% confidence bands for 1985. Y axes represent autocorrelation coefficient ( $\rho(\nu)$ ), X axes represent lag period in days ( $\nu$ ).

In summary, the two time series analysis techniques used to determine any periodicities in the OLR time series were the IMSL periodogram and the TIMESLAB correlogram. Strong spectral power in the 12-d period was evident in all four seasons in the periodogram analysis, while the correlogram showed strong 12-d fluctuations in the dry seasons of both years with weaker 12-d fluctuations evident in the wet seasons. Other spectral peaks were present during some seasons but were not as strong or as persistent as the 12-d fluctuation.



## CHAPTER VI

### ANALYSIS OF DOMINANT MODE OF CONVECTIVE ACTIVITY OVER PANAMA

#### Examination of 12-Day Oscillation

Using the spectral analysis techniques described in Chapter V, the daily-averaged OLR time series over the Panama region have all shown spectral peaks of approximately 12 d. To determine the actual strength of this 12-d oscillation, a band-pass recursive filter developed by Shanks (1967) and used by Murakami (1980) was applied to the OLR time series of Figs. 9, 10, 11, and 12. This recursive filter computes each output point as a weighted sum of input points plus a weighted sum of previously computed output points. This filter allows us to set the periods where full (1.0) and lower (0.5) amplitude responses are desired. In this study the two periods chosen were 12 d (full response) and 9 d (0.5 response), which translate into frequencies (measured by  $2\pi/\text{period}$ )  $\omega_0$  and  $\omega_1$  respectively.

The filtered time series data at day  $n$  ( $\bar{f}_n$ ) were obtained from the unfiltered data,  $f_n$ , by

$$\bar{f}_n = a(f_n - f_{n-2}) - b_1\bar{f}_{n-1} - b_2\bar{f}_{n-2},$$

$$n = 1, 2, \dots, N, \tag{6}$$

where

$$a = \frac{2\Delta\Omega}{4 + 2\Delta\Omega + \Omega_0^2},$$

$$b_1 = \frac{2(\Omega_0^2 - 4)}{4 + 2\Delta\Omega + \Omega_0^2},$$

$$b_2 = \frac{4 - 2\Delta\Omega + \Omega_0^2}{4 + 2\Delta\Omega + \Omega_0^2}, \quad (7)$$

and

$$\Delta\Omega = 2 \left| \frac{\sin\omega_1}{1 + \cos\omega_1} - \frac{\sin\omega_2}{1 + \cos\omega_2} \right|,$$

$$\Omega_0^2 = \frac{4(\sin\omega_1)(\sin\omega_2)}{(1 + \cos\omega_1)(1 + \cos\omega_2)}. \quad (8)$$

The frequencies  $\omega_1$  and  $\omega_2$  in Eq. 8 are the frequencies at which we get 0.5 response on both sides of  $\omega_0$ . Recall we have already specified the 1.0 response frequency for 12 d ( $\omega_0$ ), and the 0.5 response frequency for 9 d ( $\omega_1$ ). To obtain the other 0.5 response frequency ( $\omega_2$ ) the following relationship is used:

$$\omega_2 = \omega_0^2/\omega_1. \quad (9)$$

The filtered data are obtained by first applying Eq. (6) to the original time series data (from which the mean and any linear trends have been removed) from  $n = 3$  to  $N$  by assuming that  $\bar{f}_1 = \bar{f}_2 = 0$  to obtain tentative mean values for  $\bar{f}_n$ . Then, using these tentative mean values, the process is reversed in time (from  $N - 2$  to  $n = 3$ ) to obtain the final  $\bar{f}_n$  values. A significant advantage to using this procedure is that it results in a zero phase shift for all frequencies.

The amplitude response ( $R_n$ ) for each frequency is given by

$$R_n = a(1 - z_n^2)/(1 + b_1 z_n + b_2 z_n^2), \quad (10)$$

where  $z_n = e^{-i(2\pi/n)}$ ,  $n$  = the period in days, and  $a$ ,  $b_1$ , and  $b_2$  are calculated from Eq. (7). The actual amplitude response curve of the 12-d filter used in this study for a length of  $n = 100$  d is shown in Fig. 17.

The plots of the 12-d filtered OLR time series for each season are shown in Figs. 18, 19, 20, and 21. Note that in all seasons significant amounts of the OLR deviations have been retained after filtering for 12 d. A quantitative measure of the strength of the signal can be found by comparing the standard deviations of the unfiltered and filtered time series. The variances for the unfiltered OLR time series of Figs. 9, 10, 11, and 12 have been calculated as 334.9, 497.3, 156.3, and 449.4  $(\text{Wm}^{-2})^2$ , respectively. In comparison, the 12-d filtered OLR time series of Figs. 18, 19, 20, and 21 have variances of 98.0, 118.8, 29.2, and 94.1  $(\text{Wm}^{-2})^2$ , so roughly 20–25% of the variance of the original OLR time series has been retained after filtering for 12 d. An examination of these diagrams shows that while this 12-d oscillation is evident in each season, it is strongest and most consistent during the 1984 dry and wet seasons. Of particular interest is the 1984 wet season filtered time series, which shows an apparent modulation of the 12-d oscillation occurring every 70–80 d. This feature will be addressed in Chapter VII.

### OLR Composite Diagrams

The majority of this research to this point has concentrated on detecting periodicities in the OLR field over the Panama region. Now that a 12-d oscillation has been found, the next step is to determine the spatial extent of that oscillation.

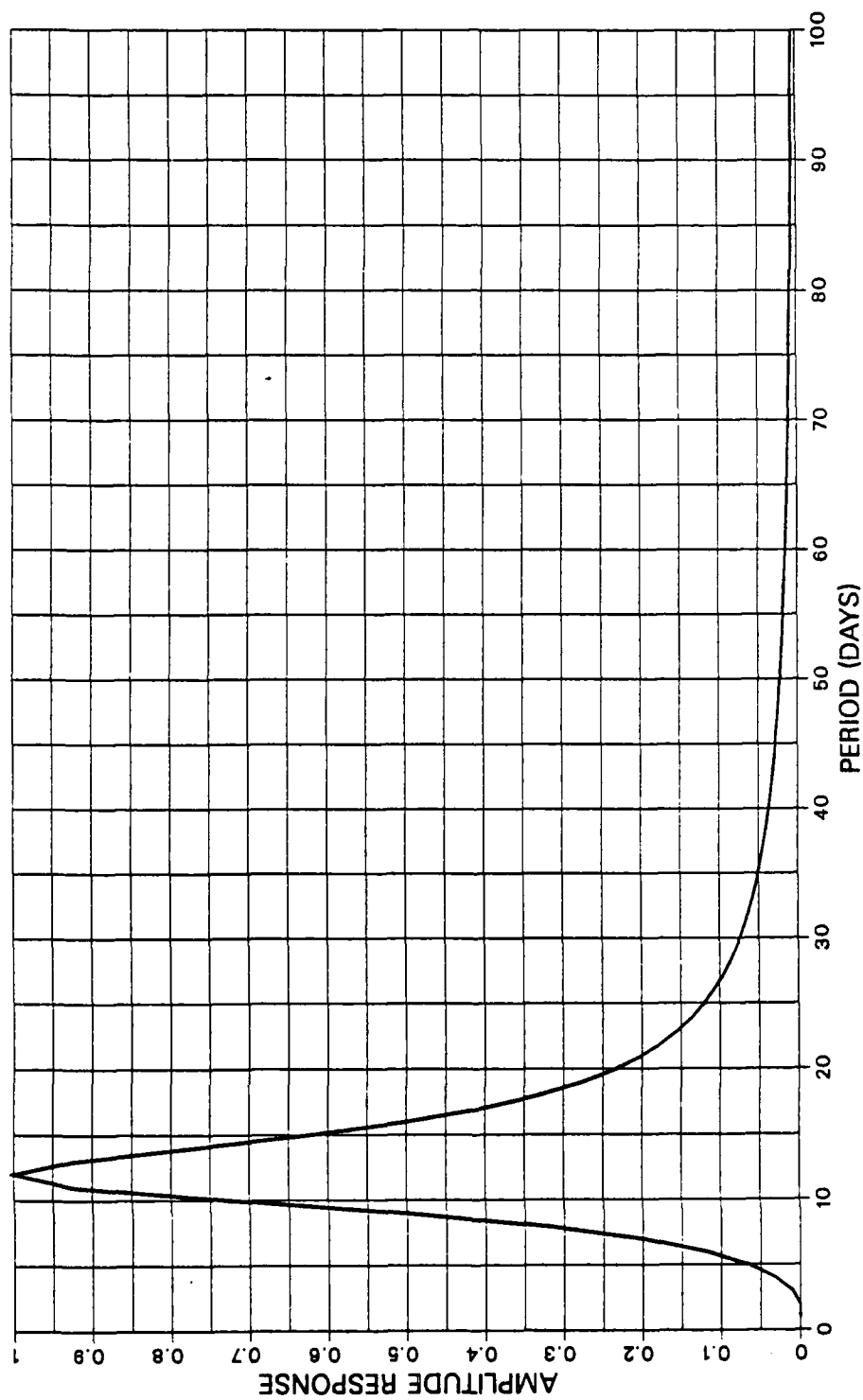


Figure 17. Amplitude response curve of 12-d filter.

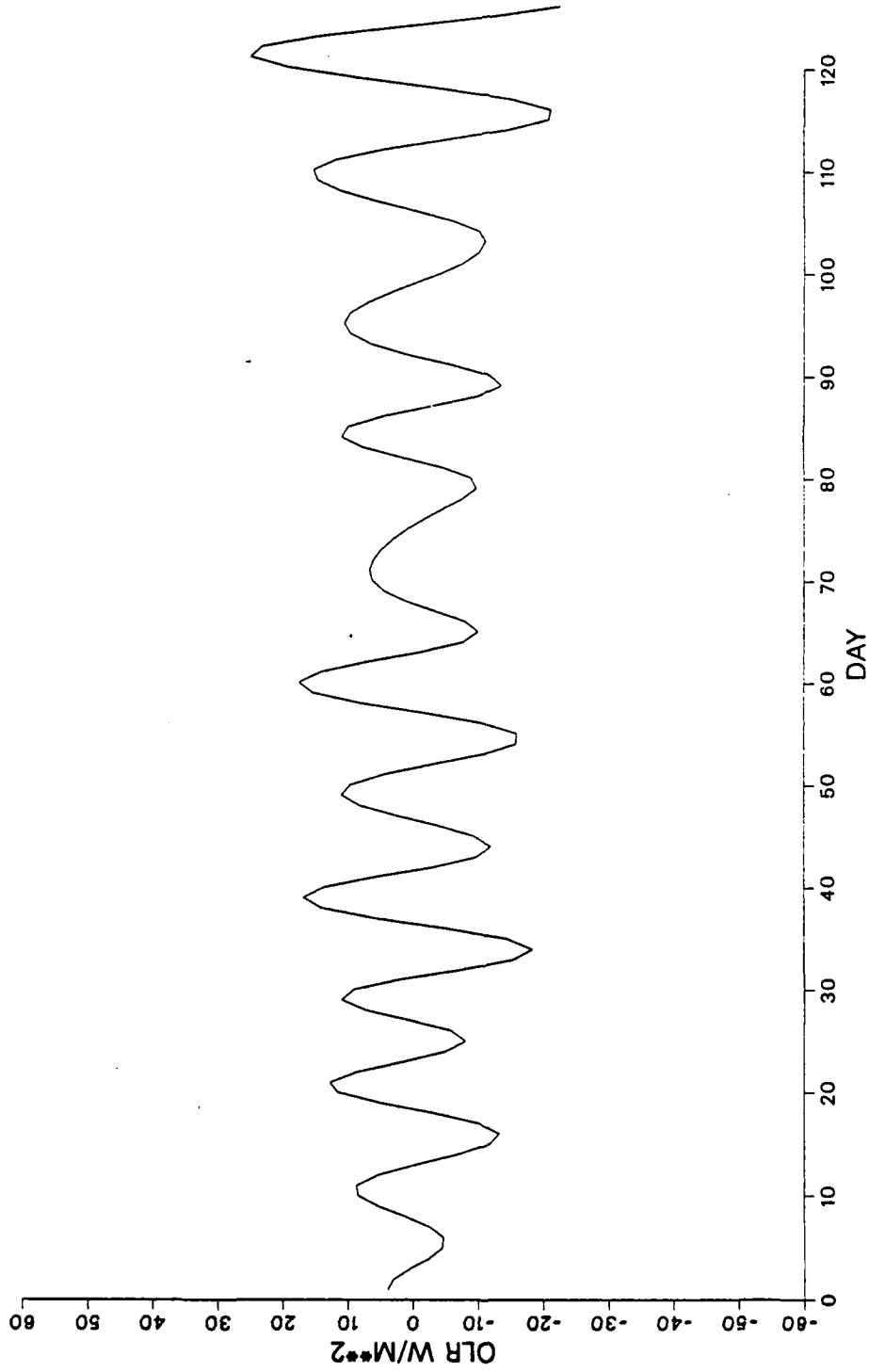


Figure 18. 12-d filtered OLR data for dry season 1984.

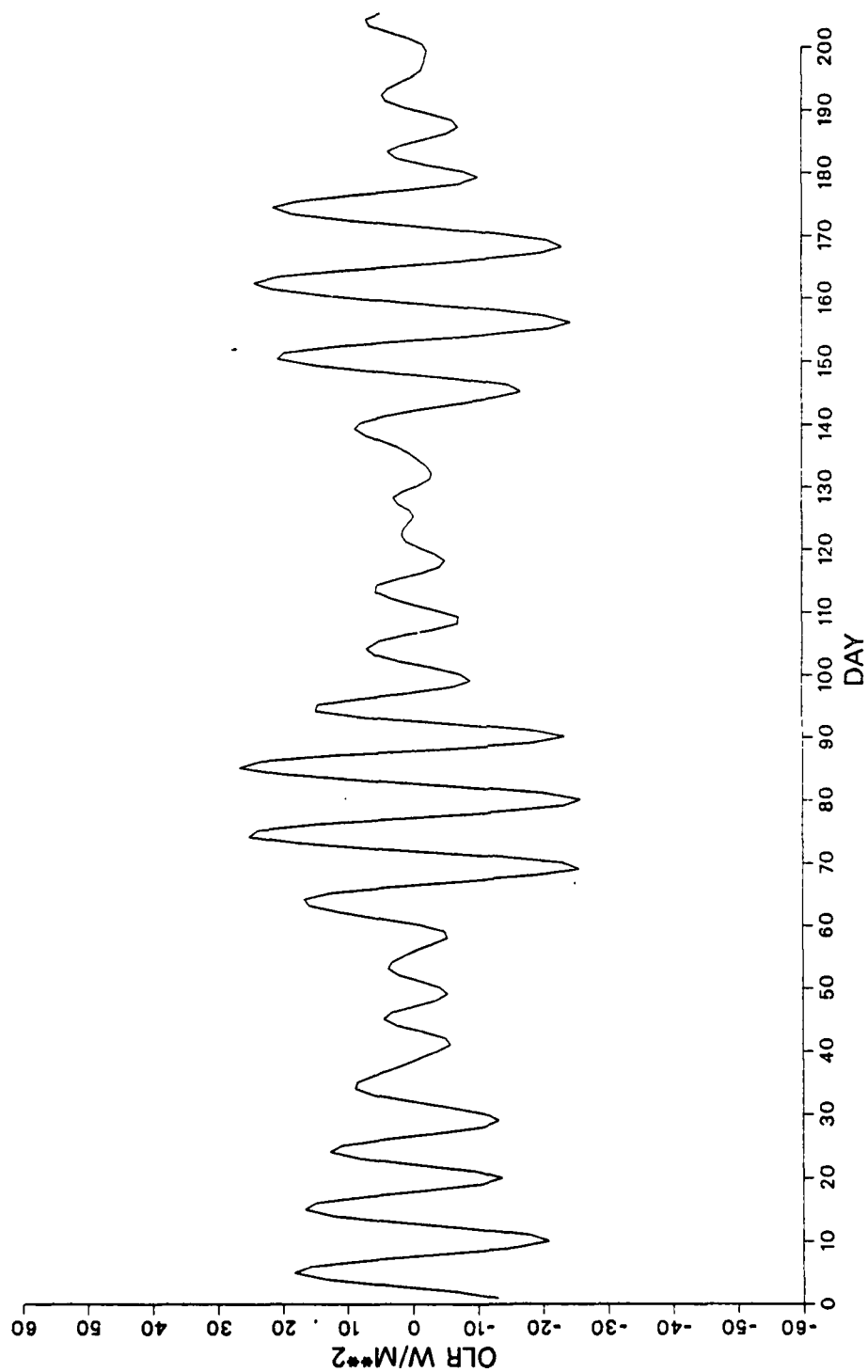


Figure 19. 12-d filtered OLR data for wet season 1984.

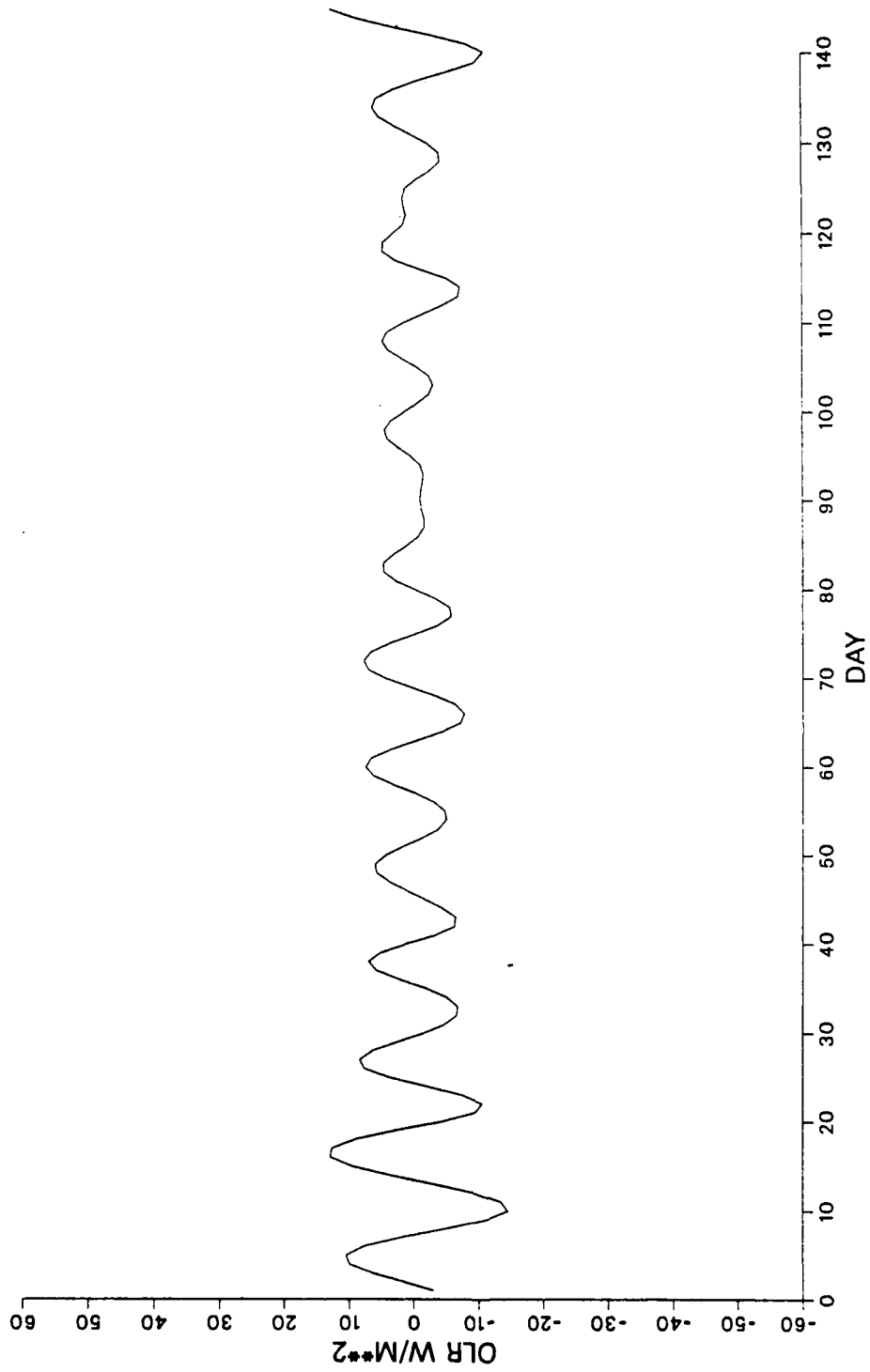


Figure 20. 12-d filtered OLR data for dry season 1985.

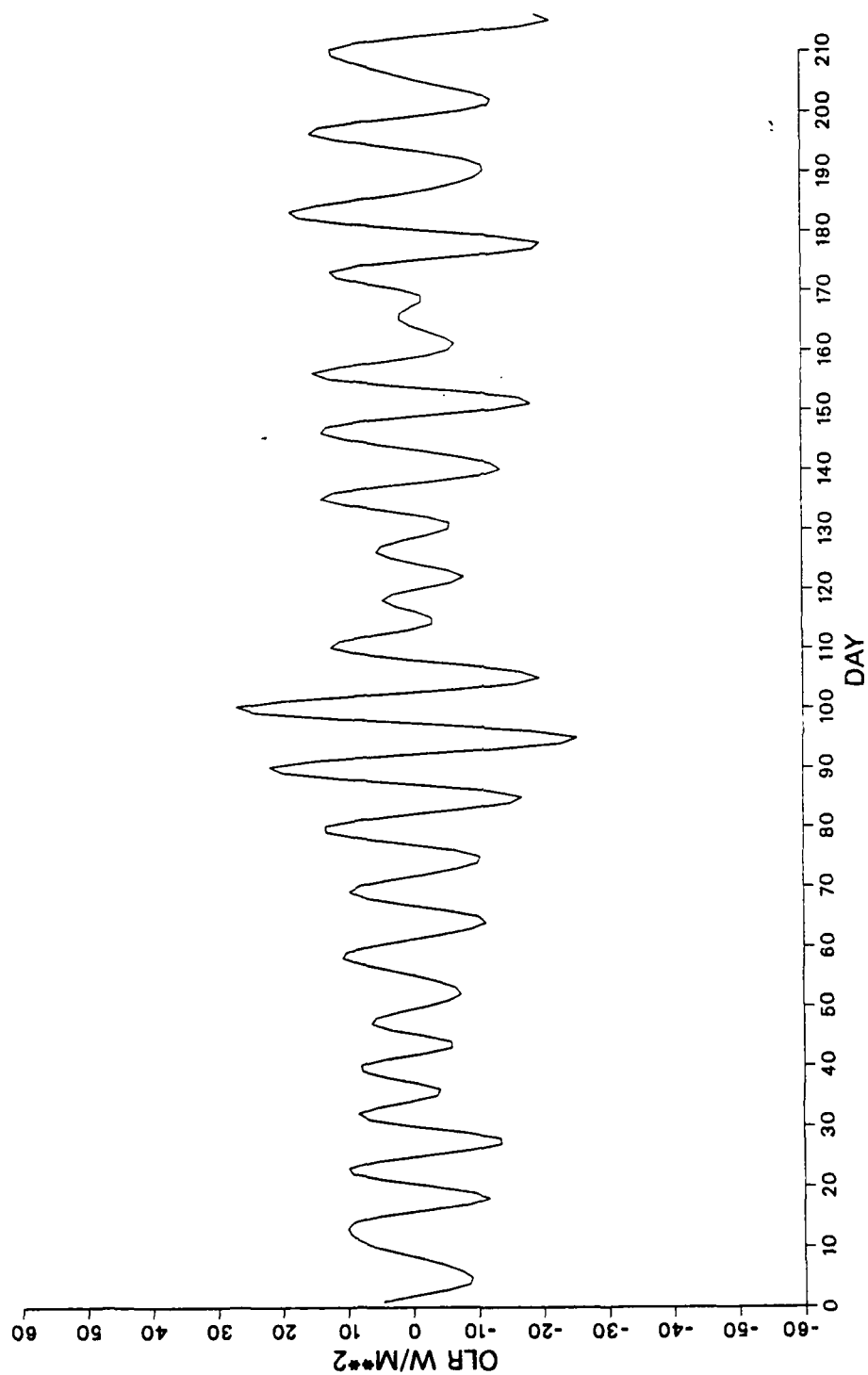


Figure 21. 12-d filtered OLR data for wet season 1985.



This was accomplished through the use of OLR composite diagrams, which were constructed as follows:

- The OLR time series of each  $2.5^\circ$  OLR grid point in the domain of Fig. 1 (957 total points) was divided into the same dry and wet seasons as the Panama area for 1984 and 1985.
- The seasonal mean and long-period trends were removed from the OLR seasonal time series at each point.
- The OLR time series for each point was filtered for 12 d in the same manner as the Panama area OLR time series.
- Cutoffs of  $\pm 1$  standard deviation were established for each of the 12-d filtered OLR time series shown in Figs. 18, 19, 20, and 21. For each season, any day in which the OLR deviation in the Panama area time series exceeded one standard deviation above the seasonal mean was considered a Maximum OLR day, or in other words, a relatively cloud-free day over the Panama area. For these same days, the corresponding OLR deviations from the 12-d filtered OLR time series for each point in the domain were collected and averaged. This produced average OLR deviations for each point in the domain corresponding to Maximum OLR days in Panama. By constructing this OLR composite diagram we can now determine whether conditions occurring over Panama with a periodicity of 12 d have any relationship with the rest of the domain. The same procedure was used to construct composite diagrams corresponding to Minimum OLR days (OLR deviations less than one standard deviation below the seasonal mean) over the Panama area.

- Composite diagrams were also constructed for the two inflection points found in the 12-d filtered time series. They correspond to the inflection point going from cloud-free to cloudy conditions (Max-to-Min) and going from cloudy to cloud-free conditions (Min-to-Max).

As was mentioned above, each individual point in the domain was filtered for 12 d without first performing a spectral analysis to determine if any spectral peaks existed in that period. The reasoning behind this procedure is that if no 12-d signal existed anywhere else in the domain, application of a 12-d filter to the OLR time series at each point would filter out all of the signal, resulting in time series that would show little or no OLR deviations. Any composite analysis using these time series would result in a diagram that would also show very small, if not zero, OLR anomalies. As will be seen in the next section, this was not the case.

Composite diagrams were constructed for both years, but since the 12-d oscillation was most evident in the 1984 OLR time series, only that year will be shown here.

#### Composite Diagrams for Dry Season 1984

The composite diagrams for dry season 1984 are shown in Figs. 22, 23, 24, and 25. Beginning the 12-d cycle with the Maximum OLR composite (Fig. 22), a large area of maximum OLR deviations implying relatively clear conditions can be seen through most of Central America extending to the west, along a latitude band of about  $2^{\circ}$ – $3^{\circ}$ N. A broad area of negative OLR anomalies, representing more cloud cover than usual, is centered at  $7^{\circ}$ N,  $105^{\circ}$ W, extending beyond the domain to the

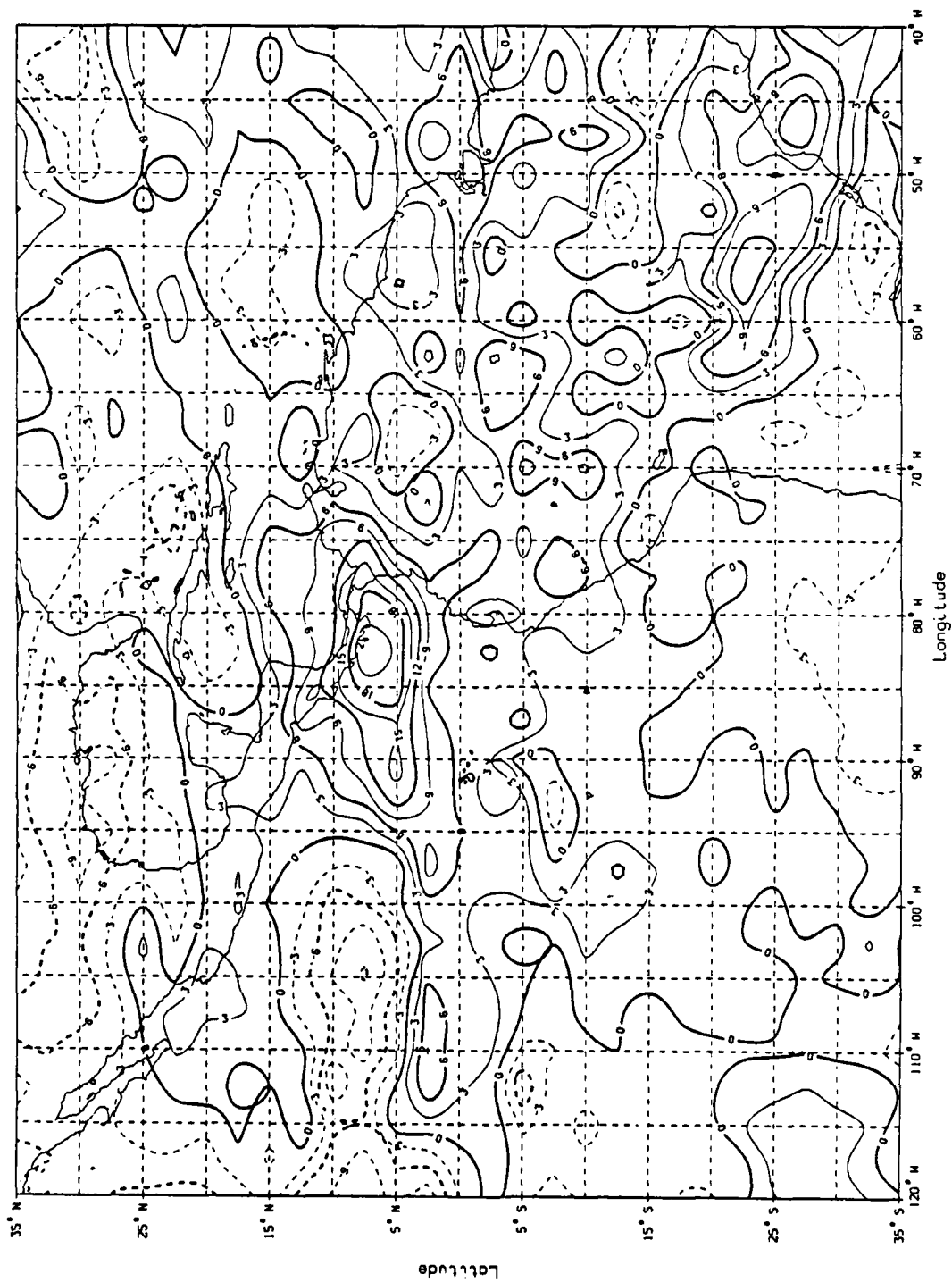


Figure 22. OLR composite diagram corresponding to Maximum OLR days over Panama for dry season 1984. Contoured values represent deviations from seasonal averages in units of  $Wm^{-2}$ .

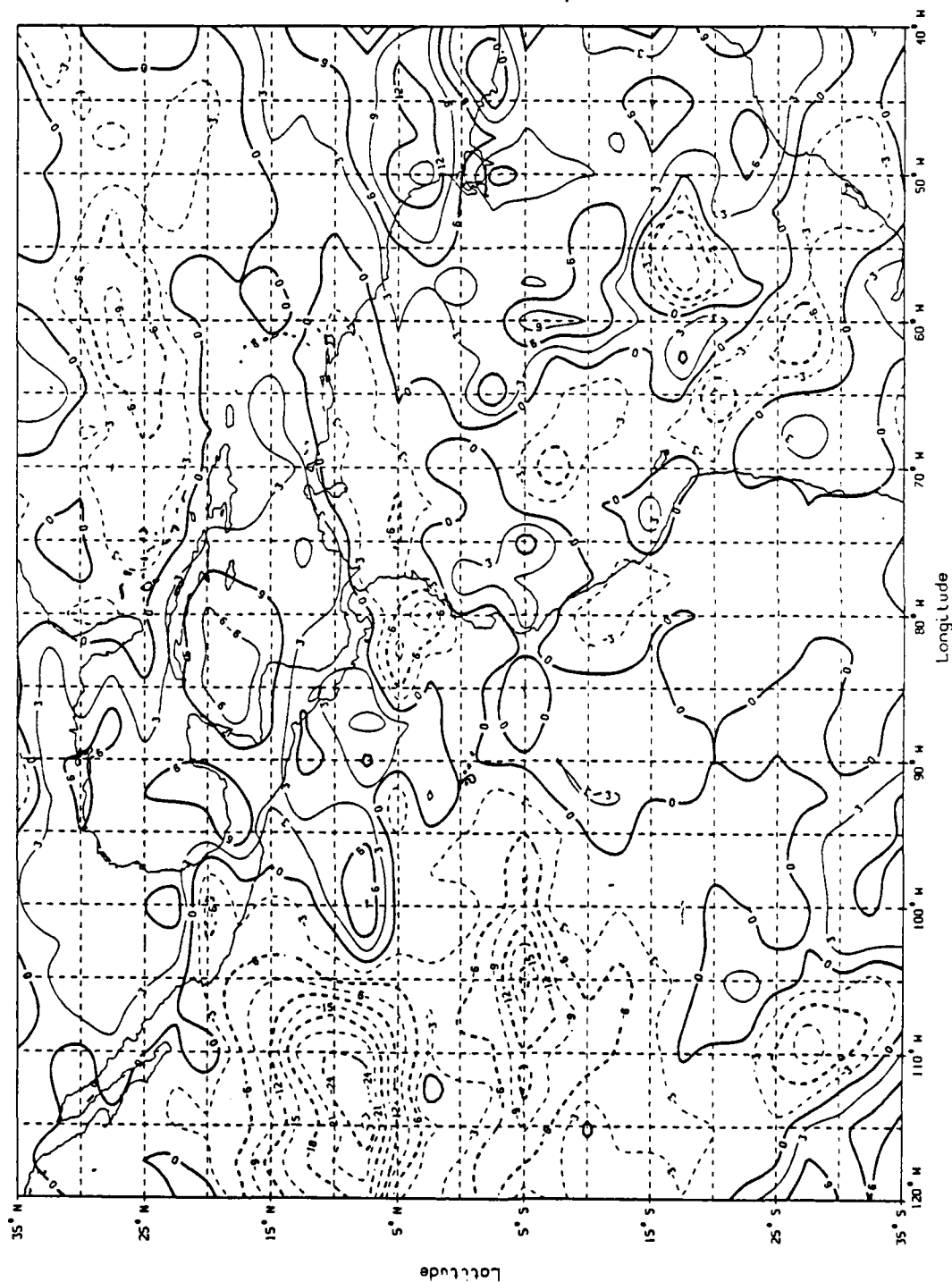


Figure 23. OLR composite diagram corresponding to Max-to-Min inflection points over Panama for dry season 1984. Contoured values represent deviations from seasonal averages in units of  $Wm^{-2}$ .

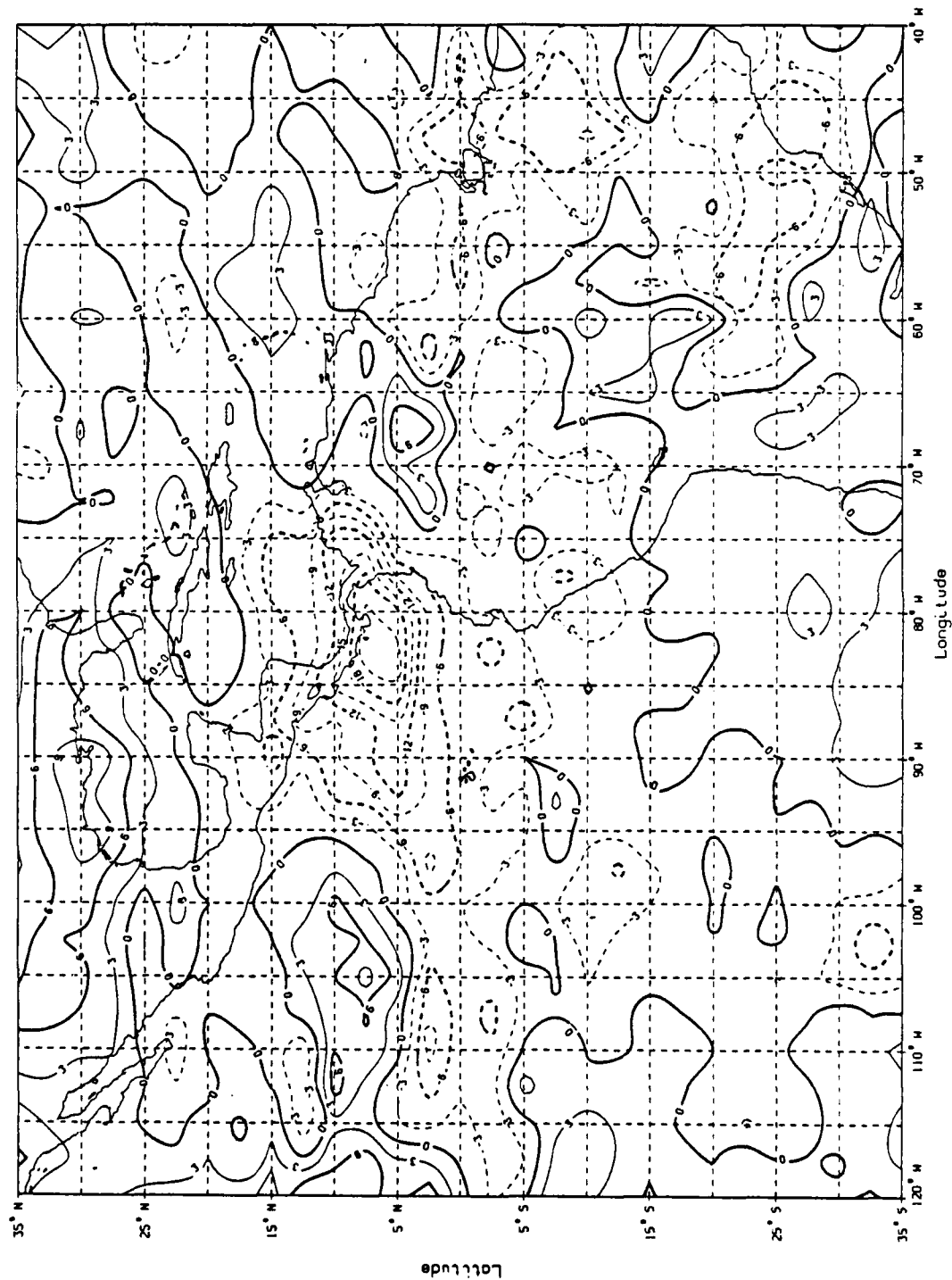


Figure 24. OLR composite diagram corresponding to Minimum OLR days over Panama for dry season 1984. Contoured values represent deviations from seasonal averages in units of  $Wm^{-2}$ .

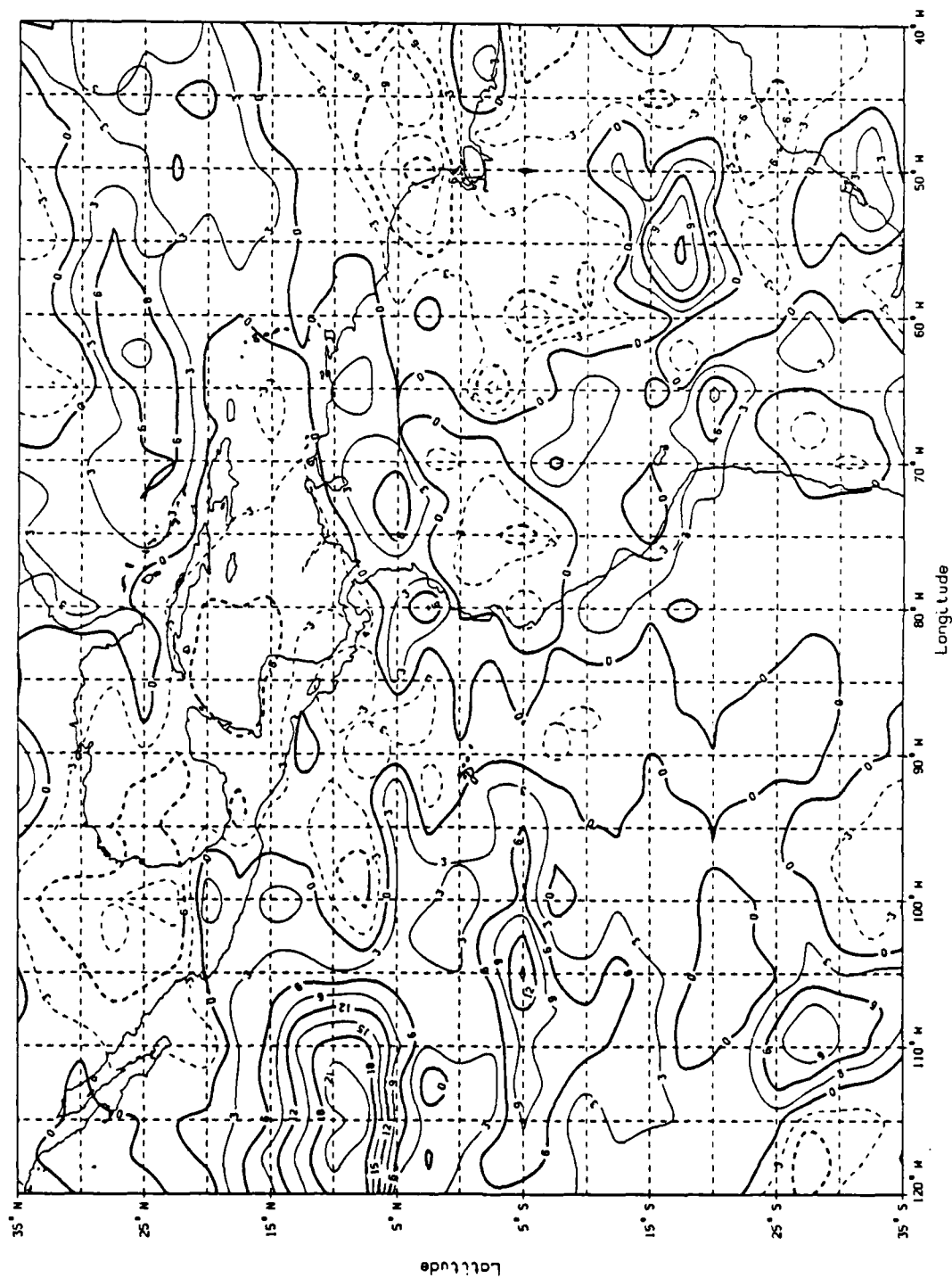


Figure 25. OLR composite diagram corresponding to Min-to-Max inflection points over Panama for dry season 1984. Contoured values represent deviations from seasonal averages in units of  $Wm^{-2}$ .

west. Three days later, the Max-to-Min inflection point composite (Fig. 23) shows the positive OLR anomalies over the Panama area have diminished and appear to have shifted slightly to the north. The major difference in this composite is the development of the strong dipole OLR anomaly centered at  $7^{\circ}\text{N}$ ,  $115^{\circ}\text{W}$  and  $5^{\circ}\text{S}$ ,  $105^{\circ}\text{W}$ . Note the intensity of the minimum values in the northern OLR minimum region, which are roughly  $-27\text{Wm}^{-2}$ . Moving ahead three more days in the cycle to the Minimum OLR composite (Fig. 24) it appears that these strong minimum OLR anomalies have built towards the east, with most of Central America now dominated by these low OLR values. The remnants of the strong negative OLR anomalies over the eastern Pacific can be seen extending from the Central American region to the west along a latitude of roughly  $3^{\circ}\text{N}$ . At around  $7^{\circ}\text{N}$ ,  $105^{\circ}\text{W}$  a new area of positive OLR anomalies can be seen developing, extending to the west beyond the boundary of the domain. An interesting comparison can be made at this point between the Maximum and Minimum composites. It appears the two are mirror images of each other, in both location and intensity of OLR anomaly centers. This comparison holds for the inflection point composites as well, as strong similarities can be seen between the Min-to-Max composite and the Max-to-Min composite. The Min-to-Max composite (Fig. 25) shows the large negative OLR anomalies over Central America have dissipated and shifted to the north, while a large dipole positive OLR anomaly has developed in the western portion of the domain. Again, this scenario is nearly the exact opposite of the Max-to-Min inflection point composite.

In summary, it appears that in the 1984 dry season a large-scale, west-to-east moving feature is responsible for creating large OLR anomalies across the

domain which extend from beyond the western edge of the domain eastward through Panama and Central America. Throughout the domain these anomalies appear to be significant in both size and strength, suggesting that this 12-d oscillation is affecting not only Panama, but much of the eastern Pacific as well.

#### Composite Diagrams for Wet Season 1984

Strong OLR anomalies during the wet season of 1984 can be seen on the composite diagrams, however, the development and apparent movement of these anomalies appears to be quite different from the dry season. Figures 26, 27, 28, and 29 correspond to OLR composites through one complete cycle of the 12-d oscillation. Beginning with the Maximum OLR composite (Fig. 26), the large positive OLR anomalies can be seen throughout Central America extending westward to the edge of the domain. An area of low OLR values is centered just off the southwest Mexico coast at  $15^{\circ}\text{N}$ ,  $100^{\circ}\text{W}$ , extending off to the northeast. This differs significantly from the negative anomaly pattern associated with the dry season maximum OLR composite diagram, as this minimum OLR anomaly is located farther to the northeast. More differences in the OLR anomaly field can be seen three days later in the Max-to-Min composite diagram (Fig. 27). It appears the large positive OLR anomaly over Panama and Central America has kept much of its original intensity despite a slight decrease in size and has shifted to the west-northwest, just south of the coasts of El Salvador and Guatemala. The negative OLR anomaly that was located off the southwest Mexico coast has expanded significantly and built farther to the west. Again, this pattern is quite different from the dry season pattern in which the OLR anomalies appeared



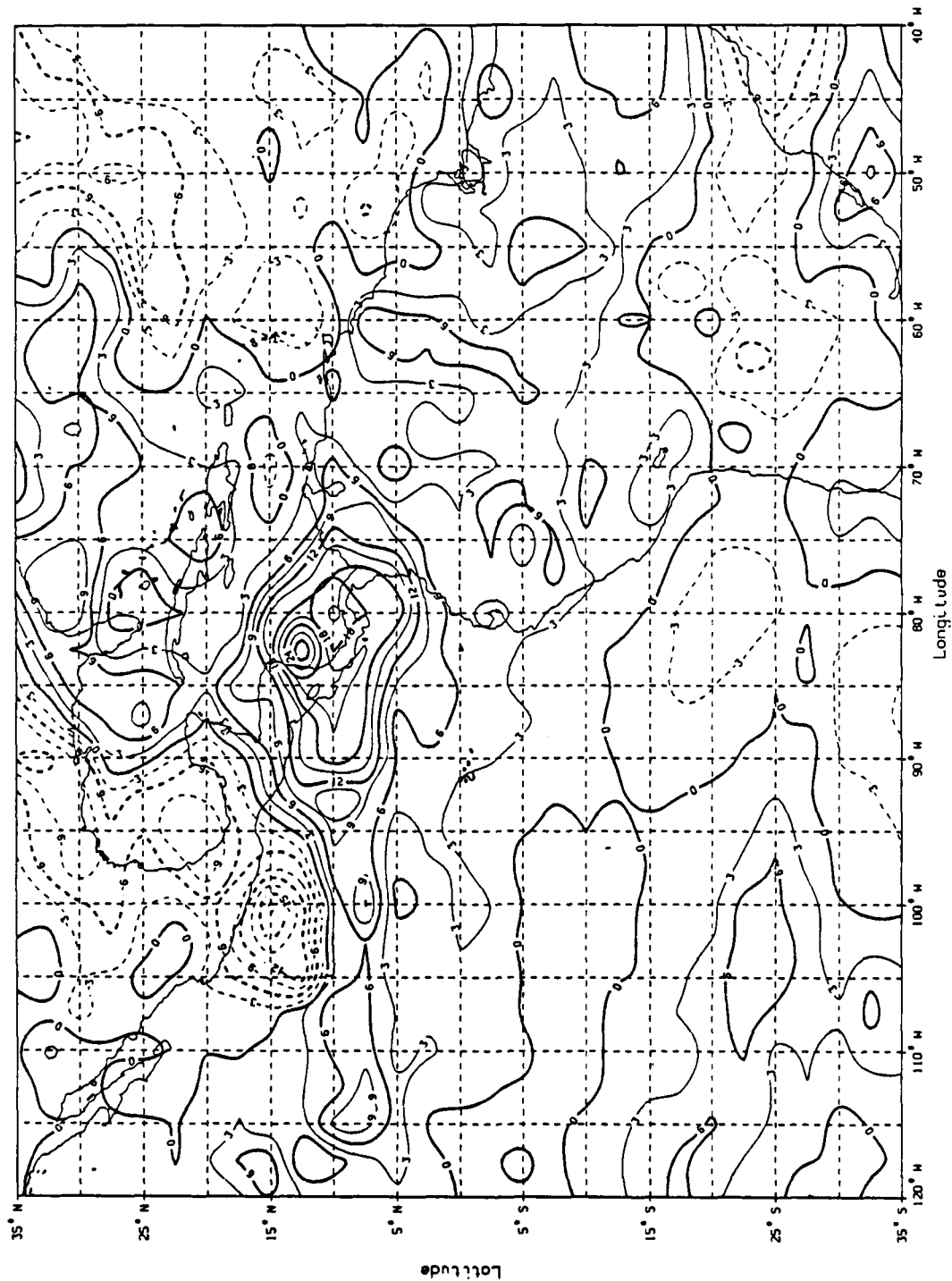


Figure 26. OLR composite diagram corresponding to Maximum OLR days over Panama for wet season 1984. Contoured values represent deviations from seasonal averages in units of  $Wm^{-2}$ .

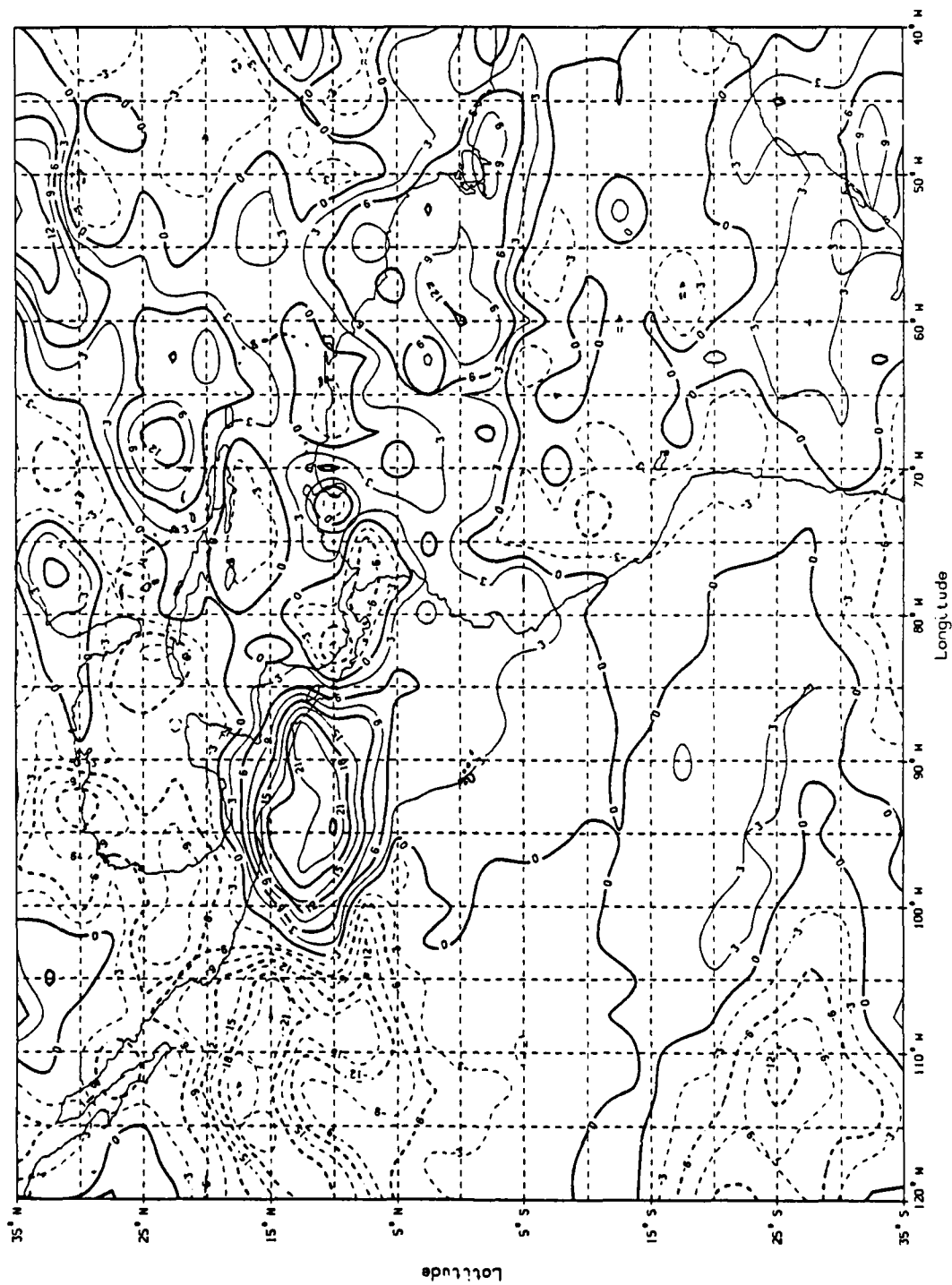


Figure 27. OLR composite diagram corresponding to Max-to-Min inflection points over Panama for wet season 1984. Contoured values represent deviations from seasonal averages in units of  $Wm^{-2}$ .

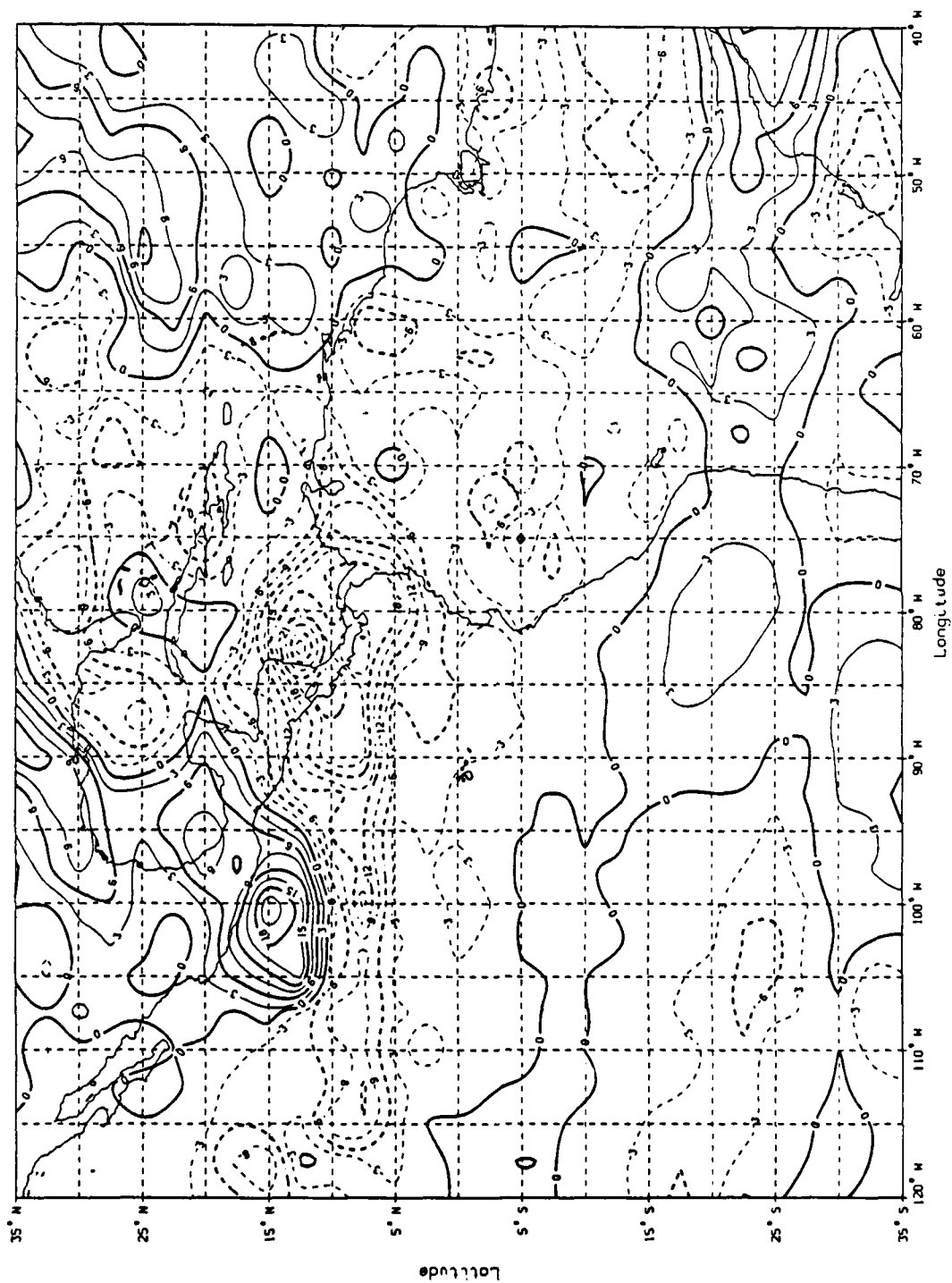


Figure 28. OLR composite diagram corresponding to Minimum OLR days over Panama for wet season 1984. Contoured values represent deviations from seasonal averages in units of  $Wm^{-2}$ .

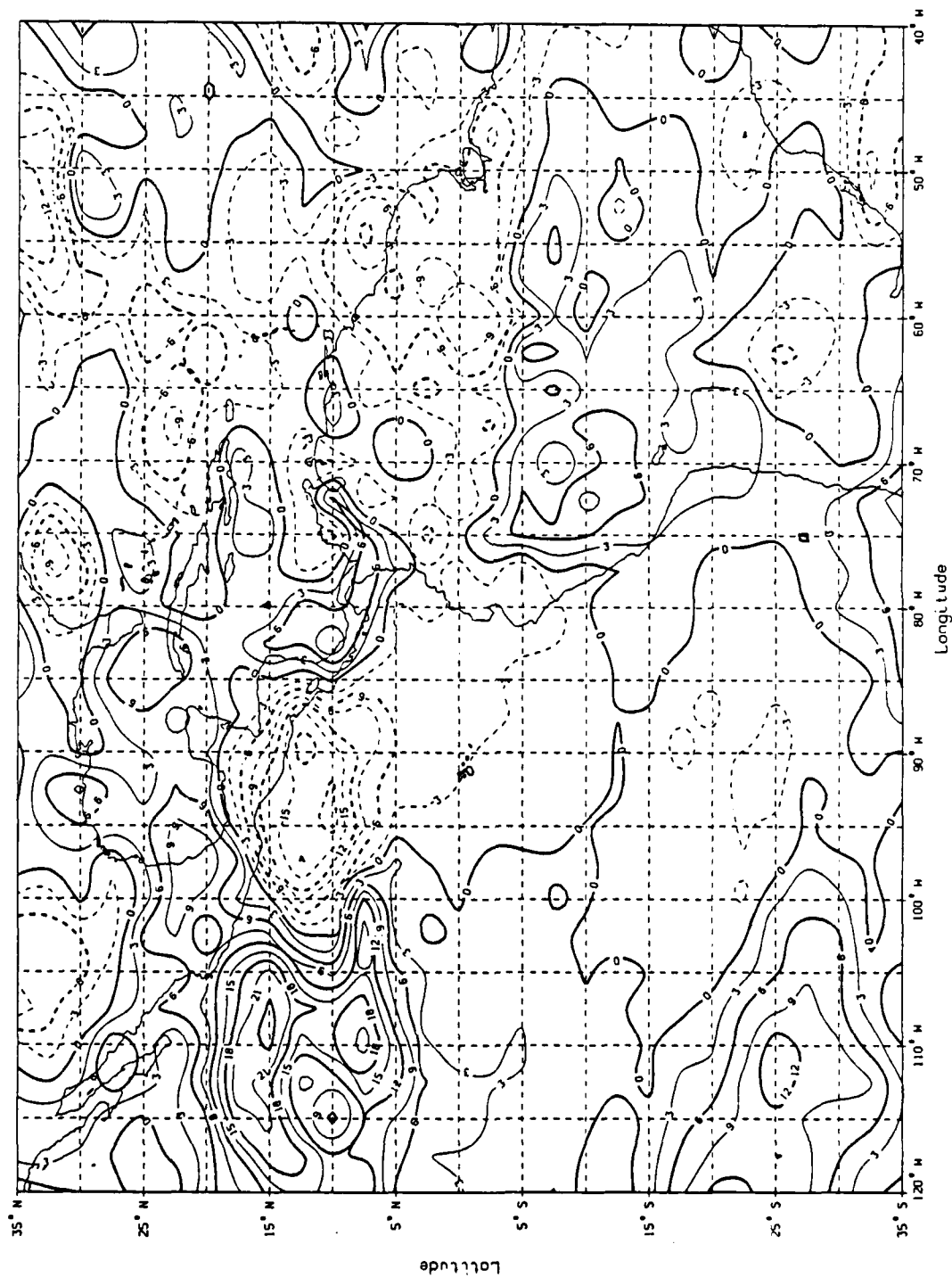


Figure 29. OLR composite diagram corresponding to Min-to-Max inflection points over Panama for wet season 1984. Contoured values represent deviations from seasonal averages in units of  $Wm^{-2}$ .

to be drifting to the east. Three days later, the Minimum OLR composite (Fig. 28) shows that convection has developed explosively throughout Central American with the lowest OLR values centered over the Costa Rica-Nicaragua region. Convection also seems to have intensified along the entire monsoon trough. Meanwhile, the positive OLR anomaly that was located off the southern coasts of El Salvador and Guatemala has diminished somewhat in size but has maintained much of its original intensity and has shifted to the west-northwest. Finally, the Min-to-Max inflection point composite (Fig. 29) shows that the large area of negative OLR anomalies centered over Costa Rica and Nicaragua 3 d earlier has diminished in size and moved to the west-northwest. One feature the wet season pattern has in common with the dry season is that the Maximum and Minimum composites, as well as the Max-to-Min and Min-to-Max inflection point composites, appear to be mirror images of each other.

In comparison with the dry season OLR anomalies, which appeared to be originating off the western boundary of the domain and building from west to east, the source region for the wet season OLR anomalies appears to be directly over the Panama region with the OLR anomalies drifting slowly to the west-northwest. However, it is impossible to infer a possible synoptic scenario associated with the development and movement of these OLR anomalies without first examining the vertical structure of the atmosphere. Also, by examining the upper-air sounding for any significant changes as the 12-d oscillation moves over Panama, forecasters may be able to use these upper-air analyses to forecast changes in cloud cover and convection associated with the oscillation.

## Vertical Structure of 12-Day Oscillation

Upper-air data from Albrook Air Force Station, Panama were studied in order to determine the vertical structure of the 12-d oscillation, as well as to determine if the movement of the oscillation through Panama could be detected. There were two methods used to obtain these goals: First, the IMSL periodogram analysis routine was performed on all three variables (u- and v-wind component and height of pressure surfaces) to determine if any spectral power in the 12-d range was present for any of the variables. Second, vertical composites for each of the four phases of the oscillation were constructed for each variable to determine if any significant deviations from the mean were evident. If these deviations were consistent over the period of the oscillation they could be used as a forecasting tool. These studies were divided into dry and wet seasons, and the procedures and results are discussed in the following sections.

### Dry Season 1984 Vertical Composites

The procedures used to study the upper-air data were similar to those used on the OLR time series. First, u- and v-wind components and height of the pressure surfaces were obtained from 10 levels (100, 85, 70, 50, 40, 30, 25, 20, 15, and 10 kPa). For each variable at every level, the seasonal mean and any long-period seasonal trends were removed, and the IMSL periodogram analysis routine was then performed. The results from the analyses (not shown) are briefly summarized as follows:

- Spectral peaks were evident at all levels for the u-wind component in the 30–60 d range, consistent with the findings of Madden and Julian (1972).

Broad spectral peaks at 15–30 d were also evident at some levels. Some spectral power at all levels was present in the 11–12 d range.

- Very broad spectral peaks in the 30–60 d range were present at some levels for the v-wind component, with another strong spectral peak detected at around 20–25 d. However, the strongest and most persistent period was found at 11–12 d.
- The strongest spectral peaks in the height field were found 30–45 and 20–25 d periods in the upper levels (40–10 kPa). Weak spectral power was detected at all levels for the period of 11–12 d.

The results of the IMSL analyses have shown that other low-frequency oscillations can be detected in each of the three variables from the Panama sounding. The 11–12 d oscillation, while not always the strongest spectral peak, was evident at each level with the strongest signal found in the v-wind component.

The next step in the analysis was to filter each variable at every level for 12 d, similar to the process used on the OLR data. Once this was accomplished, these analyses were used to construct vertical composite diagrams corresponding to each of the four phases (Maximum, Max-to-Min inflection point, Minimum, and Min-to-Max inflection point) of the Panama area 12-d filtered OLR time series (Fig. 18). These vertical composites would show the deviation from the seasonal means associated with each phase of the 12-d oscillation. Using these composites, a forecaster should be able to determine which phase of the 12-d oscillation Panama was in simply by maintaining continuity of the daily 1200 GMT upper-air analyses. The following is a brief description of the vertical composites:

- The vertical composites for the u-wind component corresponding to each of the four phases of the oscillation are shown in Figs. 30, 31, 32, and 33. The largest deviations from the seasonal average on the composites are only around 2–3 kt, but more important is the trend of the deviations through the cycle for the levels 50 kPa and above. Note that at the Maximum composite (Fig. 30) the winds have a slightly weaker easterly component from 50–30 kPa, and a slightly stronger westerly component above 30 kPa. Moving through the cycle to the Minimum composite (Fig. 32) the anomalies have reversed, with slightly stronger easterly winds from 50–30 kPa and a slightly weaker westerly component above 30 kPa. Although this only amounts to a reversal in the wind component of about 4 kt, the fact that this trend can be detected in the entire upper-level u-wind field could be a significant feature used to forecast the phase of the 12-d wave.
- The v-wind composites are shown in Figs. 34, 35, 36, and 37. A stronger trend can be seen in the v-component at the 25–20 kPa level. In the Maximum composite (Fig. 34) the v-wind at that level is only about 1 kt from the south, which is roughly 5 kt less than the seasonal average. By the time the 12-d oscillation cycle reaches the Minimum phase 6 d later (Fig. 36), the southerly wind component has increased by over 8 kt at the 25–20 kPa level.
- The composites of the height of the pressure surfaces are shown in Fig. 38. The height composites differ from the u-and v-wind composites in that



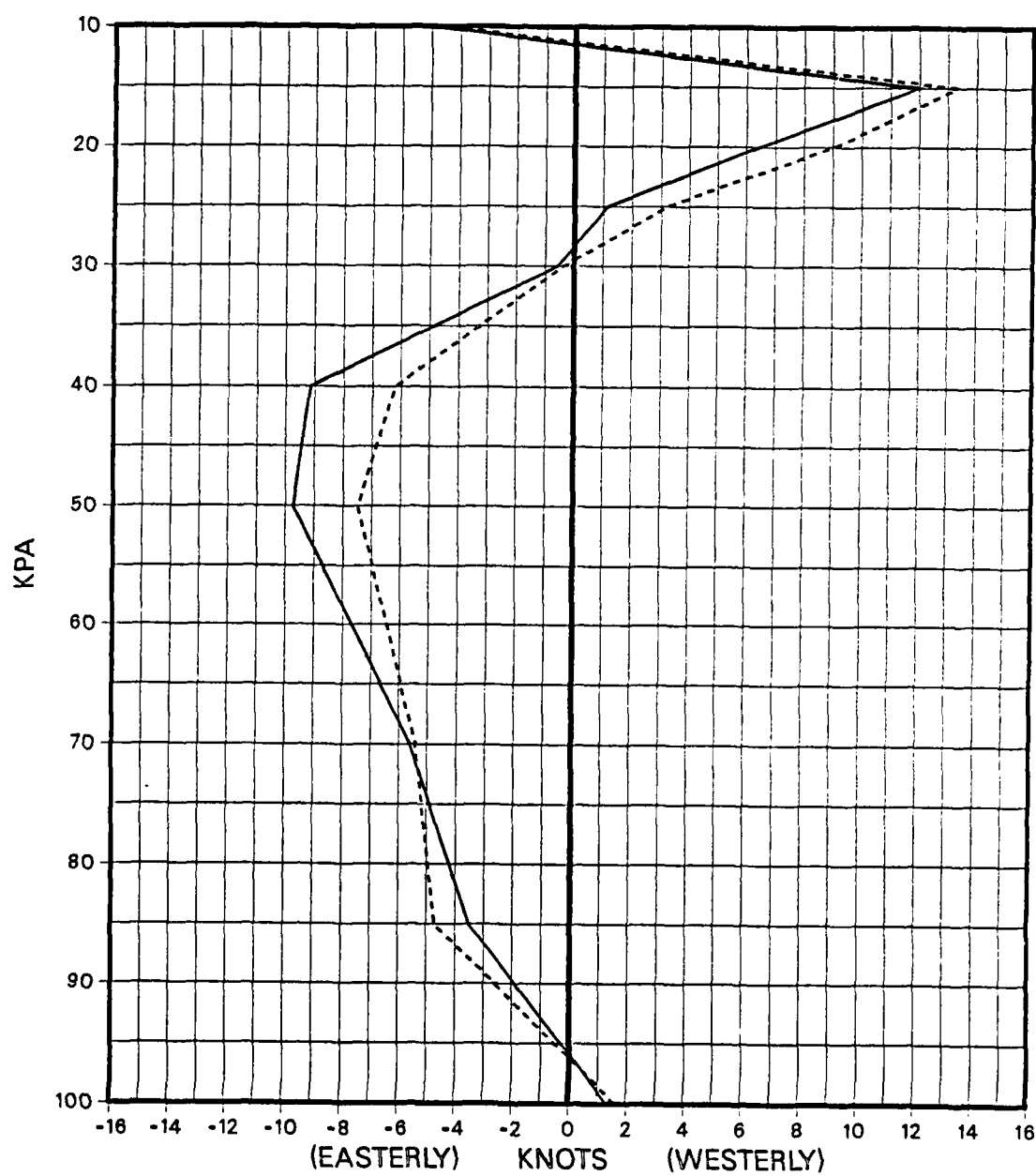


Figure 30. Vertical composite for u-wind component corresponding to Maximum OLR days, dry season 1984. Solid line represents seasonal average, dashed line represents deviation.

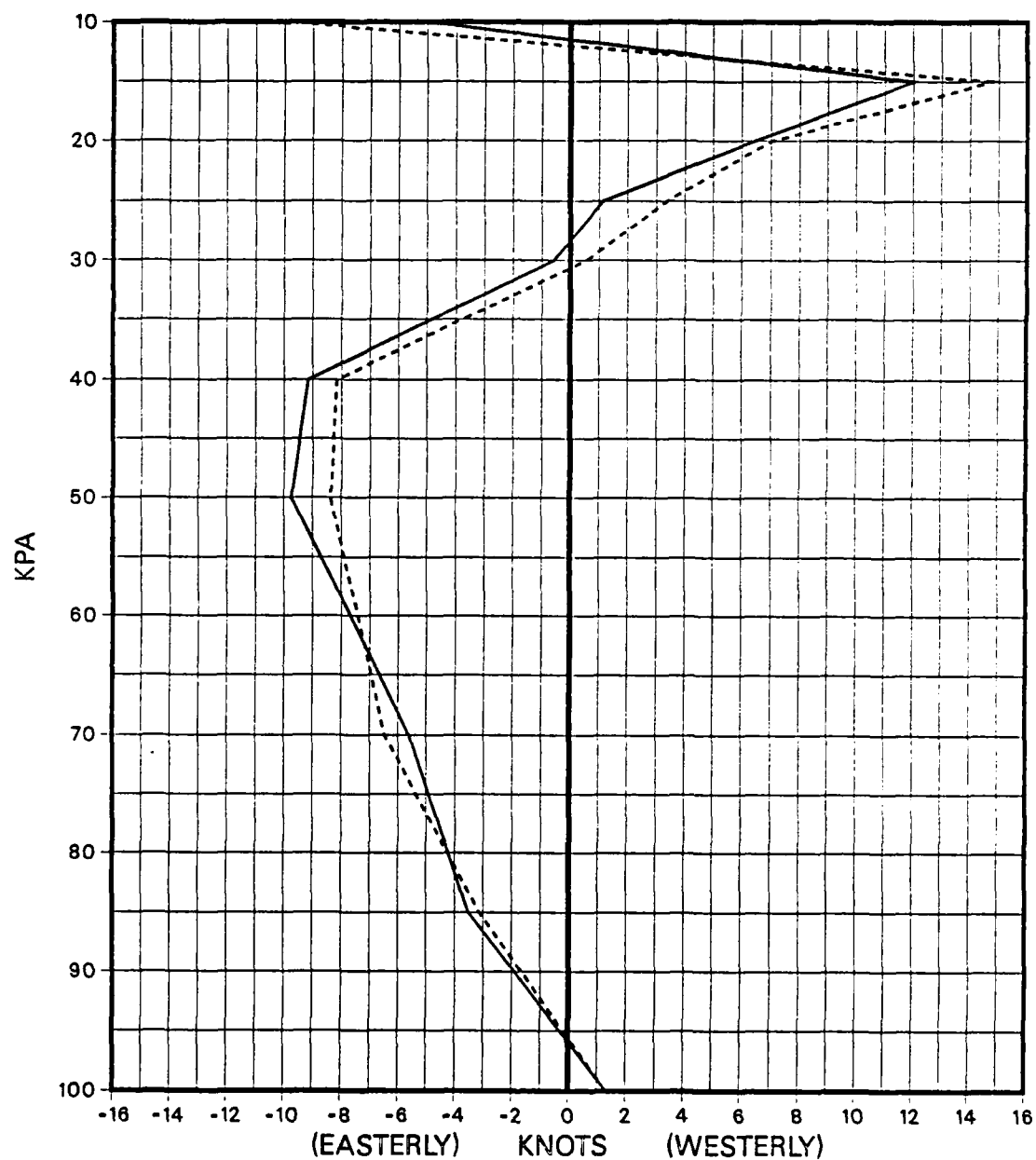


Figure 31. Vertical composite for u-wind component corresponding to Max-to-Min OLR inflection points, dry season 1984. Solid line represents seasonal average, dashed line represents deviation.

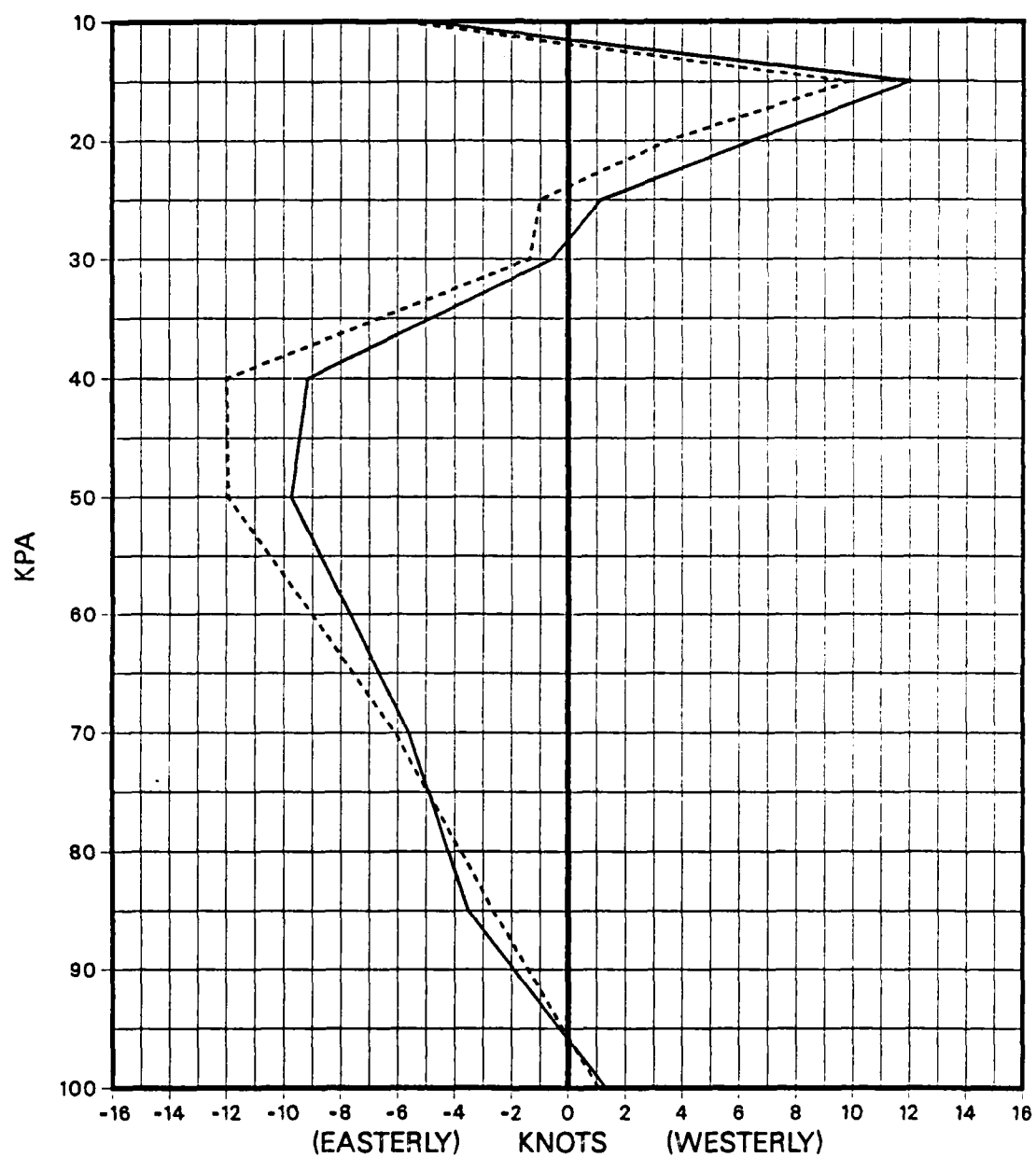


Figure 32. Vertical composite for u-wind component corresponding to Minimum OLR days, dry season 1984. Solid line represents seasonal average, dashed line represents deviation.

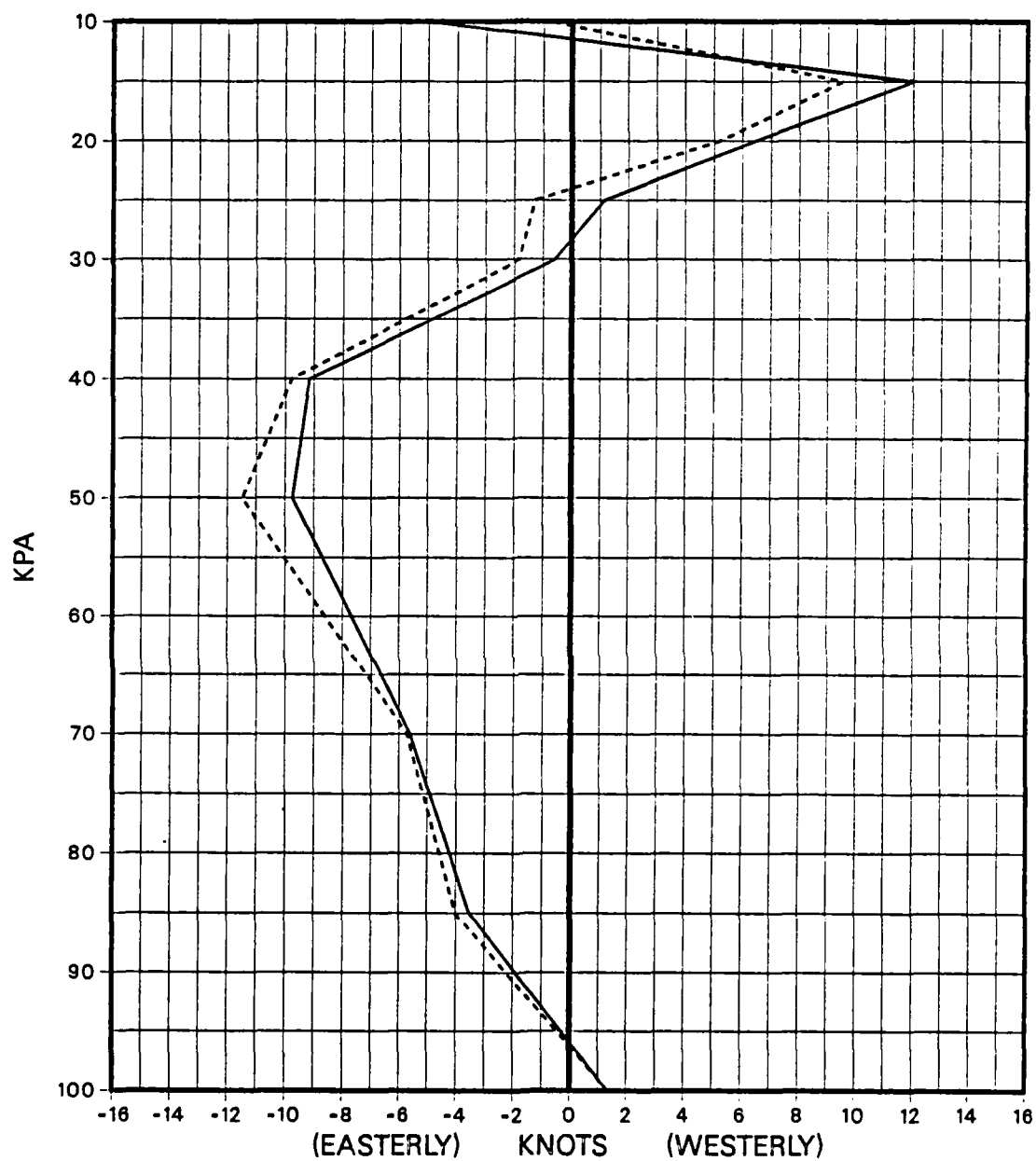


Figure 33. Vertical composite for u-wind component corresponding to Min-to-Max OLR inflection points, dry season 1984. Solid line represents seasonal average, dashed line represents deviation.

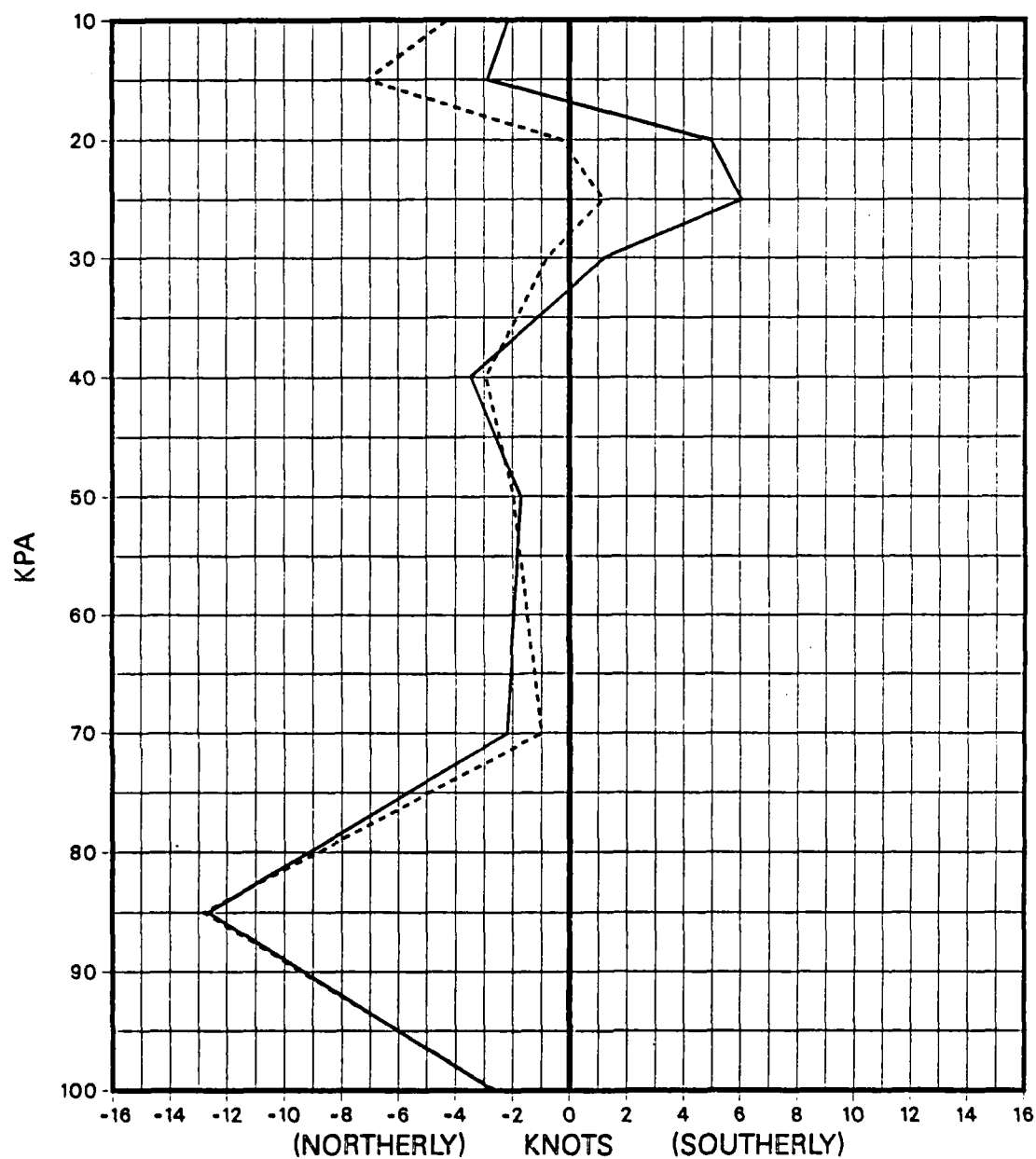


Figure 34. Vertical composite for v-wind component corresponding to Maximum OLR days, dry season 1984. Solid line represents seasonal average, dashed line represents deviation.

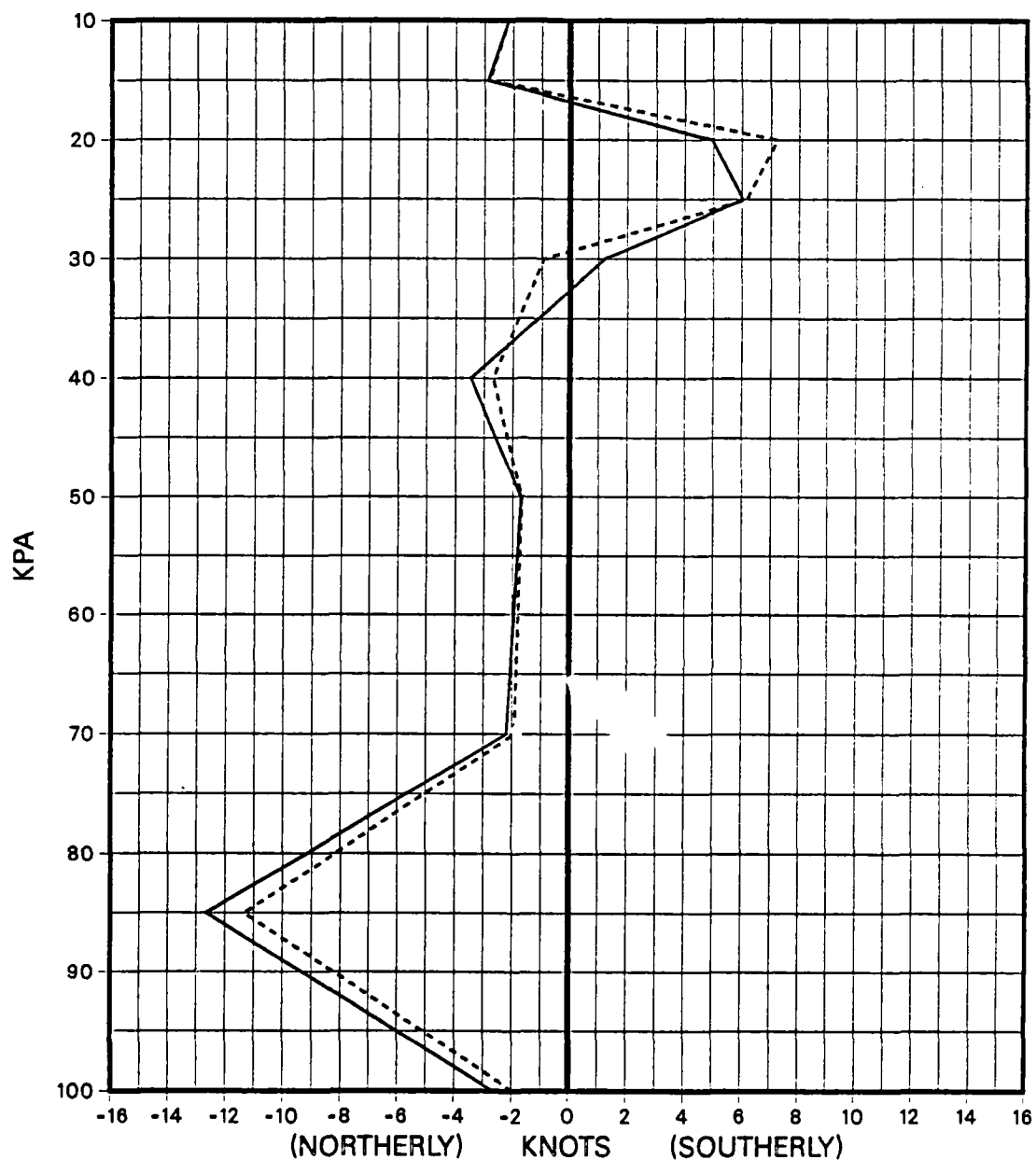


Figure 35. Vertical composite for v-wind component corresponding to Max-to-Min OLR inflection points, dry season 1984. Solid line represents seasonal average, dashed line represents deviation.

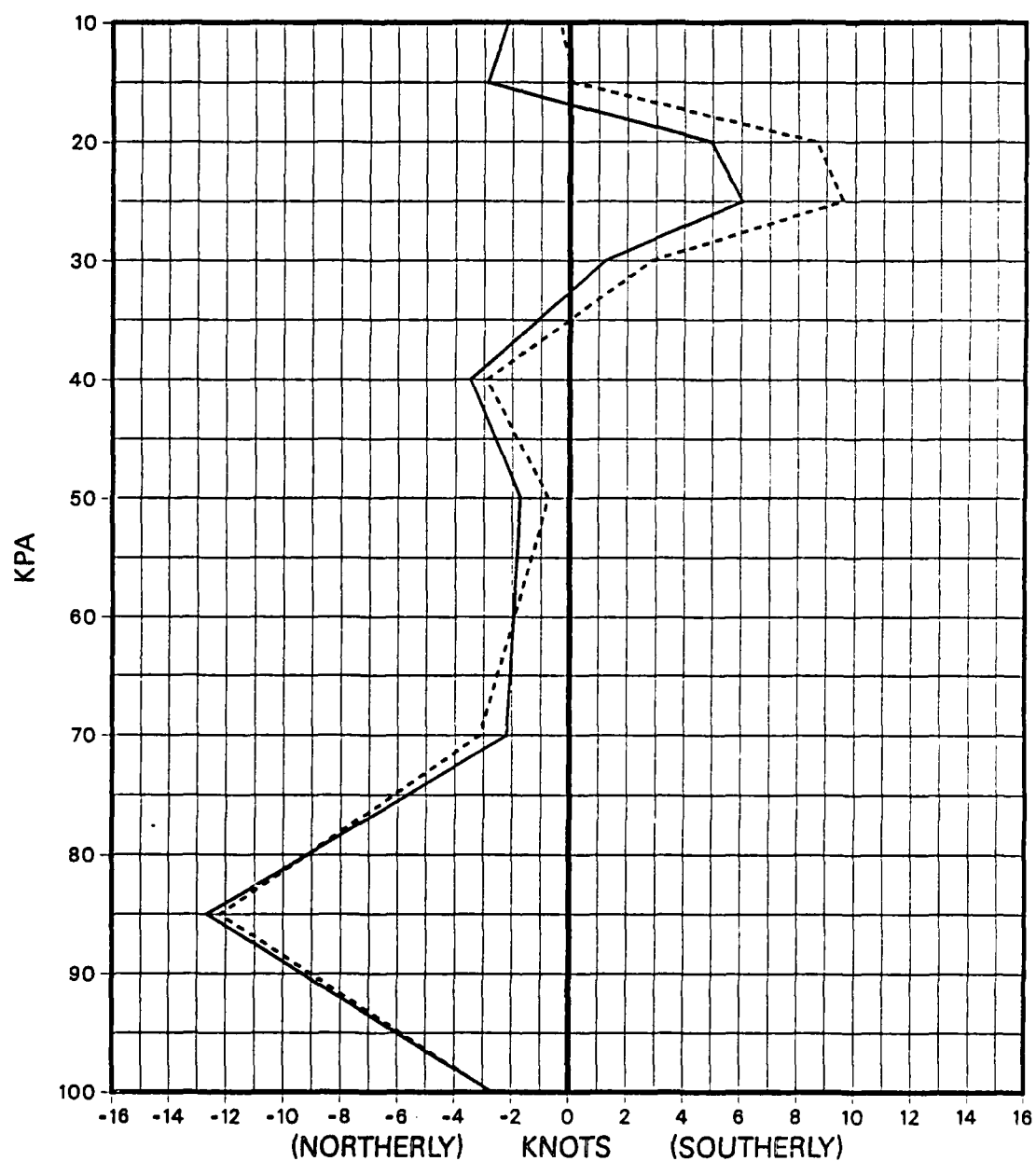


Figure 36. Vertical composite for v-wind component corresponding to Minimum OLR days, dry season 1984. Solid line represents seasonal average, dashed line represents deviation.

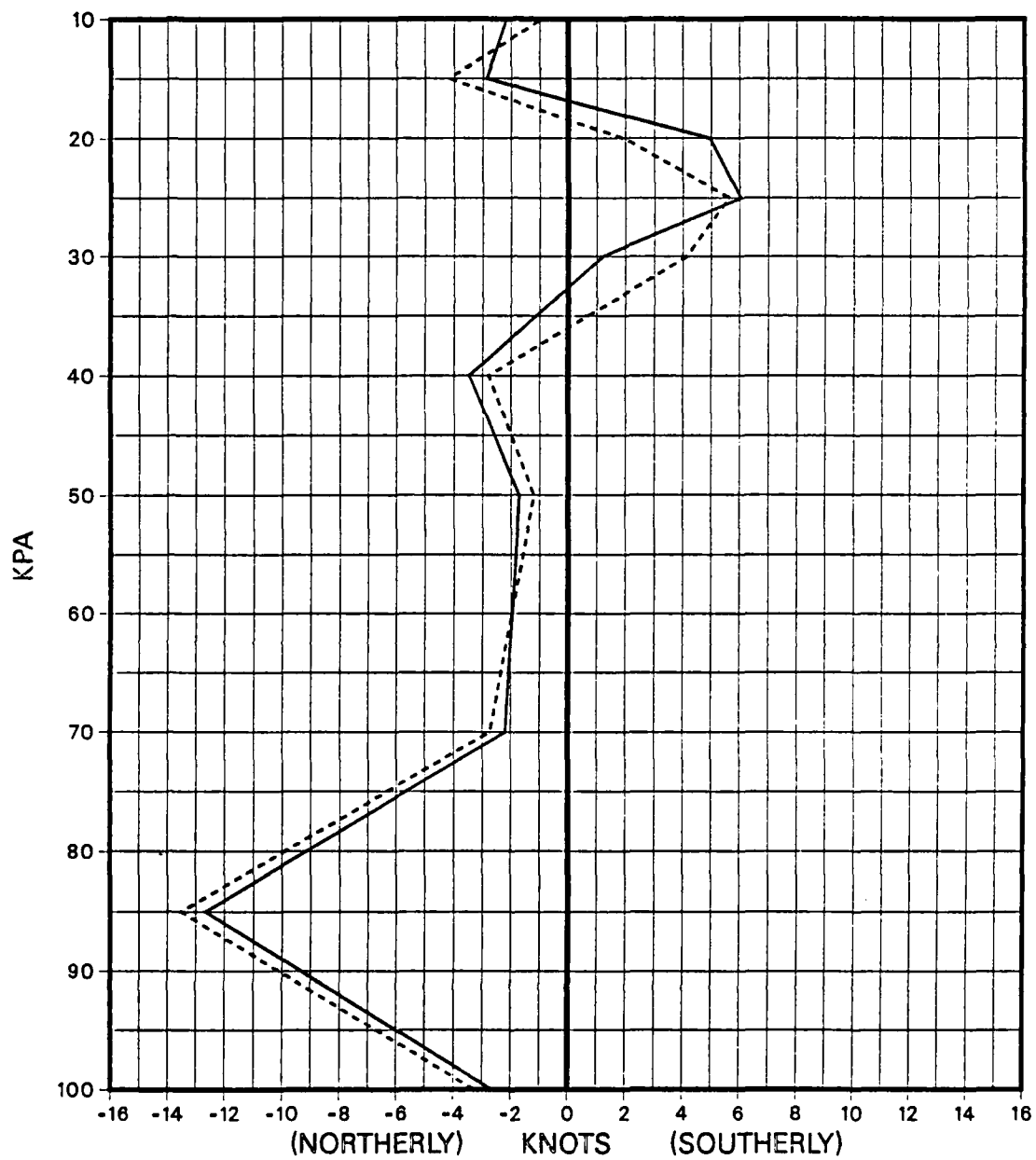


Figure 37. Vertical composite for v-wind component corresponding to Min-to-Max OLR inflection points, dry season 1984. Solid line represents seasonal average, dashed line represents deviation.



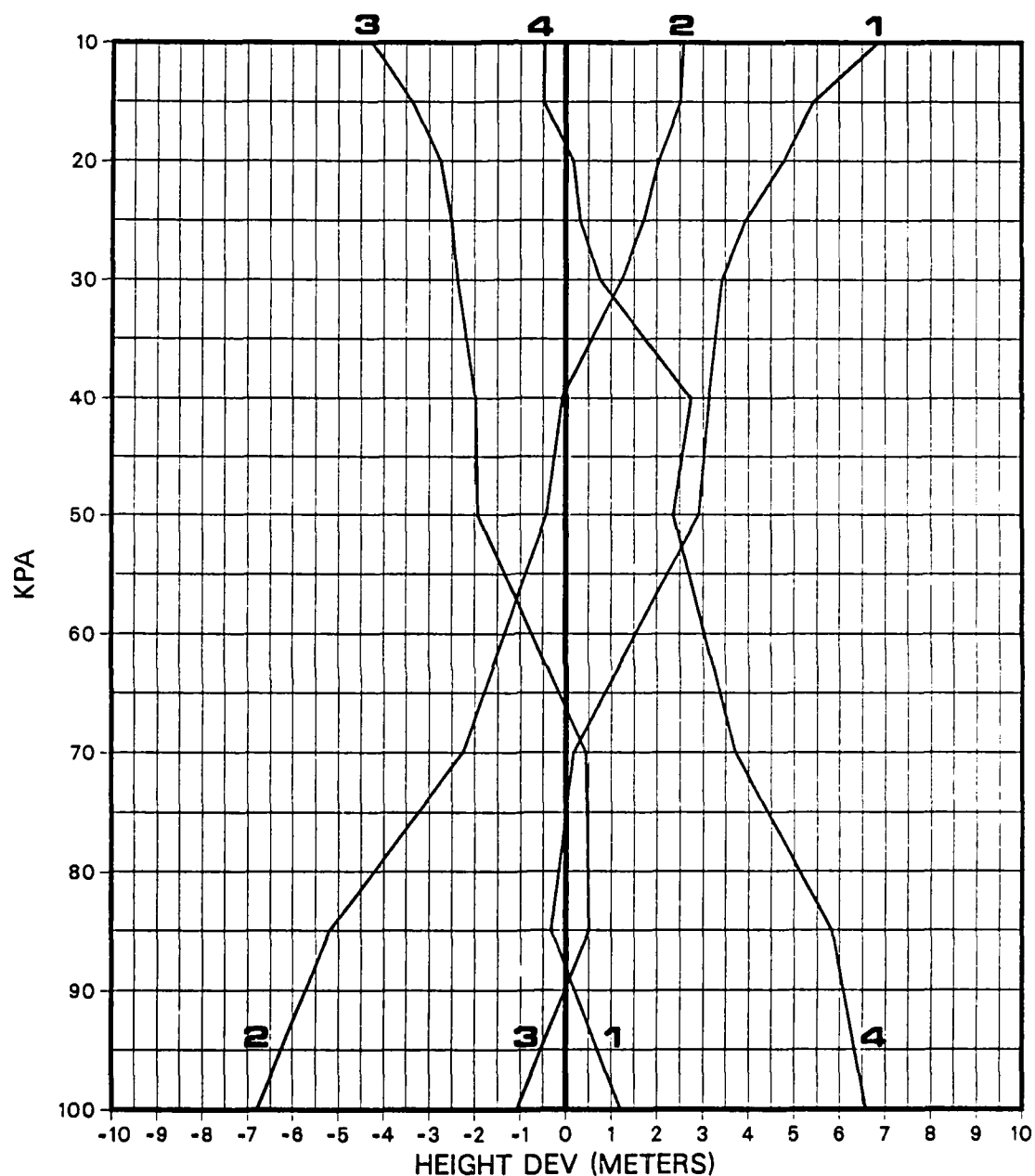


Figure 38. Vertical composite of height anomalies for dry season 1984. Solid line along zero deviation line represents seasonal mean, solid traces represent deviations from the mean. Trace 1 corresponds to Maximum OLR composite, Trace 2 to Max-to-Min OLR composite, Trace 3 to Minimum OLR composite, Trace 4 to Min-to-Max OLR composite.

the height deviations can be detected at all levels, as opposed to the wind composites which were evident at only the upper levels. Beginning with the Maximum composite (Trace 1), the upper levels show maximum height anomalies while the lower levels remain near the seasonal mean. Three days later (Trace 2), the upper levels have shifted towards the seasonal mean while the lower levels show a relatively large negative height anomaly. The minimum composite (Trace 3) shows that while the lower levels retreat towards the seasonal mean the upper levels reach a relative minimum. Finally, the Min-to-Max inflection point (Trace 4) completes the cycle as the upper-level heights shift towards the seasonal average and the lower-level heights become positive. This lag between lower and upper levels is significant because it implies a vertical structure exists in the oscillation where the lower levels lead the upper levels. This implied vertical tilt suggests the oscillation could have a baroclinic structure.

To summarize, it appears the phase of the 12-d oscillation during dry season 1984 can be detected using the vertical composites of all three variables. Although the composite anomalies may be too small to determine the phase of the oscillation using quantitative methods, the trends of the anomalies appear to be consistent and well-defined throughout the cycle of the oscillation, especially the v-wind component and height composites. These trends would allow forecasters to monitor and forecast each phase of the oscillation.

### Wet Season 1984 Vertical Composites

The composites for wet season were constructed using the same methods as the dry season. The results of the IMSL periodogram analyses (not shown) are summarized as follows:

- Very broad spectral peaks in the 30–60 d range were detected at all levels for the u-wind component. Spectral peaks corresponding to the period of 15–25 d were found at some levels. The strongest and most persistent spectral peaks were in the 11–12 d range and were found at all levels, but were strongest in the upper levels.
- Strong spectral peaks were found in the 11–12 d range at all levels for the v-wind component. Some concentration of spectral power was detected at several levels in both the 30–60 d and approximately 15–25 d periods.
- Very strong spectral peaks in the height fields were detected at around 50–60 d in the upper levels along with weak spectral peaks in the 15–30 d range. Persistent peaks in the 11–13 d period were found at all levels but were strongest in the upper levels.

The IMSL periodogram analysis results for wet season were similar to those of dry season. The 12-d oscillation was detected at all levels in all three variables, but was again strongest in the v-wind component. Next, the 12-d filter was applied to each variable at every level and composite diagrams were constructed in the same manner as for dry season. The vertical composites and a brief discussion of their trends are as follows:

- The u-wind composites are shown in Figs. 39, 40, 41, and 42. Very large deviations from the seasonal mean can be seen in the upper levels (20–15 kPa) as the composite diagrams follow the 12-d cycle. Beginning with the Maximum composite (Fig. 42), the seasonal mean shows easterly winds of about 4–6 kt in the 20–15 kPa layer, but the composite winds show a westerly wind component of around 2–3 kt during this phase. Moving ahead 3 d to the Max-to-Min inflection point composite (Fig. 43), the composite winds are nearly equal to the seasonal average. However, 3 d later in the Minimum composite (Fig. 44), the composite u-component winds are now easterly at over 10 kt. This represents a deviation of 12–13 kt in the u-wind component over the 6 d period from the Maximum composite to the Minimum composite, as well as a switch from weak westerlies to strong easterlies.
- The vertical composites for the v-wind component are shown in Figs. 43, 44, 45, and 46. Strong directional shifts in the upper-level v-wind component can also be seen in the vertical composites. Beginning with the Maximum composite (Fig. 46), the composite winds are roughly equal to the seasonal average in the upper levels. Moving to the Max-to-Min inflection point (Fig. 47), the composite wind at 20 kPa is now southerly at approximately 5 kt. Three days later at the Minimum composite (Fig. 48), the composite winds are again nearly equal to the seasonal average, but on the Min-to-Max inflection point composite the winds are now from

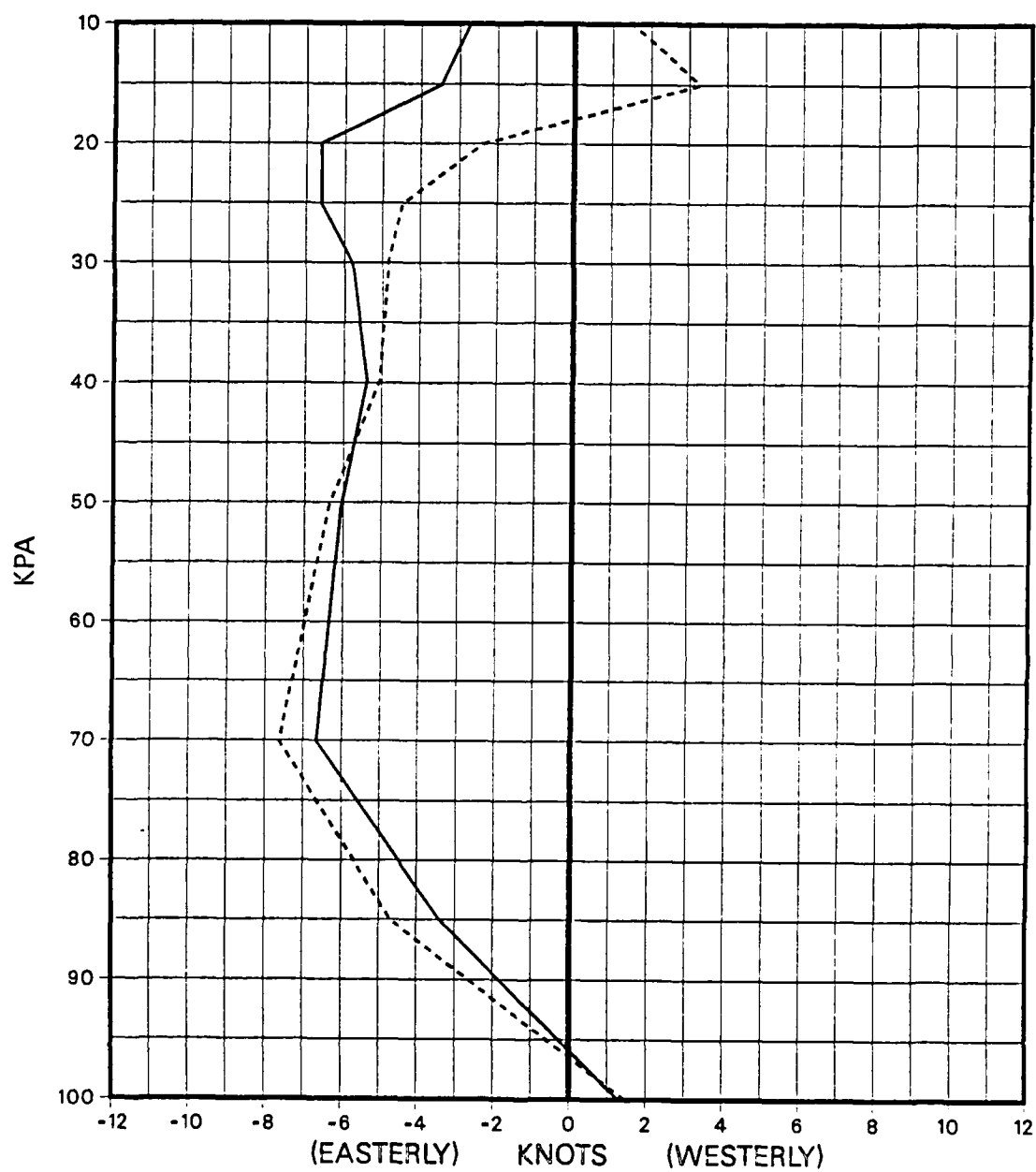


Figure 39. Vertical composite for u-wind component corresponding to Maximum OLR days, wet season 1984. Solid line represents seasonal average, dashed line represents deviation.

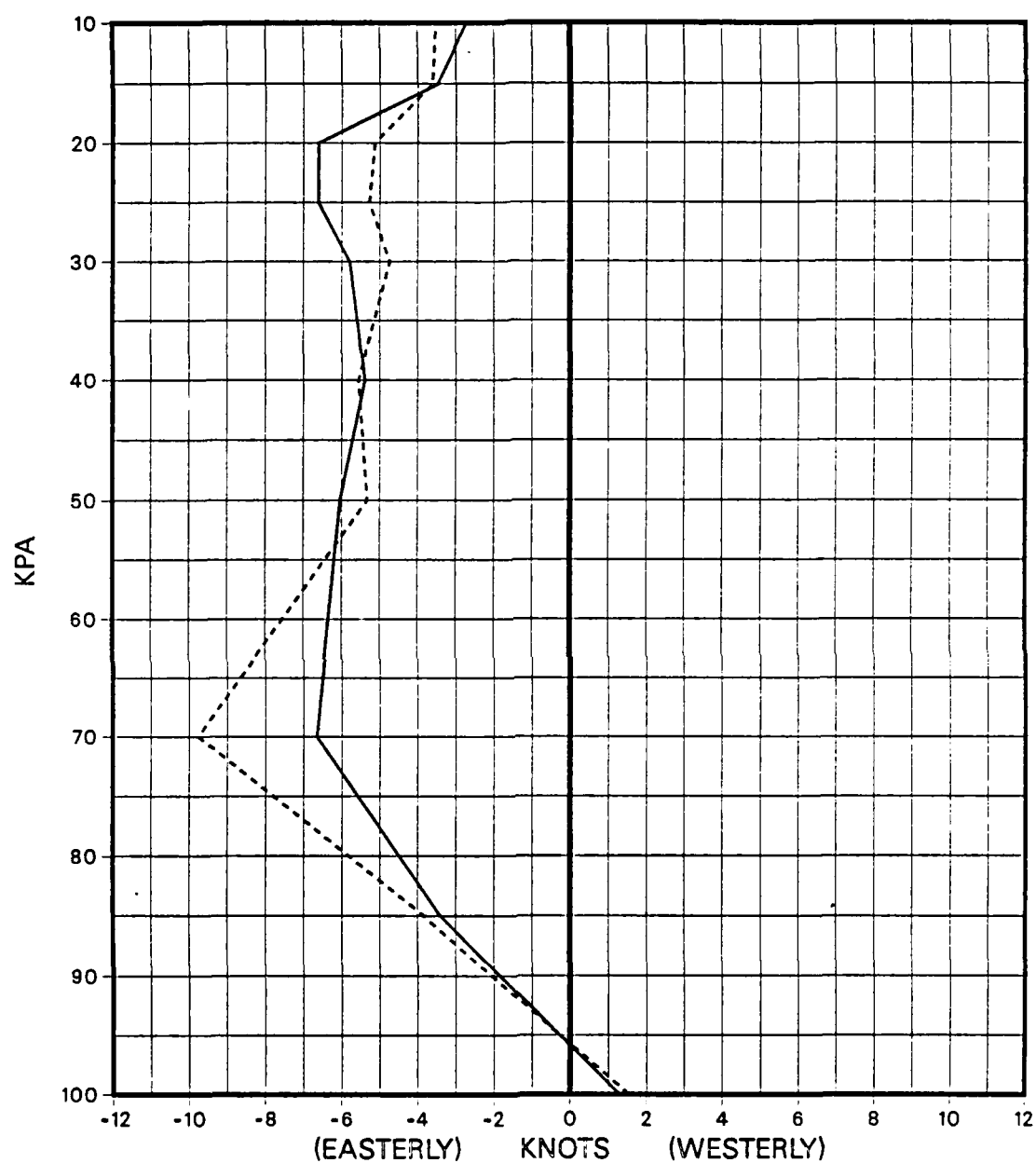


Figure 40. Vertical composite for u-wind component corresponding to Max-to-Min OLR inflection points, wet season 1984. Solid line represents seasonal average, dashed line represents deviation.

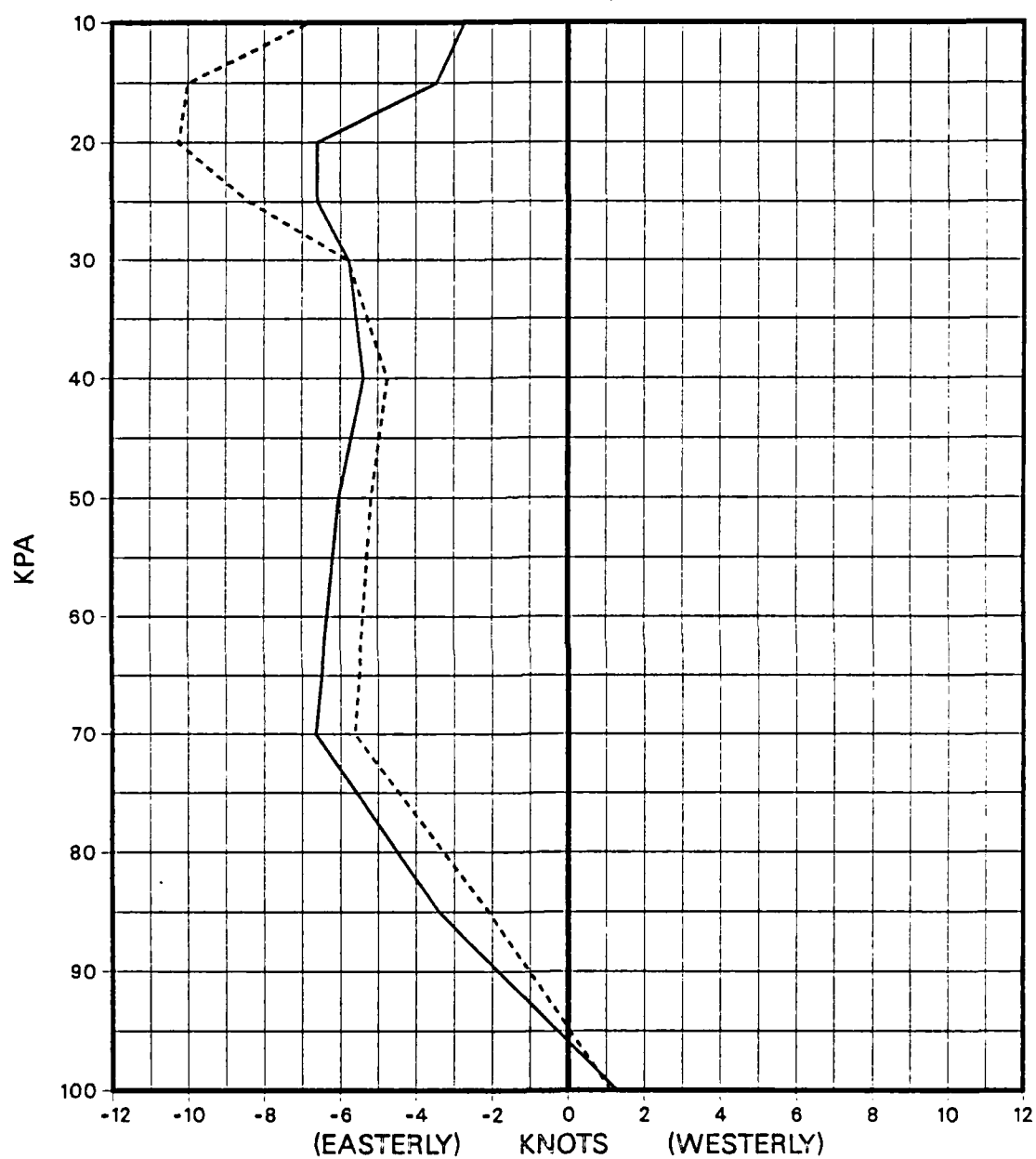


Figure 41. Vertical composite for u-wind component corresponding to Minimum OLR days, wet season 1984. Solid line represents seasonal average, dashed line represents deviation.

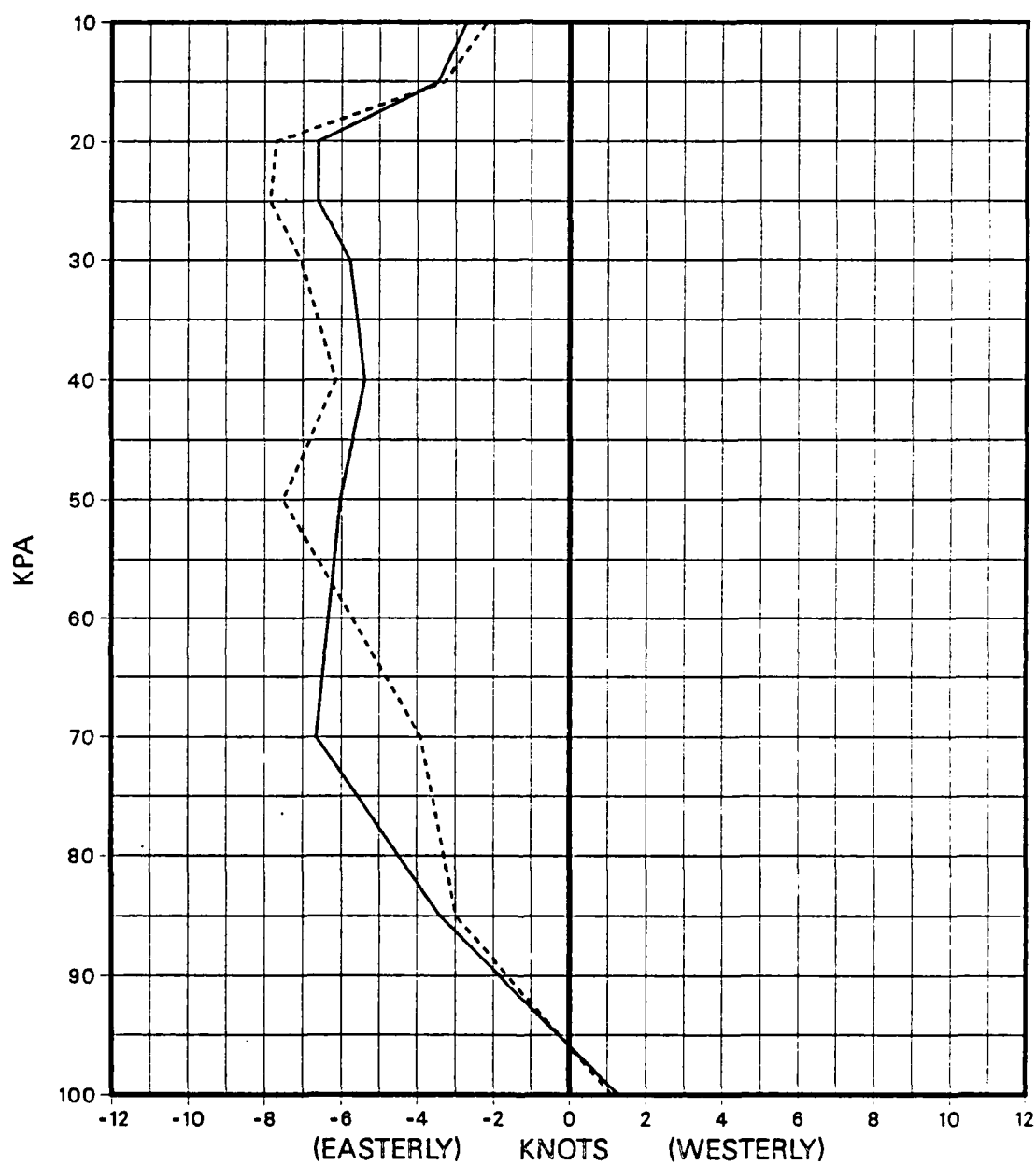


Figure 42. Vertical composite for u-wind component corresponding to Min-to-Max OLR inflection points, wet season 1984. Solid line represents seasonal average, dashed line represents deviation.



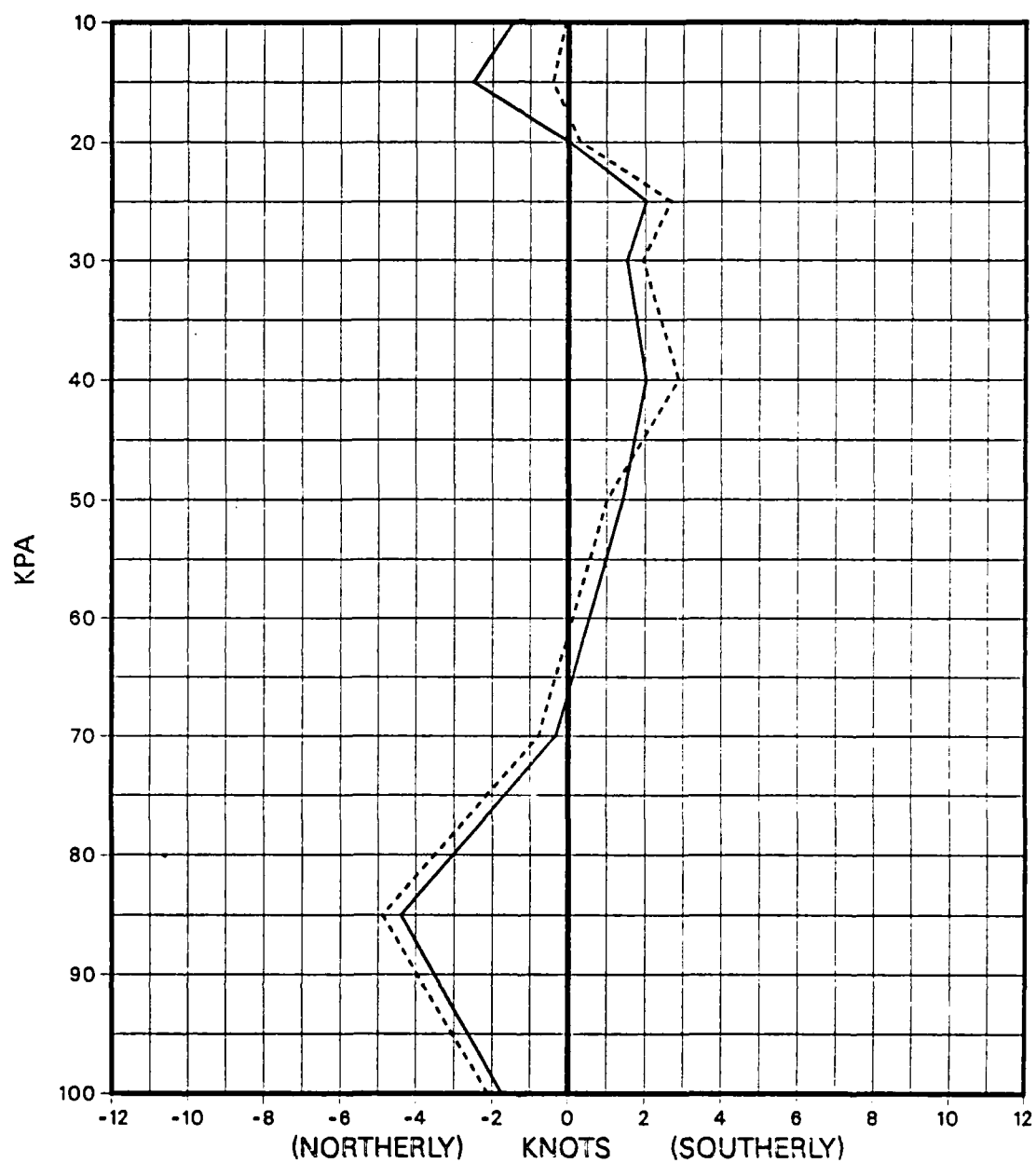


Figure 43. Vertical composite for v-wind component corresponding to Maximum OLR days, wet season 1984. Solid line represents seasonal average, dashed line represents deviation.

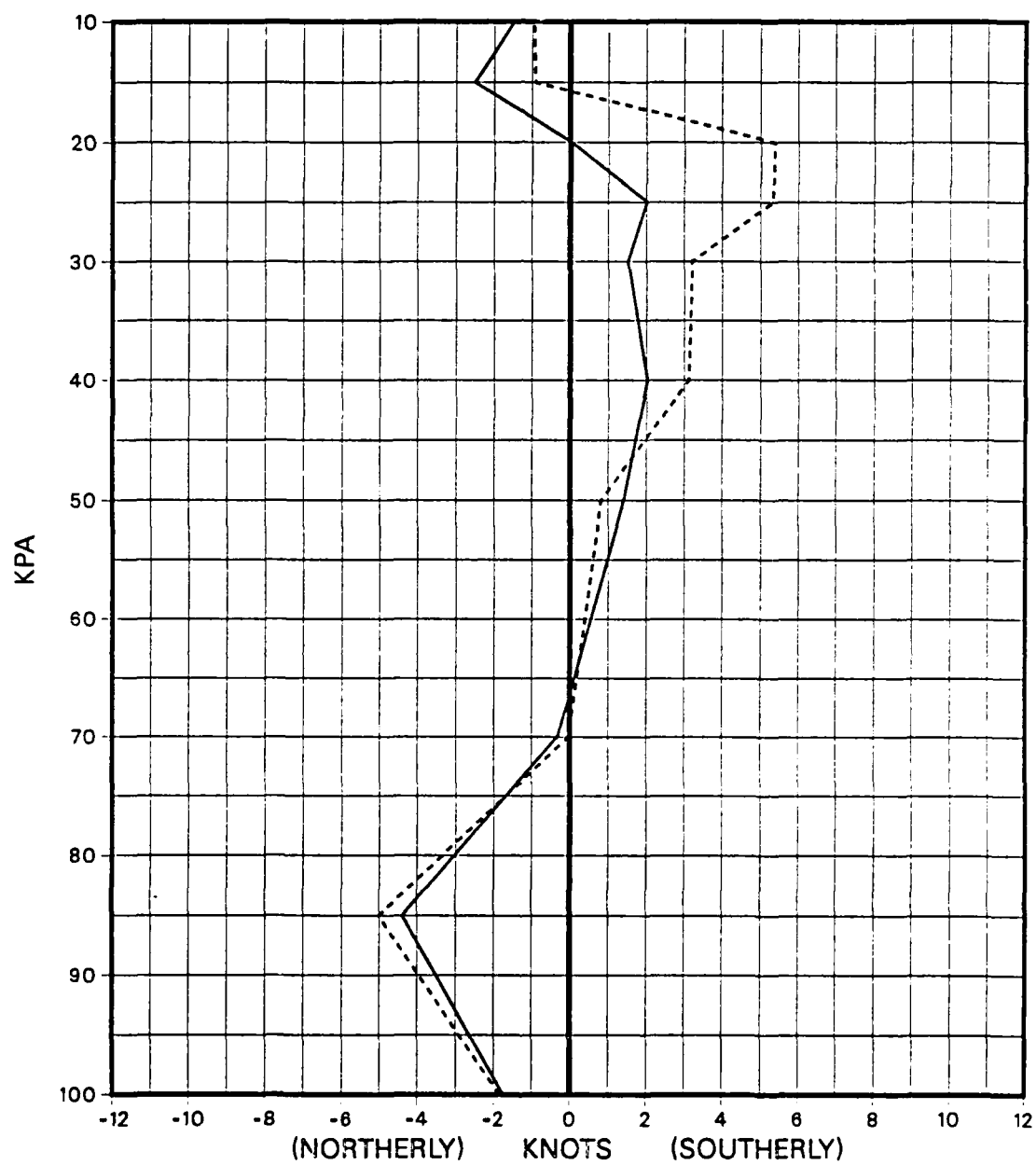


Figure 44. Vertical composite for v-wind component corresponding to Max-to-Min OLR inflection points, wet season 1984. Solid line represents seasonal average, dashed line represents deviation.

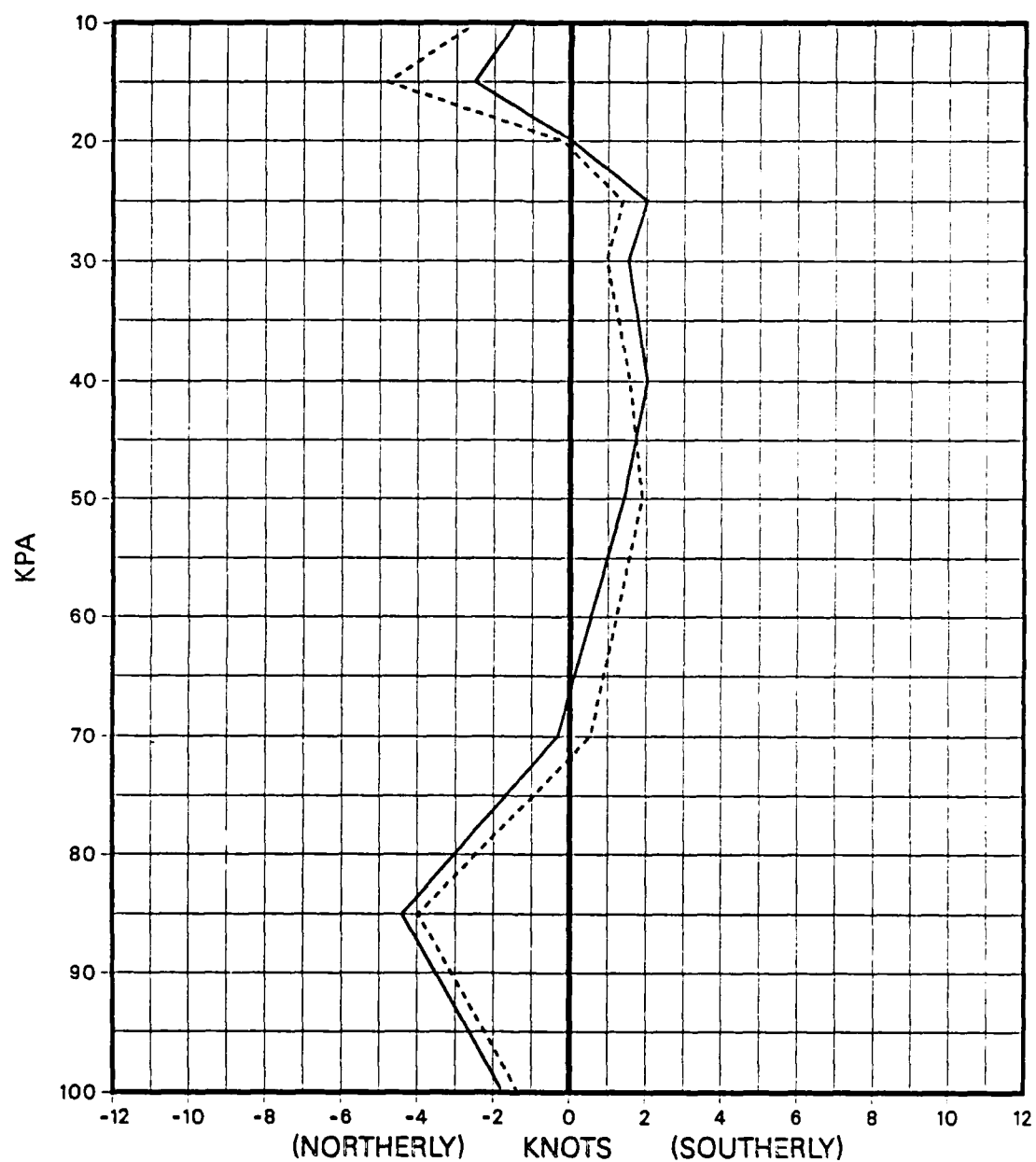


Figure 45. Vertical composite for v-wind component corresponding to Minimum OLR days, wet season 1984. Solid line represents seasonal average, dashed line represents deviation.

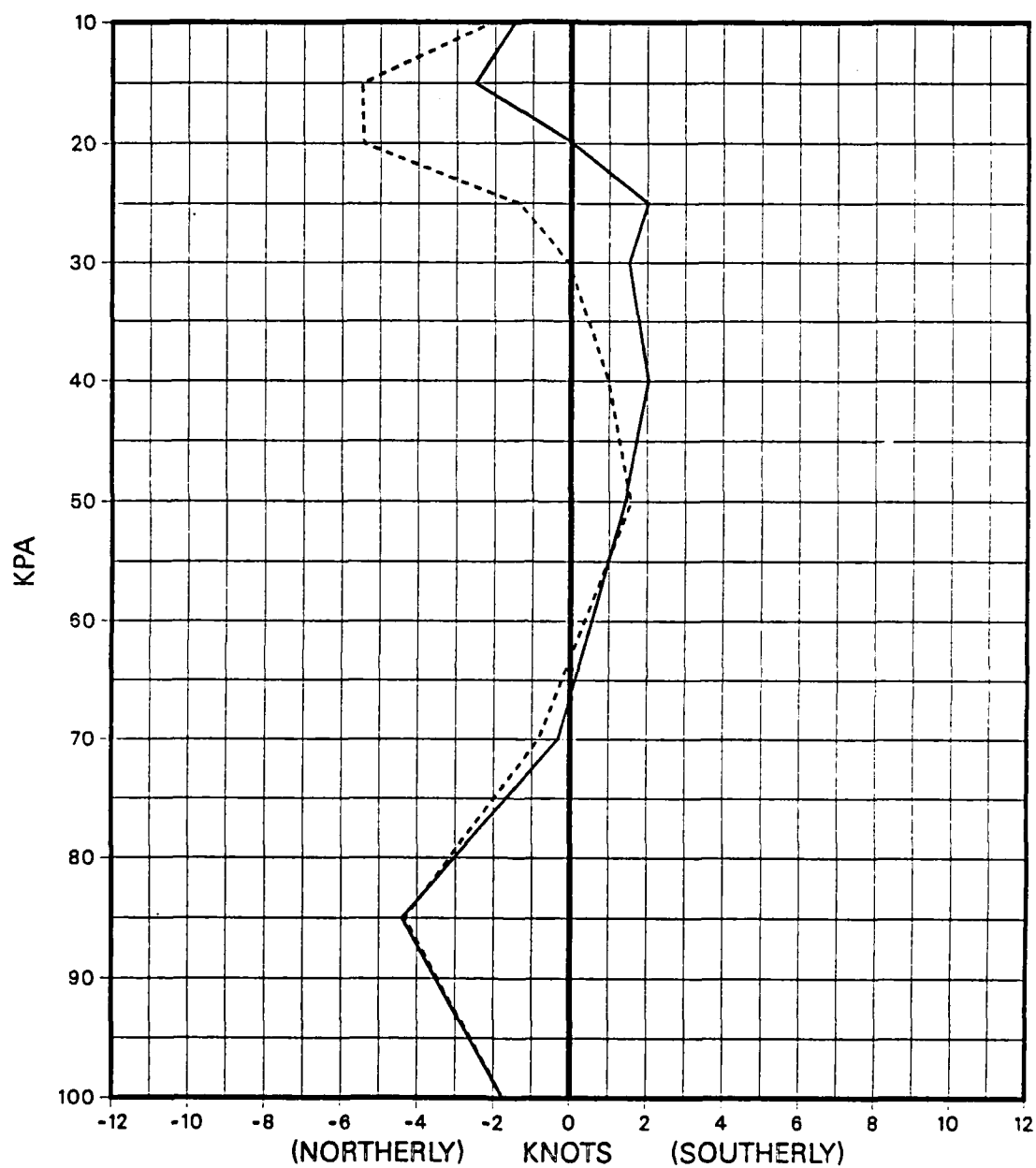


Figure 46. Vertical composite for v-wind component corresponding to Min-to-Max OLR inflection points, wet season 1984. Solid line represents seasonal average, dashed line represents deviation.

the north at roughly 5-6 kt. So again, within the span of 6 d the composite v-component winds have changed directions from a 5 kt southerly component to a 5-6 kt northerly component.

- Figure 47 shows the vertical composites of the height anomalies. The height deviations can again be detected in both the upper and lower levels, similar to the dry season height composites. However, this time the upper-level height anomalies lag the lower-level height anomalies, as can be seen from following the cycle of the 12-d oscillation in the composites. This structure is opposite from that found in the dry season and would imply that a different mechanism is responsible for the OLR anomalies associated with a period of 12 d.

The composites for wet season show that strong trends in all three variables are associated with the different phases of the 12-d oscillation, with the wet season trends are noticeably stronger than the dry season trends. The next section will attempt to describe the synoptic conditions that could be associated with the 12-day oscillation using the information obtained from the vertical composites.

### **Possible Synoptic Scenarios Associated with the 12-Day Oscillation**

#### **Dry Season 1984**

A summary of the resultant wind field and height anomalies for each phase of the 12-d oscillation during dry season 1984 is shown in Table 1. The data in this table were obtained from the vertical composites presented in the previous section.

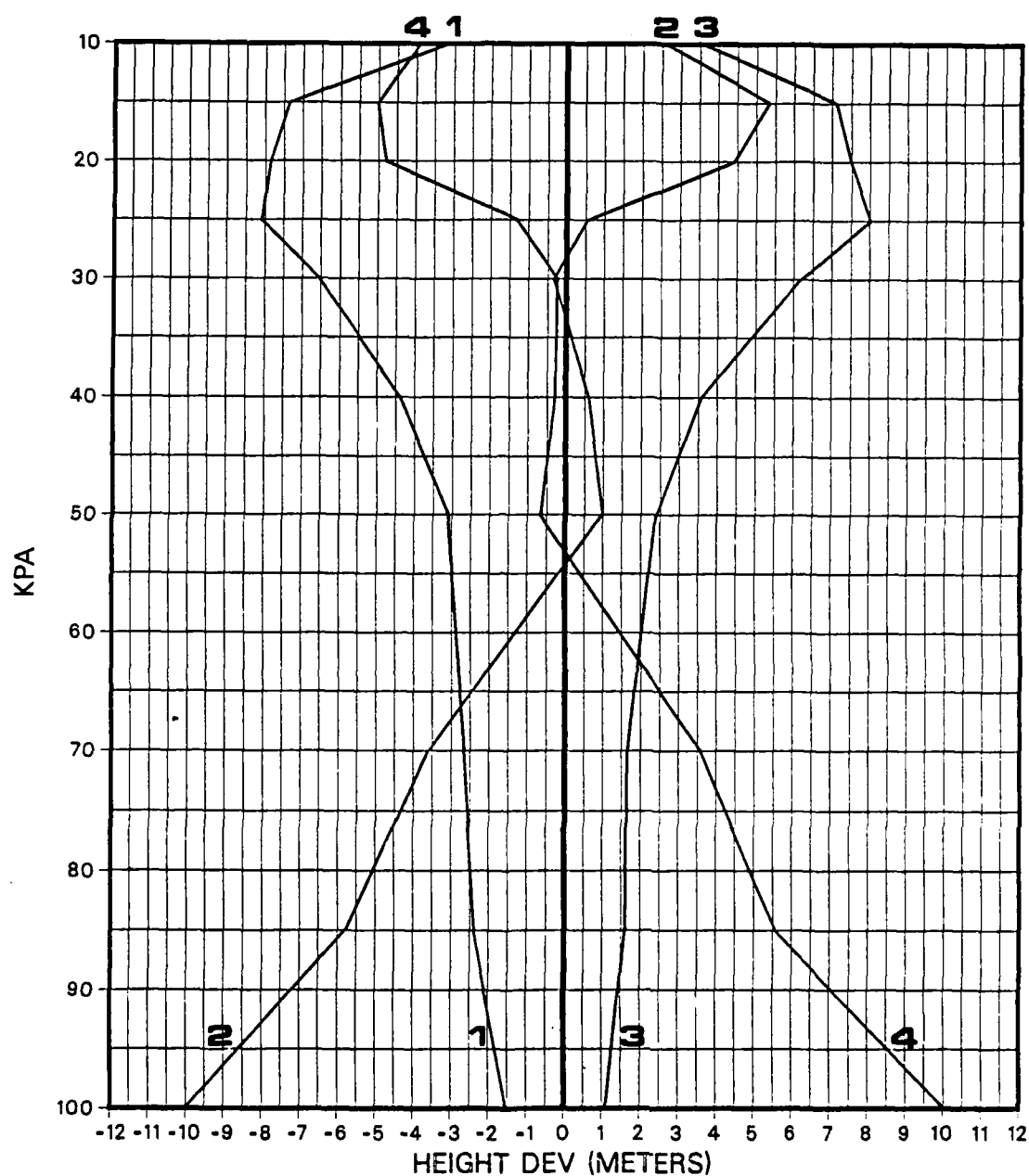


Figure 47. Vertical composite for height anomalies for wet season 1984. Solid line along zero deviation line represents seasonal mean, solid traces represent deviations from the mean. Trace 1 corresponds to Maximum OLR composite, Trace 2 to Max-to-Min composite, Trace 3 to Minimum OLR composite, Trace 4 to Min-to-Max composite.

Table 1. Resultant winds and height anomalies for Panama corresponding to the four phases of the 12-d oscillation for dry season, 1984. The resultant wind speeds are in knots.

		MAX	MAX-MIN	MIN	MIN-MAX
25 KPA	HEIGHT	+	0	-	0
	WIND	250/03	210/07	175/10	170/06
85 KPA	HEIGHT	0	-	0	+
	WIND	020/14	015/11	015/12	015/14

The height anomalies are depicted as relative maxima (+) and minima (-), while zero height anomalies indicate the height composite values were near the seasonal mean for that phase. The selection of single levels to represent the upper and lower troposphere was difficult in that the strongest anomalies for each variable were not always found at the 25 kPa and 85 kPa levels. For example, during wet season the strongest shift in the v-wind component anomalies is found at the 20 kPa level, with a weaker signal at 25 kPa. However, the forecaster trying to predict the phase of the 12-d oscillation will not have the benefit of having the current season u-and v-wind component and height anomaly composites to know which level contains the strongest signal. It is also very likely that the structure of these composites will vary a great deal from year-to-year. With that in mind, the 25 and 85 kPa levels were chosen

because they consistently capture the trend, and usually the maximum anomalies, of the deviations found throughout the 12-d cycle for both dry and wet seasons.

Starting the 12-d cycle shown in Table 1 with the Maximum phase (corresponding to maximum OLR values over Panama), positive height anomalies are found at 25 kPa while the composite heights are near the seasonal mean at 85 kPa. Moving through the four phases of the cycle it can be seen that the lower level height anomalies lead those of the upper-levels, suggesting a vertical tilt to the oscillation. The wind composites show that the majority of the fluctuation in the wind field are found in the upper-level winds, with the lower-level wind flow remaining fairly constant as the strong northeasterly winds typical of the dry season dominate. Knowing this, we will now concentrate on the fluctuations contained in the upper-level winds. Fig. 48 shows the upper-level wind flow from climatology for the month of January (Sadler (1975)), which is representative of dry season conditions. The main features around the Central American region are a weak ridge over Panama and the rest of Central America with a broad trough located to the west. Relating the upper-level wind composites of Table 1 to climatology, the following scenario is suggested (see Fig. 49):

- During the Maximum phase, the upper-level trough usually located to the west of Panama has moved to the east of the country, resulting in clear conditions (positive OLR anomalies) over the region. Weak west-southwesterly flow over Panama and positive height anomalies are the result of a broad ridge aloft just to the east of the region.



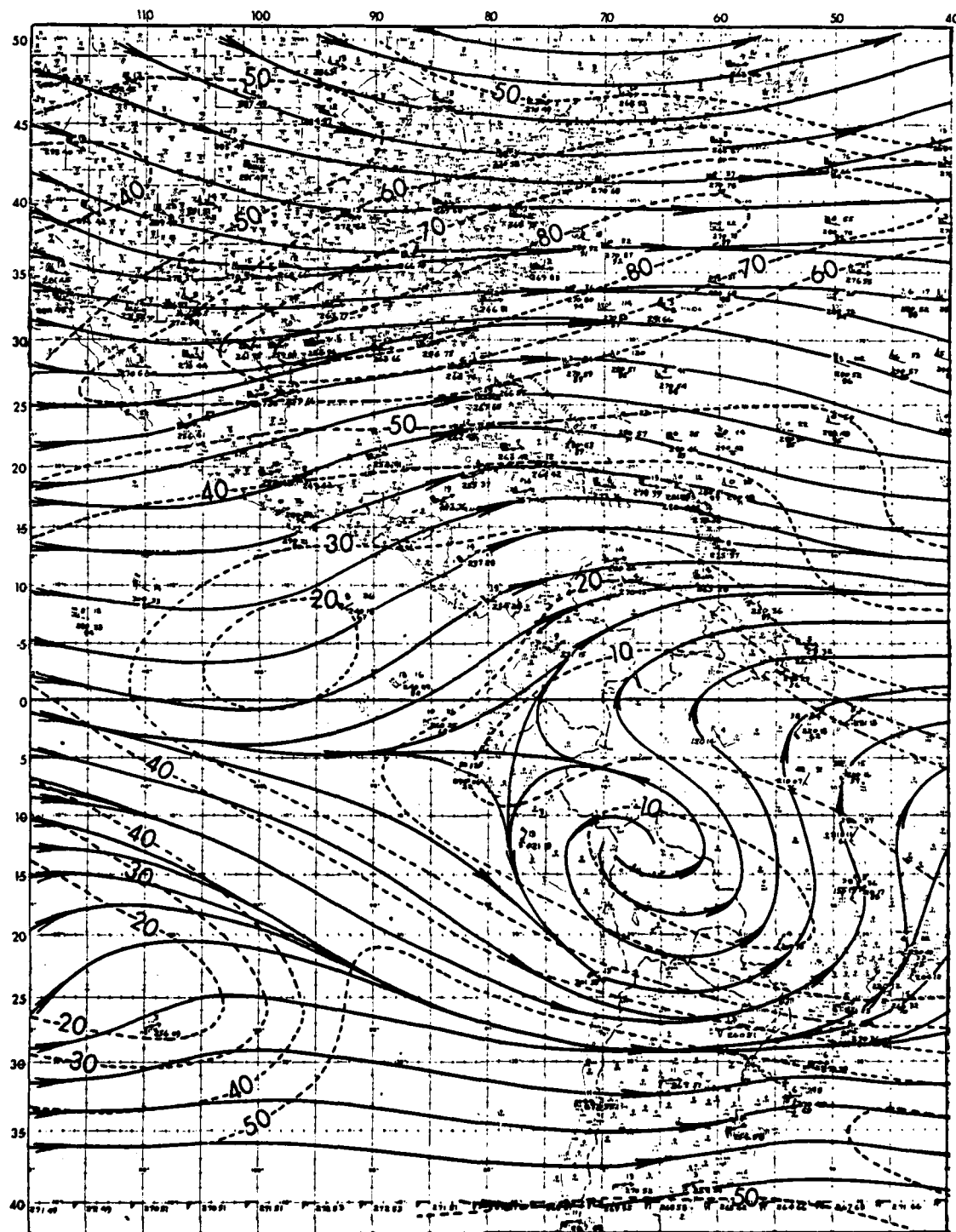


Figure 48. 20 kPa streamline climatology for January.

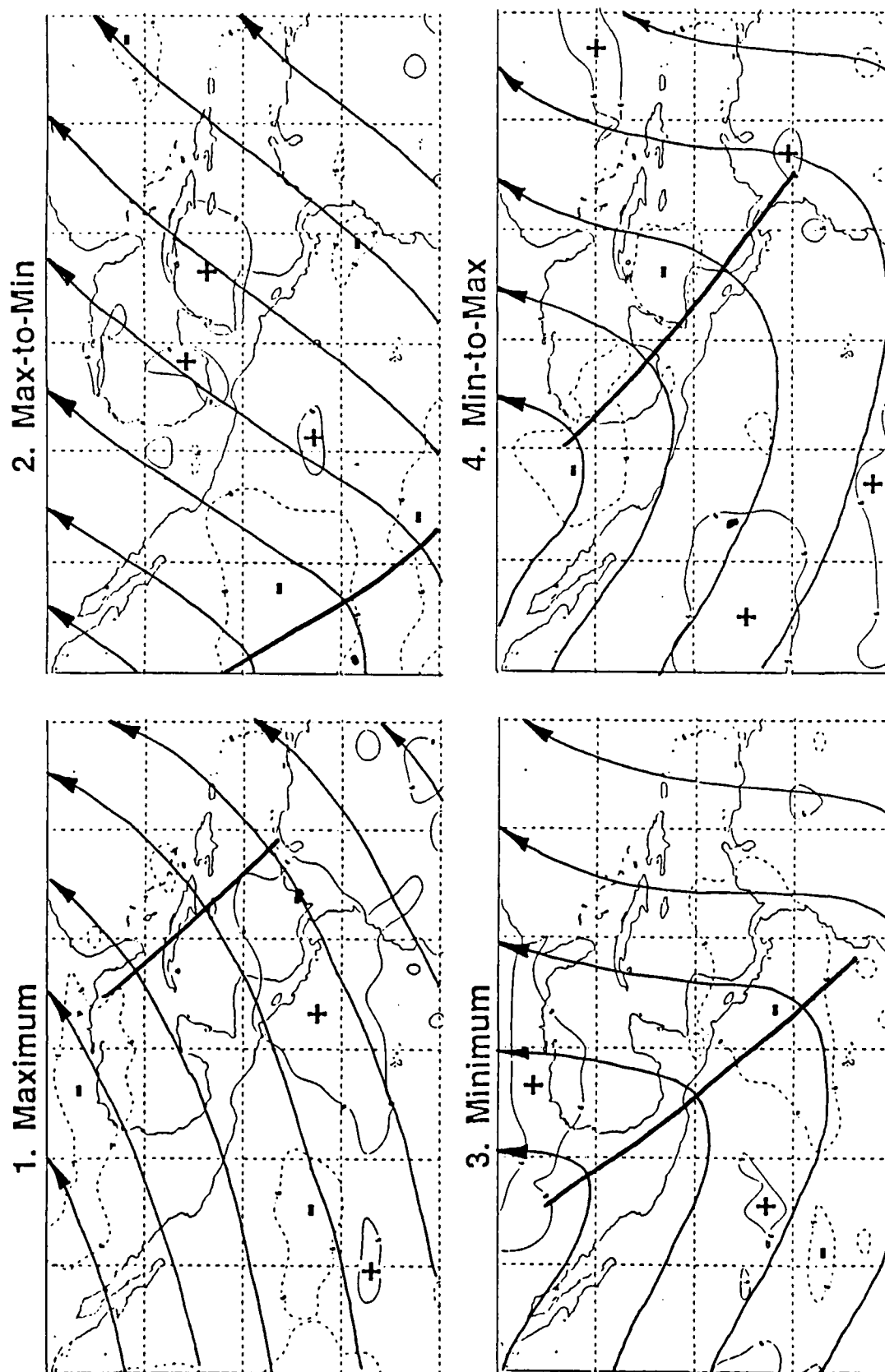


Figure 49. Possible synoptic scenario associated with the four phases of the 12-d oscillation, dry season. Contoured areas represent OLR anomalies greater than  $\pm 6 \text{ Wm}^{-2}$ .

- Three days later, a broad trough begins to build far to the west of Central America, with strong negative OLR anomalies developing just ahead of it. Southeasterly winds aloft and the decrease of the height anomalies over Panama suggest the upper-level ridge has moved off to the east.
- At the Minimum phase of the cycle the negatively-tilted trough has now moved just off the west coast of Central America and has deepened, as indicated by the relatively strong south-southeast upper-level flow and the negative height anomalies over Panama. Note that the strongest convective activity (shown by the negative OLR anomalies) is also found over Panama and Central America, just ahead of this trough.
- Three days later at the Min-to-Max inflection point it appears the trough has weakened and moved just to the northeast of Panama, as reflected by the weakened south-southeast flow and an increase in the upper-level height anomalies from a relative negative to the seasonal mean. At this point the cycle repeats again as weak ridging begins to build over the eastern Pacific.

While it is unrealistic to expect to be able to analyze the upper-level wind field of the entire domain using winds from only one location, this scenario does agree with climatology and the location of the OLR anomalies, and also provides an explanation for the apparent west-to-east movement of the OLR anomalies.

Table 2. Resultant winds and height anomalies for Panama corresponding to the four phases of the 12-d oscillation for wet season, 1984. The resultant wind speeds are in knots.

		MAX	MAX-MIN	MIN	MIN-MAX
25 KPA	HEIGHT	-	0	+	0
	WIND	120/05	140/07	100/09	080/08
85 KPA	HEIGHT	0	-	0	+
	WIND	045/07	040/06	025/04	035/05

#### Wet Season 1984

Table 2 shows a summary of the resultant winds and height anomalies for wet season 1984. The data were obtained in the same manner as dry season. As was the case in the dry season, the majority of the variation in the wind field is contained in the upper levels (25 kPa), as the lower-level winds (85 kPa) remain fairly constant from the northeast throughout the 12-d cycle. One major difference between the two seasons is that the upper-level height anomalies appear to lead those in the lower levels, which is opposite from the dry season pattern. An examination of the upper-level wind climatology for August shown in Fig. 50 reveals that the controlling feature for Panama appears to be the large anticyclone associated with the subequatorial ridge located to the northeast of Panama. The resultant wind field of Table 2, along

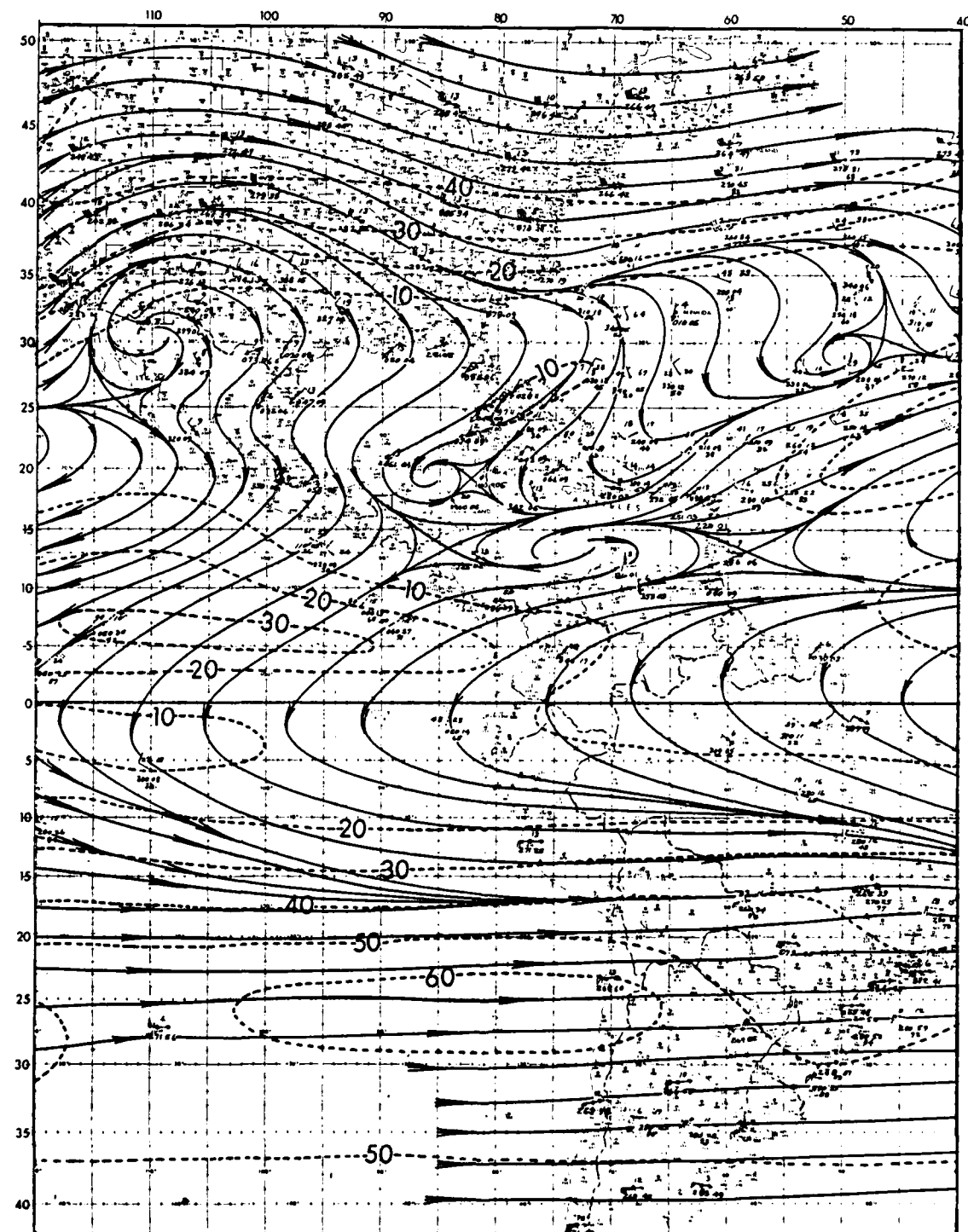


Figure 50. 20 kPa streamline climatology for August.

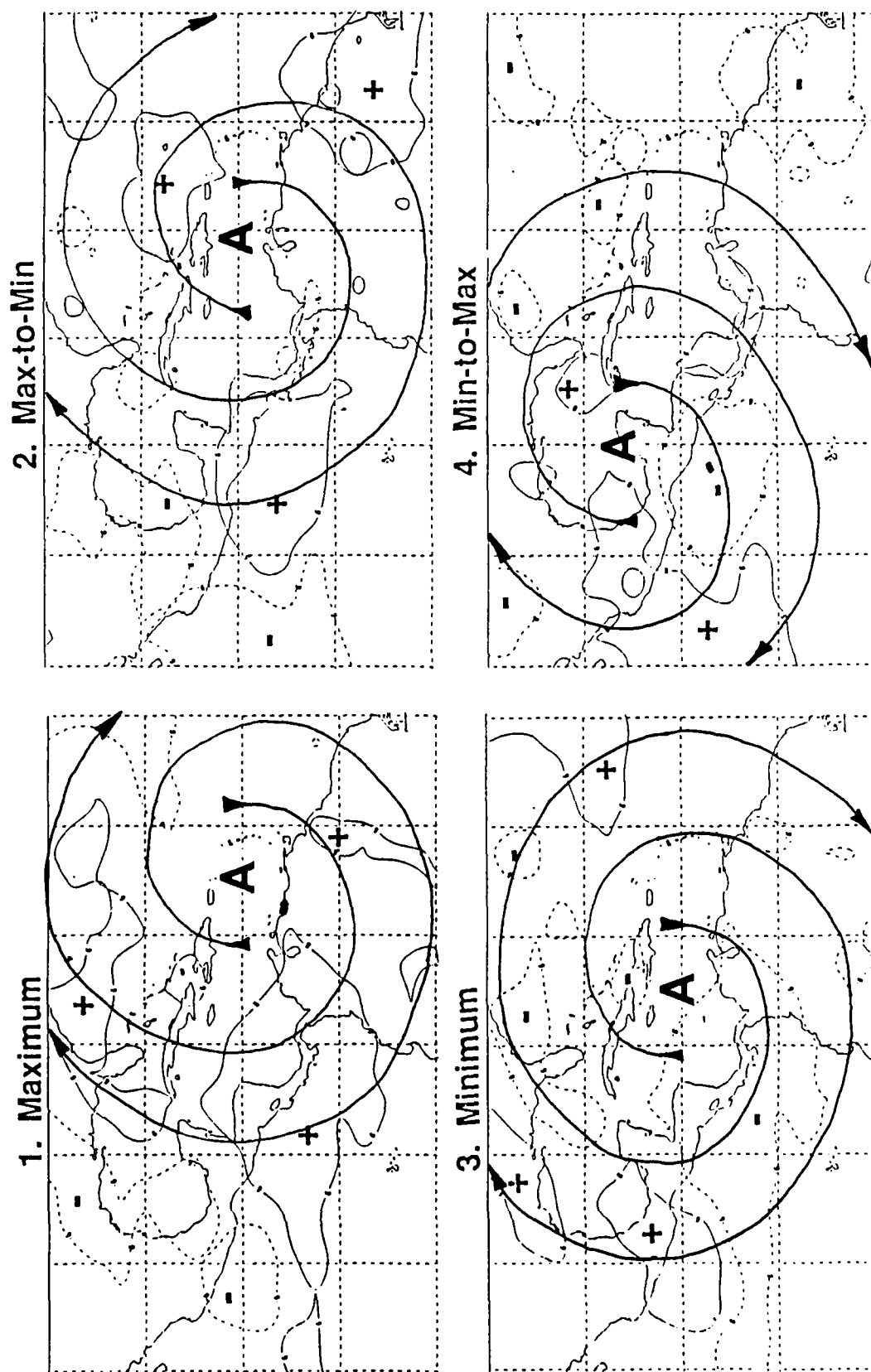


Figure 51. Possible synoptic scenarios associated with the four phases of the 12-d oscillation, wet season. Contoured areas represent OLR anomalies greater than  $\pm 6 \text{ W m}^{-2}$ .

with climatology, suggests that the following synoptic sequence (shown in Fig. 51) could be associated with the 12-d oscillation:

- Beginning with the Maximum phase, the anticyclone that is shown in climatology is located well to the northeast of Panama, resulting in weak southeasterly winds and a negative pressure anomaly. The outflow aloft associated with this anticyclone is also well to the north of the region, resulting in relative maximum OLR values over Central America.
- Three days later at the Max-to-Min inflection point, the anticyclone begins to move slowly to the west. This is reflected by the increase in convective activity over Panama and the continued southeasterly flow.
- During the Minimum phase of the 12-d oscillation the anticyclone has continued to move to the west and appears to be located just to the north of Panama, as shown by the upper-level winds which are now from the east-southeast. At this time the maximum outflow aloft associated with the anticyclone and the subequatorial ridge is located over Panama and Central America, resulting in the large area of negative OLR anomalies over the region which extends along the monsoon trough to the west.
- By the final phase of the oscillation, the Min-to-Max inflection point, the anticyclone appears to be drifting slowly to the west-northwest as Panama's upper-level winds are now from the east-northeast. The minimum OLR anomalies associated with the anticyclone have also drifted to the west-northwest and are located off the coasts of Guatemala and El Salvador. At this point it is not clear from the information available, but

it appears the anticyclone dissipates once it moves to the west and another forms to the northeast of Panama and the cycle begins again. Again, these scenarios are difficult to verify using data from only one location.

To summarize, the synoptic scenario for the wet season depicted above differs from that of dry season. In this case the factor controlling the development and movement of the OLR anomalies through the 12-d oscillation appears to be the westward movement of the anticyclone which is shown by climatology to be located to the northeast of Panama. Also, the OLR anomalies appear to develop over Panama and drift to the west-northwest during the wet season as opposed to the west-to-east movement observed during dry season.

### **Case Study**

The previous sections have concentrated on using upper-air data from a single station to detect and monitor the phase of the 12-d oscillation. This section will follow a complete cycle of the 12-d oscillation during wet season 1984 through the use of satellite imagery. The satellite imagery is from the Geostationary Operational Environmental Satellite (GOES) system. The satellite imagery shown in Figs. 52, 53, 54, and 55 are enhanced infrared photos with 7 km resolution. Clark (1983) describes the color enhancement levels as follows:

- The first level contours (medium and light gray) represent cloud tops between approximately 9,500 and 11,000 m.
- The next dark gray contour indicates thunderstorm activity with maximum cloud tops of approximately 12,500 m.



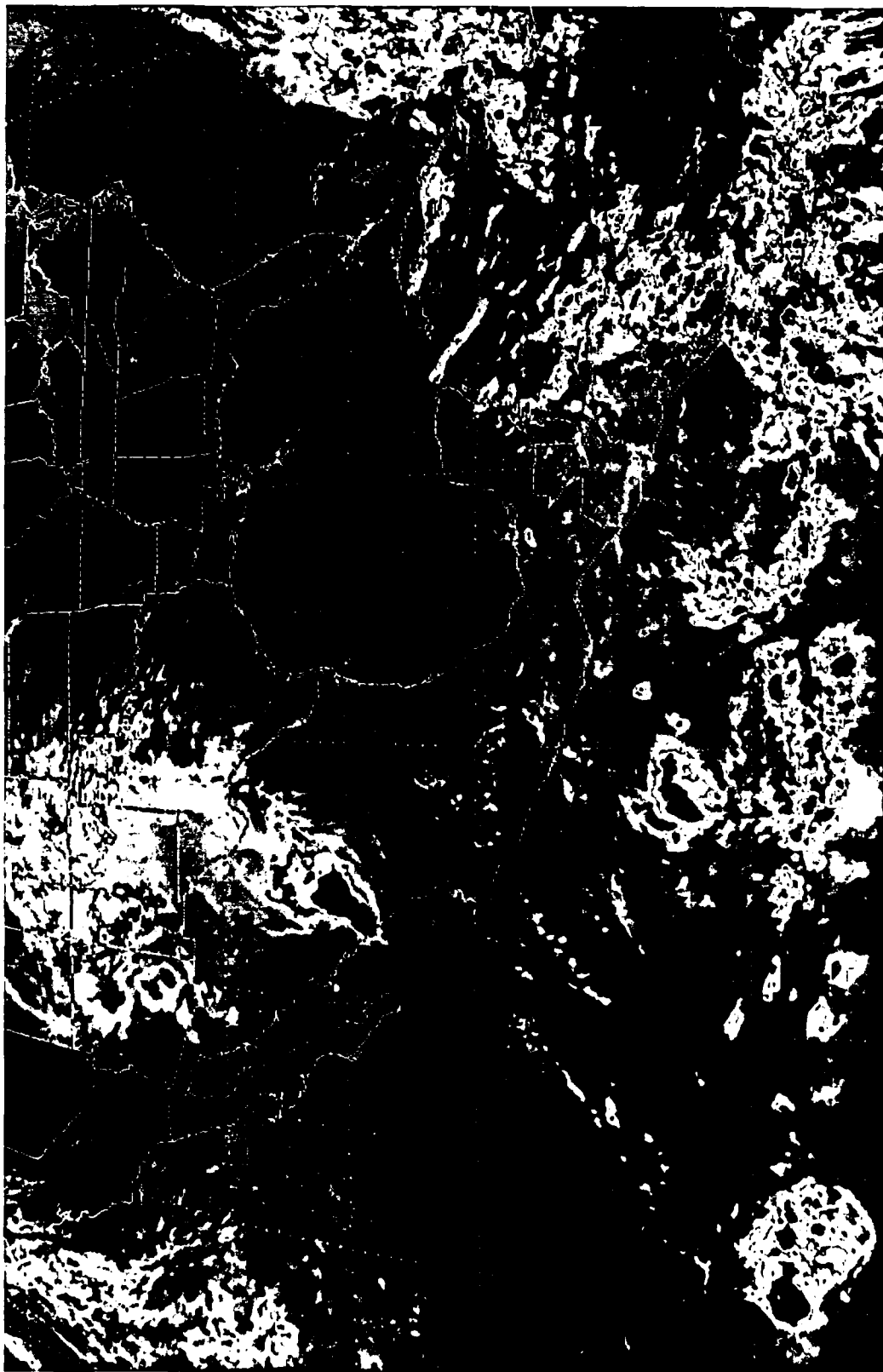


Figure 52. GOES enhanced IR satellite photo for 1800 GMT, 3 October 1984.



Figure 53. GOES enhanced IR satellite photo for 1900 GMT, 6 October 1984.

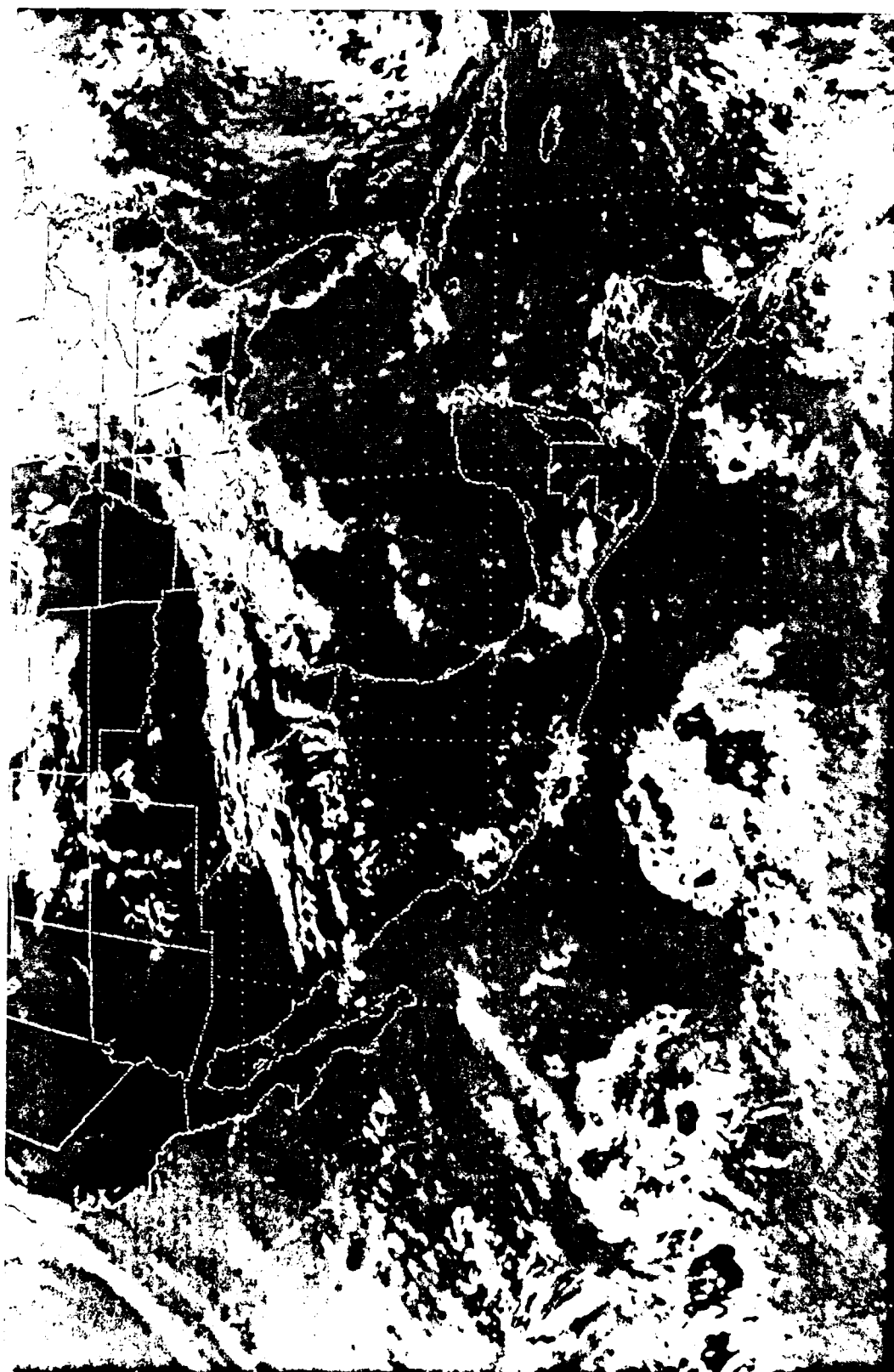


Figure 1. Aerial photograph of the study area, showing the location of the study area.

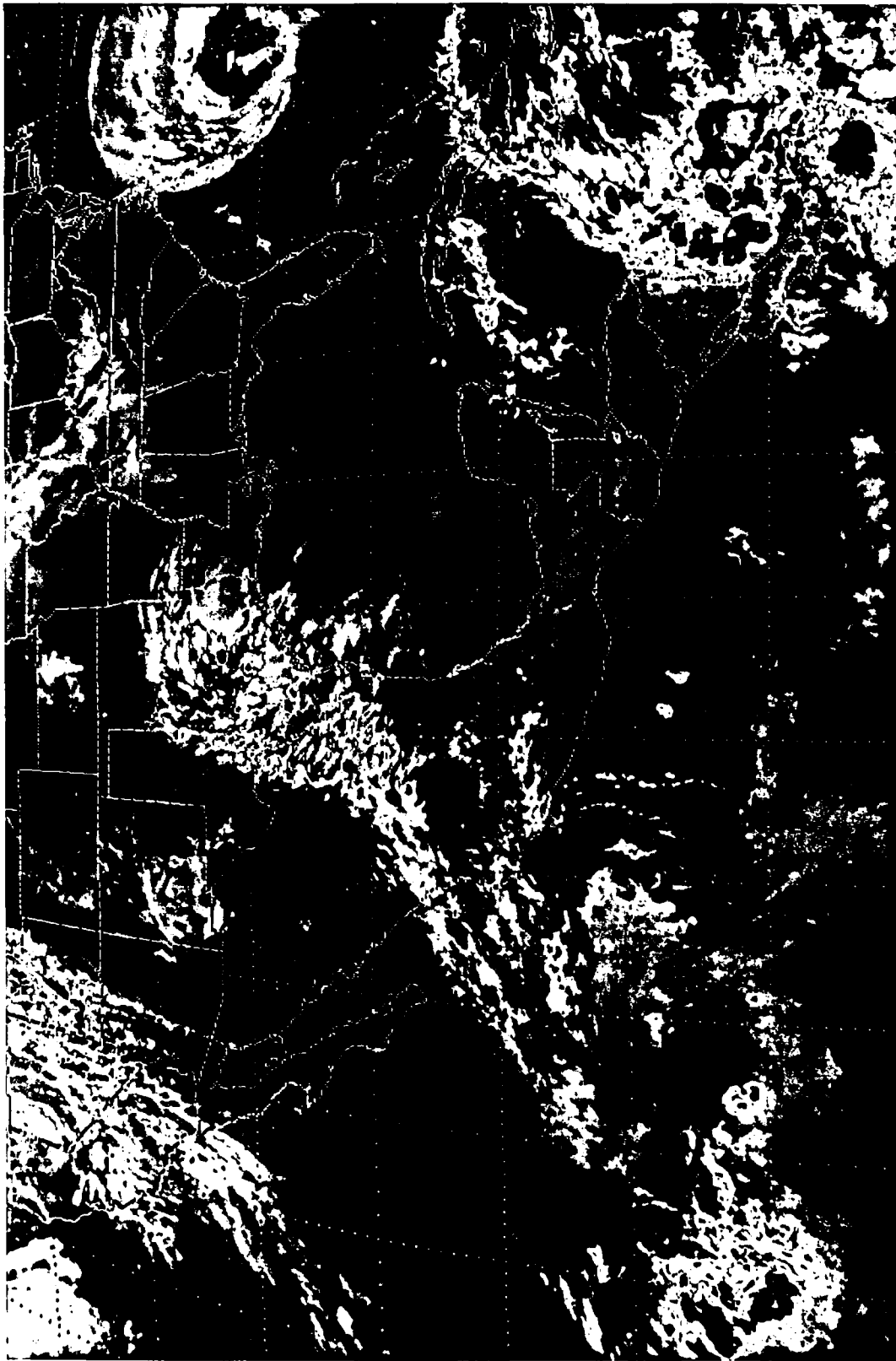


Figure 55. GOES enhanced IR satellite photo for 1800 GMT, 11 October 1984.

- The black enhancement represents cloud tops to approximately 13,400 m.
- The gray shade embedded within the black contour indicates cloud tops of approximately 14,700 m.
- The white enhancement within the black contour represents overshooting cloud tops above 14,700 m.

Using this enhancement, the thunderstorms around the Panama area are easily seen in Fig. 52. This photo is from the afternoon of 3 October 1984, in the middle of the wet season. This day was shown by the 12-d filtered OLR time series (Fig. 19) to be a Minimum OLR day, that is, a day with more convection than usual in the Panama area. Note the similarities between this photo and the Minimum OLR composite (Fig. 28). The satellite photo shows strong thunderstorm activity throughout the Panama region, extending to the west along the monsoon trough. The minimum OLR composite also depicts these conditions during this phase of the 12-d oscillation. Note the similarities at around  $15^{\circ}\text{N}$ ,  $100^{\circ}\text{W}$  where the maximum OLR anomalies of the OLR composite correspond with the relatively clear area on the satellite photo.

Moving ahead 3 d to Fig. 53 (Min-to-Max phase), the thunderstorm activity over the Panama area has decreased in intensity, and a large area of clouds and thunderstorm activity is centered at approximately  $10^{\circ}\text{N}$ ,  $95^{\circ}\text{W}$ . Comparing this photo with the Min-to-Max composite of Fig. 29, the areas of activity match up almost exactly.

The satellite photo depicting the next phase of the cycle is shown in Fig. 54, which is the Maximum OLR phase. At this time the Panama region appears to have a fair amount of high cloud cover with some embedded showers, but the cloud cover

and thunderstorm intensity has decreased significantly as compared to the Minimum and Min-to-Max phases. Also, the rest of Central America is not experiencing any significant thunderstorm activity in this afternoon photo which is unusual for this time of year. The OLR composite of Fig. 26 corresponds to this phase of the cycle, and the relatively clear conditions over Central America seen on the satellite photo are depicted on the composite. One area of thunderstorm activity on the satellite photo is centered at approximately  $10^{\circ}\text{N}$ ,  $100^{\circ}\text{W}$ , and this area matches well with the area of negative OLR anomalies shown on the composite. Also worth noting is the lack of convection along the monsoon trough as compared to the Minimum OLR phase.

The final phase of the 12-d oscillation is represented by the satellite photo in Fig. 55. At this time strong thunderstorm activity is beginning to develop over the Panama area, but the rest of Central America remains relatively cloud-free. These general conditions also show up on the composite diagram of Fig. 27.

The variations in convection and cloud cover associated with this 12-d oscillation may not always be as clear-cut as this case study. However, by following the trends of the upper-air analyses outlined in this chapter and maintaining continuity of satellite imagery, the cycle of the 12-d oscillation can be followed. This would allow for forecasts beyond 24 h to be made for above/below normal amounts of convection and cloud cover.

### **Correlation Between OLR Data and Precipitation**

This study has concentrated on determining the variability of convective activity over the Panama region through use of OLR data. One additional question that

remains concerns the ability of OLR data to infer actual rainfall totals. If low OLR values are related to convective activity, then there should be a high correlation between OLR and rainfall amounts. The long-period seasonal trends were removed from the time series of daily precipitation totals from raingauges in the Panama Canal region (see Fig. 3). This procedure was similar to that used on the daily average OLR time series. Once rainfall data were in this form, the degree of linear association between the rainfall data and the OLR time series of Figs. 9, 10, 11, and 12 was calculated using the coefficient of determination (Neter, Wasserman, and Kutner (1983)), where

$$r^2 = \left( \frac{\sum (X_i - \bar{X})(Y_i - \bar{Y})}{\sum (X_i - \bar{X})^2 \sum (Y_i - \bar{Y})^2} \right)^2. \quad (11)$$

The results of these calculations are as follows:

- Dry season 1984:  $r^2=.05$
- Wet season 1984:  $r^2=.07$
- Dry season 1985:  $r^2=.01$
- Wet season 1985:  $r^2=.13$ .

The calculations were again performed, this time using only the two OLR points from the domain (shown in Fig. 6) that were closest to Panama. Again, these two OLR points were averaged into one daily OLR value for the area and the seasonal trends were removed. The coefficient of determination values relating this smaller area and Panama rainfall are as follows:

- Dry season 1984:  $r^2=.08$

- Wet season 1984:  $r^2=.10$
- Dry season 1985:  $r^2=.04$
- Wet season 1985:  $r^2=.13$

The values of  $r^2$  can range from 0 (indicates no linear association between the two data sets) to 1 (indicates strong linear association). The values obtained here would seem to imply that there is little correlation between the OLR averages of either area and Panama rainfall. These numbers are significantly lower than what was expected, and it was thought that one possible cause for the low  $r^2$  values could be traced to the differences in the techniques used to measure the two variables. The rainfall data are comprised of 24 hourly totals from the 26 raingauge sites which record rainfall continually throughout the observation period. The OLR data are different in that they only represent snapshots of conditions taken twice a day, at approximately 0230 and 1430 LST. So it is doubtful that the OLR data, having only those two observation times, would coincide with the daily rainfall periods. One solution was to use only the 0200–0300 and 1400–1500 LST rainfall totals to correlate with the OLR data. To eliminate any bias concerning the spatial extent of the rain resulting from one raingauge recording a downpour of several inches in an hour while the other raingauges were dry, the frequency of precipitation was recorded. If any rain fell at a raingauge site during the specified hour, regardless of intensity, a '1' was recorded, while if no rain was measured a '0' was recorded. For example, if 6 of the 26 total raingauge sites recorded precipitation during 0200–0300 LST and 14 of the 26 raingauges recorded precipitation during the 1400–1500 LST period, the daily rainfall total used to correlate with the OLR daily average would be 20 (out of a total of 52



raingauge measurements). The coefficient of determination was again calculated for the both OLR domains (the 20-point area average as well as the 2-point average), however, the results (not shown) were not significantly higher.

There could be many factors contributing to the low  $r^2$  values, some of which could be:

- The OLR averages used in this study are measured and averaged over a much larger spatial scale than that of the precipitation. Even the smaller area of OLR used in the correlation study was the average of two  $2.5^\circ$  latitude-longitude areas. Local conditions, such as orographically-induced precipitation that could be causing isolated precipitation over the Panama Canal region, would not be reflected on this large scale.
- Some of the precipitation, especially over the highlands of central Panama, could be occurring with low, warm cloud tops having relatively high OLR values. This would contradict the original assumption that all precipitation over the Panama area is associated with cold cloud tops associated with intense convection.
- Both the OLR and precipitation time series are extremely noisy. A smoothing function applied to the time series may reduce some of the erratic fluctuations that could be contributing to a low  $r^2$  value.

In conclusion, it appears in this study that the OLR data set can not be used to directly predict rainfall events in the Panama Canal area. Instead, the OLR data depict fluctuations in cloud cover over the region, and these variations imply greater than or less than normal chances of precipitation over the region.

## CHAPTER VII

### MODULATION OF 12-DAY OSCILLATION

In Chapter VI it was mentioned that the 12-d filtered OLR time series for wet season 1984 (Fig. 19) appeared to contain a modulation of the signal on the time scale of 70–80 d. While looking through daily satellite imagery for case study photos an interesting relationship between the “active” and “inactive” phases of the 12-d oscillation and tropical storm activity in eastern Pacific was discovered. Figure 56 is the 12-d filtered OLR time series for wet season 1984 (which is the same as Fig. 19), which has been subjectively divided into active and inactive phases. Active phases are periods when the 12-d signal is strongest, while inactive phases contain relatively weak 12-d signals. The black bars running along the horizontal axis show the duration in days of tropical systems that developed in the eastern Pacific (Gunther and Cross (1985)). Note the large number of systems that existed during the inactive phases as compared to the active phases. Quantitatively, the total number of systems that developed during the inactive phases was 16 (5 tropical depressions, 2 tropical storms, and 9 hurricanes) compared to only 8 (3 tropical depressions, 3 tropical storms, and 2 hurricanes) for the active phase. A slight modulation of the 1985 wet season 12-d filtered time series (Fig. 21) can be seen, but it is not nearly as strong as that of 1984 wet season.

The reasons for this connection between the relative strength of the 12-d oscillation and the development of tropical storms in the eastern Pacific are not apparent from this research. Possibly a north-south oscillation of the subequatorial

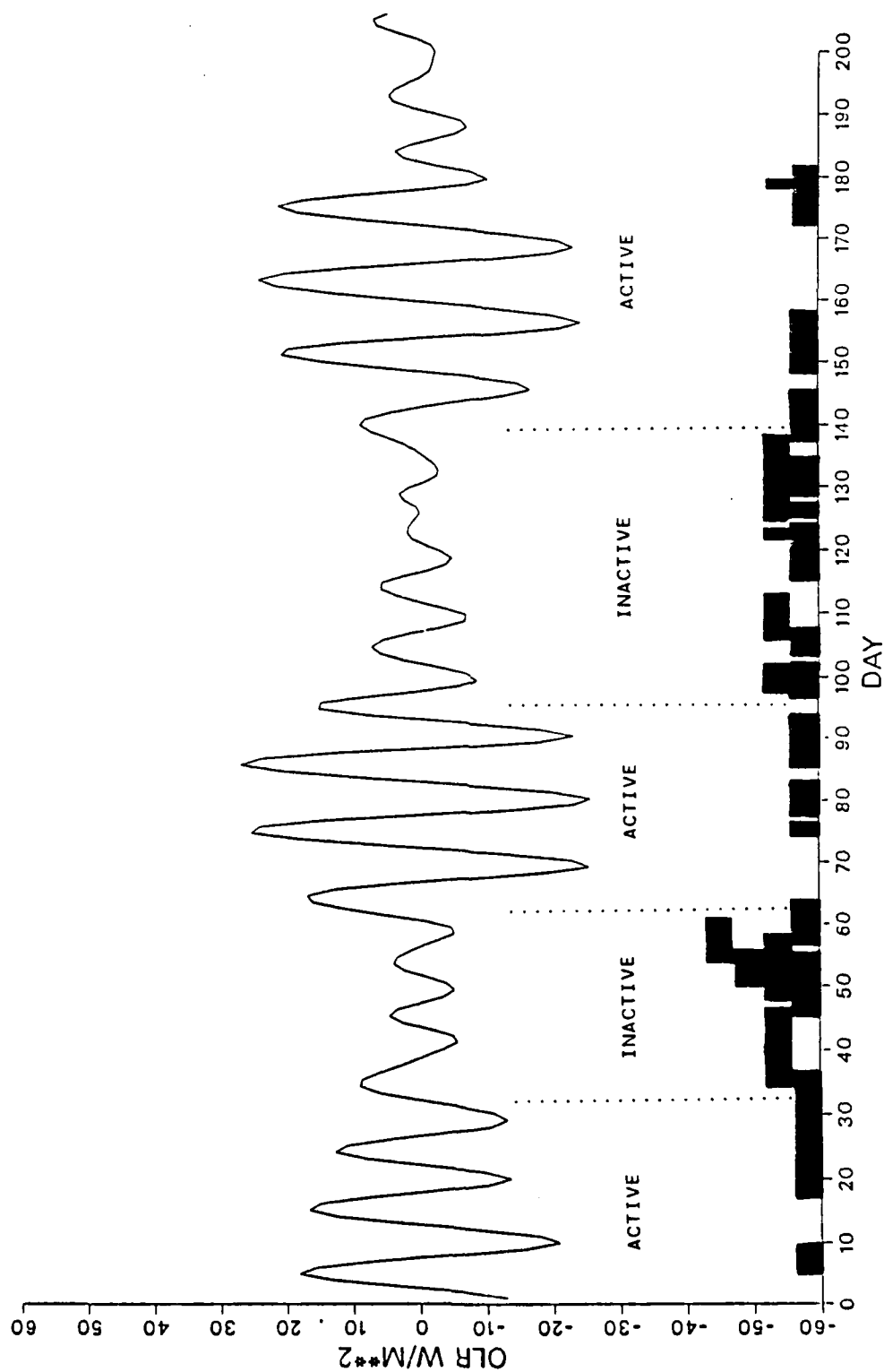


Figure 56. 12-d filtered OLR time series for wet season 1984 showing active and inactive phases of 12-d oscillation. Dark lines along horizontal axis represent tropical cyclone activity.

ridge exists during the wet season which creates favorable and unfavorable upper-level environments for tropical storm development in the eastern Pacific. During the inactive phase when favorable conditions exist in the eastern Pacific for tropical storm development, the upper-level anticyclone associated with the subequatorial ridge (see Figs. 50 and 51) could be too far to the north of Panama. This could result in a weaker 12-d oscillation by removing the outflow mechanism thought to be responsible for the periodic fluctuations in convection. However, significantly more research needs to be done on this subject before any theories can be proven.

## CHAPTER VIII

### SUMMARY AND AREAS FOR FURTHER STUDY

Convective variability over the Panama region was examined through spectral analysis of OLR time series data. The strongest and most persistent spectral peak was found in the 12-d range, with weaker spectral power evident in the 30-60 d and 15-30 d ranges. The OLR time series for the Panama region was filtered for 12 d, and composite diagrams corresponding to each of the four phases (Maximum, Minimum, and two inflection points) of the 12-d oscillation were constructed for the domain. The following conclusions were drawn from the composite analyses:

- The composites for dry season 1984 revealed west-to-east propagating OLR anomalies that appear to originate in the eastern Pacific and build to the east over Panama.
- The composites for wet season 1984 differed significantly from dry season in that the OLR anomalies appear to originate over the Panama region and drift slowly to the west-northwest.

Vertical composites of upper-air data from Albrook Air Force Station were then constructed to correspond to each of the four phases of the 12-d oscillation. Composites of u- and v-wind components and height of the pressure surfaces were examined in order to determine the vertical structure of the oscillation. The vertical composites revealed the following:

- In dry season 1984, 12-d fluctuations from the seasonal mean were evident in both the u- and v-wind components in the upper-levels, with the v-wind component showing the strongest fluctuations. Cyclic fluctuations were present in the height composites at all levels during the dry season. These height fluctuations reflected a baroclinic structure to the oscillation as the lower-level height anomalies led the upper-level height anomalies by approximately a quarter-cycle.
- Fluctuations of 12-d were again evident in the upper-level u- and v-wind composites and at all levels of the height composites during the wet season. These fluctuations were significantly stronger than those detected in the dry season. The major difference between the two seasons was found in the height composites. These composites suggest the vertical structure of the oscillation is reversed in the wet season as the upper-level height anomalies now lead the lower-level height anomalies by approximately a quarter-cycle.

The fluctuations of the departures of the three variables from their seasonal means would appear to be difficult to track from a purely quantitative standpoint, especially since the seasonal mean for the season in progress can not be determined. However, the trends of each variable through each of the four phases appear to be strong enough to enable forecasters to monitor the progress of the 12-d oscillation and the associated variations in convective activity.

Using OLR and upper-air composites as well as upper-level wind climatology, synoptic scenarios associated with the 12-d oscillation were constructed for each season. The results are as follows:

- The upper-level climatological winds show predominantly westerly flow with a broad trough embedded in this flow, located to the west of Central America in the eastern Pacific. The vertical composites suggest that this trough periodically deepens and moves to the east of Panama, resulting in enhanced convective activity ahead of it.
- The wet season pattern is significantly different from that of dry season. During this time, climatology shows the upper-levels over Panama to be dominated by the subequatorial ridge and an associated anticyclone to the northeast of Panama. The composites show indications that this anticyclone moves slowly to the west-northwest, and the increased outflow aloft associated with this anticyclone enhances convective activity over Panama as it passes just north of the region. This convection associated with the anticyclone continues appears to drift slowly to the west-northwest until the anticyclone weakens, then it seems another anticyclone develops to the northeast of Panama and the cycle begins again.

Another interesting feature associated with this 12-d oscillation is the apparent link between tropical cyclone activity in the eastern Pacific and 70–80 d fluctuations in the strength of the 12-d oscillation over Panama. In the wet season, during the periods when the 12-d oscillation over Panama was strong (active periods), tropical cyclone activity over the eastern Pacific was relatively weak (3 tropical depressions,

3 tropical storms, and 2 hurricanes). By comparison, during the periods when the 12-d oscillation over Panama was weak (inactive periods), a significant increase in eastern Pacific tropical cyclone activity (5 tropical depressions, 2 tropical storms, and 9 hurricanes) was noted. Although the cause for this modulation was not addressed in this research, one possible cause could be periodic north-south oscillations in the position of the subequatorial ridge. A northward migration of the ridge could result in a weaker 12-d signal by weakening the outflow mechanism necessary for strong convection over Panama, while at the same time creating favorable conditions for tropical cyclone development further north over the eastern Pacific where the low-level monsoon trough lies.

This research discussed the 12-d oscillation and its effects on convective activity over the Panama region. There are still many aspects of the 12-d oscillation to be examined. They are:

- Examine several years of OLR data to determine the interannual variability of the oscillation. The 12-d signal was very strong in 1984, but was not quite as strong in 1985. Perhaps some general circulation feature (El Nino, quasi-biennial oscillation) is connected with it.
- Although not shown, the 1985 OLR composites showed fairly strong connections between Panama and portions of South America with a period of 12 d. If several more years of data were examined it could be determined if this was just a one-time occurrence or if a connection does exist between the northern and southern hemispheres.



- The dry season OLR composites showed the OLR anomalies appeared to extend to the west from beyond the western edge of the domain at  $120^{\circ}\text{W}$ . The domain could be expanded to the west to determine the western extent of the oscillation.
- A more detailed study of the upper-level features associated with this oscillation could be performed by using hemispheric wind data. As was noted, it is difficult to imply conditions over the entire domain from only one vertical sounding. A hemispheric wind study could confirm the synoptic patterns inferred in this research.
- A closer examination could be made of the relationship between tropical cyclone activity in the eastern Pacific and the relative strength of the 12-d oscillation over Panama.

## REFERENCES

- Atkinson, G. D., 1971: Forecasters' guide to tropical meteorology. AWS Technical Report 240, 360 pp.
- Cahalan, R. F., D. A. Short, and G. R. North, 1982: Cloud fluctuation statistics. *Mon. Wea. Rev.*, **110**, 26-43.
- Chatfield, C., 1980: *The Analysis of Time Series: An Introduction*, Chapman and Hall, 268 pp.
- Clark, J. D., 1983: The GOES User's Guide, US Dept. of Commerce, NOAA, 162 pp.
- Daily Rainfall Map. Panama Canal Commission, n. d.
- Dunn, G. E., 1940: Cyclogenesis in the tropical Atlantic. *Bull. Amer. Meteor. Soc.*, **6**, 133-146.
- Gruber, A., and J. S. Winston, 1978: Earth-atmosphere radiative heating based on NOAA scanning radiometer measurements. *Bull. Amer. Meteor. Soc.*, **59**, 1570-1573.
- Gruber, A., and A. F. Krueger, 1984: The status of the NOAA outgoing longwave radiation data set. *Bull. Amer. Meteor. Soc.*, **65**, 958-962.
- Gunther, E. B., and R. L. Cross, 1985: Eastern North Pacific tropical cyclones of 1984. *Mon. Wea. Rev.*, **113**, 1393-1410.
- Hartmann, D. L., and J. R. Gross, 1988: Seasonal variability of the 40-50 day oscillation in wind and rainfall in the tropics. *J. Atmos. Sci.*, **45**, 2680-2702.
- The International Mathematical and Statistical Library User's Manual*, The IMSL Inc., 1987.
- Knutson, T. R., and K. M. Weickmann, 1987: 30-60 day atmospheric oscillations: Composite life cycles of convection and circulation anomalies. *Mon. Wea. Rev.*, **115**, 1407-1436.
- Knutson, T. R., K. M. Weickmann, and J. E. Kutzbach, 1986: Global-scale intraseasonal oscillations of outgoing longwave radiation and 250 mb zonal wind during northern hemisphere summer. *Mon. Wea. Rev.*, **114**, 605-623.

- Lau, K. -M., and P. H. Chan, 1983: Aspects of the 40-50 day oscillation during the northern summer as inferred from outgoing longwave radiation. *Mon. Wea. Rev.*, **114**, 1354-1367.
- Lyons, S. W., 1981: Planetary-scale aspects of outgoing longwave radiation and vorticity over the global tropics during winter. *Mon. Wea. Rev.*, **109**, 1773-1787.
- Madden, R. A., and P. R. Julian, 1971: Detection of a 40-60 day oscillation in the zonal wind in the tropical Pacific. *J. Atmos. Sci.*, **28**, 702-708.
- Madden, R. A., and P. R. Julian, 1972: Description of global-scale circulation cells in the tropics with a 40-50 day period. *J. Atmos. Sci.*, **29**, 1109-1123.
- Merritt, E. S., 1964: Easterly waves and perturbations, a reappraisal. *J. Appl. Meteor.*, **3**, 367-382.
- Murakami, T., 1980: Empirical orthogonal function analysis of satellite-observed outgoing longwave radiation during winter. Part I. Long-period (15-30 day) oscillations. *Mon. Wea. Rev.*, **108**, 408-426.
- Neiswanger, W. A., 1948: *Elementary Statistical Methods*, Macmillan, 740 pp.
- Neter, J., W. Wasserman, and M. H. Kutner, 1983: *Applied Linear Regression Models*, Irwin, 547 pp.
- Newton, J. H., 1988: *TIMESLAB: A Time Series Analysis Laboratory*, Wadsworth and Brooks/Cole, 623 pp.
- Ohring, G., A. Gruber, and R. G. Ellingson, 1984: Satellite determinations of the relationship between total longwave radiation flux and infrared window radiance. *J. Climate Appl. Meteor.*, **23**, 416-425.
- Panama. Map. U. S. Central Intelligence Agency, 1981.
- Panofsky, H. A., and G. W. Brier, 1968: *Some Applications of Statistics to Meteorology*, The Pennsylvania State University, 224 pp.
- Riehl, H., 1945: Waves in the easterlies and the polar front in the tropics. Dept. of Meteorology, University of Chicago, Misc. Rept. 17, 79 pp.
- Sadler, J. C., 1967: On the origin of tropical vortices. Proc. of the Working Panel on Tropical Dynamic Meteorology, NWRP 12-1167-132, Navy Weather Research Facility, 39-76.

- Sadler, J. C., 1975: The upper tropospheric circulation over the global tropics. Dept. of Meteor., University of Hawaii, UHMET-75-05, 36 pp.
- Shanks, J. L., 1967: Recursion filters for digital processing. *Geophysics*, **32**, 33-51.
- Wallace, J. M., and C. -P. Chang, 1969: Spectrum analysis of large-scale wave disturbances in the tropical lower troposphere. *J. Atmos. Sci.*, **26**, 1010-1025.
- Weickmann, K. M., 1983: Intraseasonal circulation and outgoing longwave radiation modes during northern hemisphere winter. *Mon. Wea. Rev.*, **111**, 1838-1858.
- Weickmann, K. M., G. R. Lussky, and J. E. Kutzbach, 1985: Intraseasonal (30-60 day) fluctuation of outgoing longwave radiation and 250 mb streamfunction during northern winter. *Mon. Wea. Rev.*, **113**, 941-961.
- Yasunari, T., 1980: A quasi-stationary appearance of 30-40 day period in the cloudiness fluctuations during the summer monsoon over India. *J. Meteor. Soc. Japan*, **58**, 225-229.

## VITA

Christopher Stephen Strager [REDACTED]  
[REDACTED] to Frank and Mary Lou Strager. Chris completed his secondary education at South Allegheny High School in Liberty Borough, Pennsylvania in June 1978. Later that same month he enlisted in the United States Air Force in the weather career field. After completing Basic Training at San Antonio, Texas and a 12-week Weather Specialist Course at Chanute AFB, Illinois he was assigned to Griffiss AFB, New York as a Weather Observer. It was during that assignment that the Air Force granted him an R.O.T.C. scholarship to The Pennsylvania State University to obtain his Bachelor of Science degree in Meteorology (1983).

Upon his commissioning in May 1983, Chris was assigned to K.I. Sawyer AFB, Michigan as Wing Weather Officer in support of Strategic Air Command aircraft. His next assignment in September 1984 was to Panama, where he served as Weather Officer to the United States Southern Command at Quarry Heights. It was during this tour that Chris became interested in studying the tropical weather patterns of Panama and Central America. In August 1987 he carried this interest with him to his next assignment at Texas A&M University, where he is working towards a Masters of Science Degree through the Air Force Institute of Technology.

Chris is married to the former Crystal Jenyne Brooks of Mililani Town, Hawaii.

[REDACTED]